DYNAMIC ANALYSIS OF SPUR GEARS

A THESIS SUBMITTED TO

THE GRADUATE SCHOOL OF NATURAL AND APPLIED SCIENCES

OF

THE MIDDLE EAST TECHNICAL UNIVERSITY

BY
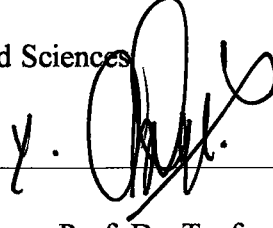
CAN ULAŞ DOGRUER

82566

IN PARTIAL FULLFILLMENT OF THE REQUIREMENTS FOR THE DEGREE

OF

MASTER OF SCIENCE

IN

THE DEPARTMENT OF MECHANICAL ENGINEERING

JUNE 1999

Approval of the Graduate School of Natural and Applied Sciences

Prof. Dr. Tayfur ÖZTÜRK

Director

I certify that this thesis satisfies all the requirements as a thesis for the degree of Master of Science.

Prof. Dr. Ediz PAYKOÇ

Head of Department

This is to certify that we have read this thesis and that in our opinion it is fully adequate, in scope and quality, as a thesis for the degree of Master of Science.
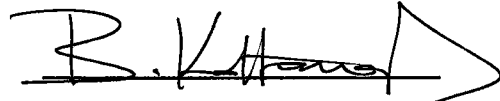
Prof. Dr. H. Nevzat ÖZGÜVEN

Supervisor

Examining Committee Members :

Prof. Dr. Bilgin KAFTANOĞLU (Chairman)

Prof. Dr. H. Nevzat ÖZGÜVEN

Prof. Dr. Metin AKKÖK

Prof. Dr. Sahir Arıkan

Assoc. Prof. Dr. Ozan TEKİNALP

ABSTRACT

DYNAMIC ANALYSIS OF SPUR GEARS

DOGRUER, Can Ulaş

M. S., Department of Mechanical Engineering

Supervisor: Prof. Dr. H. Nevzat ÖZGÜVEN

June, 1999, 147 pages

This study deals with dynamic analysis of spur gear systems which consist of shafts on elastic bearings, and coupled by a non-linear three degree of freedom gear mesh interface. The mathematical model and the software (NLGRD) developed in a previous study is extended to compute natural frequencies and dynamic bearing forces. The software NLGRD is also modified further by including an interface for a friendly use. The software NLGRD analyzes non-linear gear-shaft system by using the output of the so-called LDP version 10.1 which was developed at the Ohio State University. LDP computes loaded static transmission error and mesh compliance for the contact points in a typical mesh cycle of spur and helical gears. Although a constant mesh stiffness is assumed in the mathematical model of this study, it includes the excitation effect of time varying mesh stiffness through a periodic displacement representing loaded static transmission error.

Computer program which was originally written for main frame computer is modified and extended by including a friendly user interface

(NLGRD version 2.0). Multi disk, multi bearings, stepped shafts and gear meshes can be modeled through NLGRD interface easily. The program calculates dynamic to static load ratio, dynamic transmission error, reaction forces and displacements at bearings. The code, NLGRD version 2.0, is validated by analyzing some example cases, and comparing the results with available experimental data as well as results found in literature.

Several case studies are examined by changing various parameters of an example system, and the effects of some system parameters, such as mean load , module, center distance, on system response are studied. It is found that there is a logarithmic relation between maximum dynamic to static load ratio and module of the gear. It is believed that this empirical relation may have an important application. Parabolic and linear profile modifications are applied to spur gears. Within the limits of this study, it is found that there is a linear relation between maximum dynamic to static load ratio and amount of modification. Finally, effects of backlash and damping ratio on tooth separation are studied

Key words: Dynamic to static load ratio, Gear dynamics, Gear mesh interface, Non-linear, Non-linear gear dynamics, Mathematical modeling, Spur gears, User-interface

ÖZ

DÜZ DISLILERIN DINAMIK ANALIZI

DOGRUER, Can Ulaş

Yüksek Lisans, Makina Mühendisliği Bölümü

Tez Yöneticisi : Prof. Dr. H. Nevzat ÖZGÜVEN

Haziran, 1999 147 Sayfa

Bu çalışma, doğrusal olmayan, üç serbestlik derecesine sahip dişli ara birimiyle birleştirilmiş, elastik yataklar üzerindeki millerden oluşmuş, düz dişli sistemlerinin analizini kapsamaktadır. Bir önceki çalışmada geliştirilmiş olan, matematiksel model ve yazılım (NLGRD), doğal frekansları ve dinamik yatak kuvvetlerini hesaplamak üzere genişletilmiştir. Bu yazılım modellemeyi kolaylaştırmak amacıyla, kullanıcı arabirimi de eklenerek gelişmiş hale getirilmiştir. Bu yazılım, NLGRD, Ohio State University'de geliştirilmiş olan LDP versiyon 10.1'in çıktısını kullanarak doğrusal olmayan dişli mil sistemini inceler. LDP, statik iletim hatasını ve dişliler arasındaki direngenliği tipik bir düz veya helisel dişli döngüsündeki temas noktaları için hesaplar. Matematiksel modelde sabit bir kavrama direngenliği olduğu varsayılmasına rağmen, model dolaylı yoldan, statik iletim hatasını temsil eden periyodik bir yerdeğiştirme fonksiyonu aracılığı ile zamanla değişen kavrama direngenliğinin tahrik etkisini içermektedir.

Daha önce merkezi bilgisayar sisteminde kullanılmak amacı ile

v

yazılmış olan bilgisayar programı bir kullanıcı arabirimi eklenerek değiştirilmiş ve genişletilmiştir. Çok sayıda disk, çok sayıda yatak, değişken çapta mil ve dişli çifti, kullanıcı arabirimi ile kolaylık ile modellenebilir. Yazılım dinamik faktörü, dinamik iletim hatasını, tepki kuvvetlerini ve yataklardaki yerdeğiştirmeyi hesaplamaktadır. NLGRD versiyon 2.0 yazılımı, bazı örnek uygulamalar analiz edilerek ve bunların sonuçları, elde edilen deneysel veriler ve literatürde bulunan sonuçlarla karsılaştırılarak doğrulanmıştır.

Bir çok uygulamalı çalışma, örnek bir sistemdeki çeşitli parametreler değiştirilerek yapılmış ve statik yük, modül, merkezler arasındaki uzaklık gibi bazı sistem parametrelerinin etkileri incelenmiştir. Maksimum dinamik faktör ile dişlinin modülü arasında logaritmik bir bağıntı olduğu bulunmuştur. Bu ampirik bağıntının önemli sonuçları olabileceğine inanılmaktadır. Düz dişlilere parabolik ve doğrusal profil modifikasyonları uygulanmış ve bu çalışmanın sınırları çerçevesinde, maksimum dinamik faktör ile modifikasyonun miktarı arasında doğrusal bir bağıntı olduğu bulunmuştur. Son uygulamalı çalışmada, diş boşluğunun ve sönümlenmenin sistem tepkisi üzerindeki etkileri incelenmiştir.

Anahtar kelimeler : Dinamik faktör, Dişli dinamiği, Dişli arabirimi, Doğrusal olmayan, Doğrusal olmayan dişli dinamiği, Düz dişliler, Kullanıcı arabirimi

If I have been able to see a little farther than other

man, it is because I stood on the shoulder of giants.

Sir Isaac Newton

ACKNOWLEDGEMENTS

TABLE OF CONTENTS

LIST OF TABLES

LIST OF FIGURES

NOMENCLATURE

'	Differentiation with respect to position
*	Differentiation with respect to time
$\{\ \}^T, [\ ]^T$	Transpose of $\{\ \}, [\ ]$
a, b	Coefficients of Fourier series
$[C]$	Damping matrix
$\varepsilon_g, \varepsilon_p$	Geometric eccentricities of gear and pinion respectively
$e_t(t)$	Internal displacement excitation at the gear mesh point
$\{f\}$	Vector of forces
$\{F\}$	Complex amplitude vector of forces
$F^{gp}(t)$	Translational force vector acting on gear
$f(P)$	Backlash non-linear function
$\{G\}$	Complex amplitude vector of internal quasi-linear forces
$[H]$	Structural damping matrix
I_g, I_p	Mass moment inertia of gear and pinion respectively
I_L, I_M	Mass moment inertia of load and motor respectively
j	Unit imaginary number
k_h	Average mesh stiffness
$[K]$	Stiffness matrix
$K^{gp}(t)$	Mesh stiffness matrix
$[M]$	Mass matrix
$\{N\}$	Vector of internal non-linear forces
p	Relative displacement along the pressure line between

	meshing gear
P	Complex amplitude of relative displacement p
$\underset{\sim}{Q}^{gp}(t)$	Generalized force vector
$\underset{\sim}{\bar{Q}}^{gp}$	Static component of generalized force vector
$\underset{\sim}{Q}_m^{gp}(t)$	Vibratory component of generalized force vector
$\underset{\sim}{Q}_{md}^{gp}(t)$	Dissipative vibratory force
$\underset{\sim}{Q}_{me}^{gp}(t)$	Elastic vibratory force
q_m	Mean of relative displacement, normalized relative to backlash
q_a	Time-varying component of relative displacement, normalized relative to backlash
$q_g(t)$	Position vector of gear body
$\bar{q}_g$	Mean position of gear body
$q_{gm}(t)$	Time-varying component of position vector of gear body
$q_{mg}^i(t)$	Time-varying dynamic component of displacement
$q_{mo}^i(\theta^*)$	Spatially-varying component of displacement
$\{q\}$	Displacement vector
$\bar{R}_g$	Mean translation of gear origin with respect to inertial frame
$\bar{R}_{gm}(t)$	Time-varying component of translation vector
r_g, r_p	Base circle radii of gear and pinion respectively
$T^{gp}(t)$	Moment vector acting on gear
W	Static transmitted load

$\{X_1\}$	Non-linear coordinates associated with gear mesh interface
$\{X_2\}$	Linear coordinates
X,Y,Z	Inertial frame
X_g,Y_g,Z_g	Non-rotating geometric reference frame
y_g,y_p	Displacement in y direction of gear and pinion respectively
Y_g,Y_p	Complex amplitude of displacements in y direction gear and pinion respectively
$[\alpha]$	Quasi-linear receptance matrix
$\delta_m^{gp}(t)$	Vector of equivalent displacement
$\delta_e^{gp}(t)$	Deviation of gear tooth profile from perfect conjugate
$\delta_q^{gp}(t)$	Gear body Displacement
$[\Delta]$	Generalized quasi-linear receptance matrix
$[\gamma]$	Linear receptance matrix
η_H	Hysteric loss factor
η_v	Viscous damping factor
v_{kj}	Describing function corresponding to the non-linear element n_{kj}
θ_1,θ_2	Total angular rotations of pinion and gear respectively
$\bar{\theta}_g$	Mean angular misalignment vector of gear origin
θ_g,θ_p	Fluctuating parts of rotations of gear and pinion respectively
Ω_g,Ω_p	Spin speed of gear and pinion respectively
ω	Excitation frequency
ω_n	Gear mesh torsional resonance frequency

ABBREVIATIONS

dof	Degree(s) of freedom
DF	Describing function
DSLR	Dynamic to static load ratio
DYTEM	Dynamic Transmission Error Program-Multi degree of freedom
FFT	Fast Fourier Transformation
LDP	Load Distribution Program
NLGRD	Non-Linear Geared Rotor Dynamics
sdof	Single degree of freedom
OSU	Ohio State University
STEP	Static Transmission Error Program
VB 5.0	Visual Basic, version 5.0

CHAPTER I

INTRODUCTION

1.1 General

Gear noise is a major factor in the design of transmission systems such as automotive, aerospace, industrial, marine and appliance geared systems. While the contribution of the transmission to the total sound level is relatively minor, many consumers associate gear whine with mechanical problems within the transmission.

In extreme situations the vibrations associated with the gear mesh frequency will cause mechanical failure of the gears or the neighboring hardware.

The usual approach followed in reducing gear noise is to reduce the effective transmission error by the use of stringent quality control measures in gear manufacture and perhaps through the use of profile modifications. While these steps are beneficial, they seldom provide dramatic reductions in gear noise and they fail to recognize the contribution of the system dynamics to the problem.

A more thorough design study will include a consideration of the effects of gear train dynamics. In many instances the system dynamics cause the design to be extremely sensitive to manufacturing induced transmission error. In

applications that are sensitive to gear noise it is advantageous to minimize the design sensitivity through the use of dynamic analysis.

Quite gearing can be designed by considering design modifications directed at two different aspects of the system dynamics:

Dynamic Mesh Force Control: Design of the rotating components in order to limit the amount of dynamic mesh force developed at the mesh due to the transmission error. In this approach, basically, the dynamic compliance is included into the system. It is one of the most effective approaches to quite gearing design. The magnitude of the dynamic mesh stiffness plays a major role in determining the sensitivity of a transmission design to gear noise.

Control of the Force Transmissibility: This involves the design of the shafts and their supports to reduce the transmissibility of the force from the mesh location to the housing. What fraction of the dynamic force developed between the mating gear teeth actually is transmitted to the housing is the major consideration.

The problem of geared rotor dynamics is difficult to handle due to the change of the number of meshing gear teeth pair in one tooth contact cycle, which leads to variable mesh stiffness. Therefore even in the absence of geometric and material type of non-linearities the problem is formulated as a parametrically excited system with linear differential equations. Presence of backlash and other type of non-linearities will complicate the problem further. Therefore several assumptions must be made before modeling the system. It is obvious that the type of the model, that should be used for a reliable dynamic analysis, depends on the object of the study as well as the relative dynamic properties of different elements in the system and its configuration. (Özgüven and Houser, 1988b)

Some of the important parameters in gear dynamic models are :

2

- Backlash

- Elements considered in the model that affect the degrees of freedom of the system. They are:

  1. Gear mesh interface

  2. Prime mover and load inertia

  3. Shaft inertia and stiffness

  4. Bearings stiffness

- Gyroscopic effects

- Friction at gear mesh

- Symmetry

  1. Symmetric stator

  2. Symmetric rotor

- Off line of action of the contact

- Excitations

  1. *External excitations*: This group includes excitations due to rotating mass unbalances, geometric eccentricities, and prime mover and/or load torque fluctuations. Such excitations are typically at low frequencies, which are the first few multiples of the input shaft speed. Practical problems include rattle problem in lightly loaded automotive transmissions and machine tools.

3

2. *Internal excitations*: This group includes the high frequency excitations caused by the manufacturing related profile and spacing errors, and time dependent tooth stiffness. Under static conditions, all such mechanisms can be combined with elastic deformation due to all other elastic members (such as shafts and bearings) to yield an overall kinematic error known as the S*tatic Transmission Error*. In gear dynamic problems STE is used as a periodic displacement excitation at the mesh point along line of action.

- Solution techniques:

1. *Digital simulation* : Gives time response history of the system

2. *Modal Analysis* : Gives steady state response of the system

3. *Analytical Methods* : Available only for some systems (Harmonic Balance Method - Method of Multiple Scales) (Kahraman and Singh, 1990; 1991a)

- Assumptions: There may be several assumptions in the model used. A well accepted assumption is to use an average linear time-invariant mesh stiffness with a periodic displacement excitation at the mesh point along the line of action which represents the loaded static transmission error (Özgüven and Houser, 1988b). Thus a system of equations with time varying coefficients reduces to a system of constant coefficient linear differential equations. The steady state response of the resulting system due to the excitation representing STE, which is approximated by FFT, can be found by modal analysis.

4

1.2 Literature Survey

There are many models in literature, which consider different aspects of gear dynamics problem. An extensive review of the literature on dynamic modeling of gears, has been given by Özgüven and Houser (1988a).

The mathematical models developed in gear dynamics can be classified into five main categories:

1.2.1 Simple Dynamic Models

This group includes most of the early studies in which a dynamic factor that can be used in gear root stress formulae is determined. These studies include empirical and semi-empirical approaches as well as recent dynamic models constructed for the determination of a dynamic factor.

Although the history of studies on gear loads dates back almost two centuries, the dynamic factor (which was then called speed factor) was originally suggested in 1868 by Walker (Fisher, 1968). It is defined as :

$$DF = \frac{SL}{DL} \tag{1.1}$$

where DF is the dynamic factor, SL is the static load and DL is the dynamic load. Concept of speed factor was originally introduced on the basis of strength consideration. In the earliest studies, dynamic factors were determined empirically by comparing the gear size and strength calculations with records of tooth failures at different speeds. Carl G. Barth expressed the dynamic factor, based on Walker's original factor as

$$DF = \frac{600}{600 + V} \tag{1.2}$$

5

where V is the pitch line velocity in fpm (feet per minute).

In 1927, Ross found that even the lowest dynamic factor (which gives the highest stress) was too conservative for velocities over 4000 rpm and recommended a modified form:

$$DF = \frac{78}{78 + \sqrt{V}} \qquad (1.3)$$

Both the Barth equation and several modified forms of it are still used in some field of design and are given in design books. The formulae that are widely used in gear standards of American Gear Manufacturing Association are modified versions of these equations. However, these modifications were made after the 1950s.

The results of several works conducted by the ASME Researches Committeon Strength of Gear Teeth were published in 1931 by Buckingham. After the development of the dynamic load equation in this report, which is more popularly known as Buckingham's Equation, little was done until the 1950s.

In 1950 a new era in gear dynamics was initiated which incorporated the use of vibratory models in the gear dynamic analysis of gears. Such mathematical models made it possible to study dynamic properties of the geared systems in addition to the dynamic loads. However the earlier dynamic models were very simple and therefore could provide little additional information beyond the dynamic load for the gear system.

In the first spring-mass model, which was introduced by Tuplin, an equivalent constant mesh stiffness was considered and gear errors were modeled as insertion and withdrawal of wedges with various shapes at the base of the spring.

6

The work of Strauch (1953) seems to be the first study in which periodic excitation was considered. He considered the step changes in the mesh stiffness due to changing from single pair to double tooth contact. He analyzed the forced vibrations that might build up as a result of the continuo's error between two unmodified involute gears.

Zeman (1957) considered the effects of periodic profile errors, assuming a constant mesh stiffness. He analyzed transitory effects of four different forms of gear errors.

1.2.2 Models with Tooth Compliance

In such models tooth stiffness is the only energy storing element in the system. That is, the flexibilities of shafts, bearings, etc. are neglected. In such studies the system is model as single degree of freedom spring-mass system.

The resulting models are either translational or torsional. With torsional models one studies the torsional vibrations of gears in mesh, whereas with translational models the tooth of gear is considered as a cantilever beam and one can study the forced vibrations of teeth. In either of these models, transmission error is simulated by a displacement excitation at the mesh.

Nakada and Utagawa (1956) considered varying elasticities of the mating teeth in their vibratory model. The time variation of stiffness was approximated as a rectangular wave, and closed form solutions of piecewise linear equations were obtained for different damping cases for accurately manufactured gear tooth profile.

Harris's (1958) work was an important contribution. In his single degree of freedom model, Harris considered three internal sources of vibration: manufacturing errors, variation in the tooth stiffness, and non-linearity in tooth

7

due to loss of contact. Harris seems to have been the first to point out to the importance of transmission error.

Gregory et al. (1963) extended the theoretical analysis of Harris. Gregory et al. included sinusoidal type stiffness variation as an approximation. They treated the excitation as periodic, and solved the equations of motion analytically for zero damping and on an analog computer for non-zero damping. He pointed out that non-linear effects are significant when the system is lightly damped.

Nakamura (1967) investigated the separation of tooth meshing with a single degree of freedom model. He accounted for single and double tooth pair contact with a square wave tooth mesh stiffness variation and used a sinusoidal representation of tooth errors.

1.2.3 Models for Gear Dynamics

Such models include the flexibility of the other elements as well as the tooth compliance. Of particular interest have been the torsional flexibility of shafts and lateral flexibility of the bearings and shafts along the line of action.

In some models, the lateral vibrations of gear blank in mutually perpendicular directions are considered. However considering two coupled lateral vibrations of a gear shaft system makes the problem a rotor dynamics problem.

Tordion (1963) presented a torsional model in which the torsional vibrations of two gear shafts were coupled by a constant mesh stiffness. In his model all non-linear effects, including backlash, were neglected and the general receptance technique was used to obtain the system response when there is a periodic transmission error that was then called *error in action.*

8

An important contribution in this area came from Kohler, Pratt and Thomson (1970). They developed a six degrees of freedom dynamic model with four torsional degrees of freedom and one lateral degree of freedom in the direction of tooth force on each shaft. They assumed constant tooth mesh stiffness in their model.

Rettig (1975) modeled a single gear stage with six degrees of freedom, four lateral and two torsional, with all lateral degree of freedom being in the same direction He considered a variable tooth mesh stiffness and presented simplified formulae for the calculation of dynamic factors in three different regions: sub-critical, main resonance and super critical regions.

Toda and Tordion (1979) proposed a four degrees of freedom torsional model for a gear system in which they included the non-linearity of tooth mesh stiffness, damping and tooth separation, and studied the effects of the transmission error excitation on the dynamic response of the system.

An eight degree of freedom model of Küçükay (1984) for single stage spur and helical gears included the axial vibrations of rigid disks that represented gear blanks, as well as torsional, transverse and tipping motion. Periodic tooth mesh stiffness, tooth errors, and external torque were considered in his model, as well as load dependent contact ratio and non-linearities due to the separation teeth. Steady state solutions for dynamic tooth displacements and loads were found by using perturbation methods and the linearized model.

Lin and Huston (1986) used a torsional model to develop a computer program for the design of spur gear systems. Variable tooth mesh stiffness was calculated by taking a tooth as cantilever beam and also considering the flexibilities of the fillet, foundation and the local compliance due to contact forces. Damping due to lubrication of gears and shafts were expressed with constant damping coefficients and the friction between gear teeth was included in the model with a frictional torque. This model was

developed for low-contact ratio gear pairs, and the transverse flexibilities of the shafts and bearings were not considered in the model. A linearized-itrative procedure was used for the numerical solution.

Özgüven and Houser (1988b) studied single degree of freedom torsional model of a gear pair that are coupled by a non-linear mesh stiffness. They used STEP that was developed at OSU to find mesh stiffness and STE. They computed DSLR and concluded that using constant mesh stiffness with a displacement excitation at the mesh point representing the loaded STE is a very good approximate approach for including the time variation of mesh stiffness into the analysis.

Özgüven (1989) developed a six degrees of freedom non-linear semi-definite model with time varying mesh stiffness for the analysis of spur gears. The dynamic response to internal excitation has been calculated by using the static transmission error method. The software prepared (DYTEM) is capable of calculating dynamic tooth forces, dynamic transmission error, dynamic bearing forces and torsion of shafts.

Kahraman and Singh (1990) examined the non-linear frequency response characteristics of a spur gear pair with backlash for both external and internal excitations. Two solution methods, namely the digital simulation technique and the method of harmonic balance, have been used to develop the steady state solutions. They concluded that chaotic and subharmonic resonances may exist in a gear pair depending upon the mean or design load, mean to alternating force ratio, damping and backlash. The mean load determines the conditions for no impacts, single-sided and double-sided impacts.

Kahraman and Singh (1991a) developed a three degrees of freedom model that includes non-linearities associated with radial clearances in the radial rolling element bearings and backlash between a spur gear pair. Linear time-invariant gear mesh stiffness is assumed. Several key issues such as non-linear

10

modal interactions and differences between internal static transmission error excitation and external torque excitations are discussed. Additionally parametric studies are performed to understand the effects of system parameters such as bearing stiffness to gear mesh stiffness ratio, alternating to mean force ratio and radial preload to mean force ratio on the non-linear dynamic behavior.

Kahraman and Sing (1991b) developed a three degrees of freedom model with time varying mesh stiffness and clearance non-linearities associated with gear backlash and rolling element bearings, which is excited by STE under a mean torque load. Model is solved by digital simulation technique. They investigated interactions between the mesh stiffness variation and clearance non-linearities. A strong interaction between time-varying mesh stiffness and gear backlash is found whereas the coupling between time-varying mesh stiffness and bearing non-linearities is weak.

Kahraman (1993) studied planetary gear trains that are also known as epicyclical gears. They have numerous advantages over simple counter-shaft gear drives, including higher torque-to-weight ratio, compactness, decreased radial bearing loads and reduced noise. In his study he proposed a simplified purely torsional model of a single stage planetary gear set. Closed form expressions for torsional natural frequencies are derived in terms of a limited number of system parameters.

Rook and Singh (1993) studied reverse idler gear system to gain a better understanding of the non-linear behavior. Results of the Galerkin method (multi-term harmonic balance) are compared with results of numerical integration techniques.

Lin et al. (1994) conducted a computer simulation to investigate the effects of both linear and parabolic tooth profile modifications on the dynamic response of low-contact-ratio-spur gears. The effects of the total amount of modification and length of the modification zone were studied at

11

various loads and speeds to find the optimal profile modification for minimal dynamic loading.

Litvin et al. (1995) proposed an approach for the design and generation of low-noise helical gears with localized bearing contact. The approach is applied to double circular arc helical gears and modified involute gears. The reduction of noise and vibration is achieved by application of predesigned parabolic function of transmission errors that is able to absorb a discontinuous linear function of transmission errors caused by misalignment. Computerized simulation of meshing and contact of designed gears demonstrated that the proposed approach will produce a pair of gears that has a parabolic transmission error function even when misalignment is present.

Cai (1995) developed a vibration model for helical gears, assuming that there are no spacing error and no shaft run-out, in consideration of non-linear tooth separation phenomenon. In the model, a simple modified stiffness function, including the effect of tooth numbers and addendum modification coefficients, is proposed for a helical involute tooth pair.

Blankenship and Singh (1995) developed a new model that describes mesh force transmissibility in a helical gear pair. New spectral stiffness and transmissibility matrices are developed, based on linear theory, which completely characterize the steady state forced response of a helical gear pair. They concluded that additional degree of freedom must be included in the gear mesh interface model in those geared systems analyses which attempts to predict structure borne noise and casing vibration associated with power transmission systems.

Vinayak et al. (1995) developed a model for multi-mesh transmissions with external, fixed center, helical or spur gears. Each gear is modeled as a rigid body with six degrees of freedom. Excitation to the system is

considered in the form of either external torque pulsation or internal static transmission error. They compared the results with finite element model results.

Yoon and Rao (1996), presented a method to minimize the STE using cubic splines for gear tooth profile. They conducted a parametric study to establish the superiority of cubic spline based gear profile over the involute profile as well as other profiles based on the use of linear and parabolic tip reliefs.

1.2.4 Models for Geared Rotor Dynamics

In some studies, the transverse vibrations of the gear-carrying shafts are considered in two mutually perpendicular directions, thus allowing the shaft to whirl. In such models, the torsional vibration of the system is generally considered.

Pioneer models of this group are those for studying whirling of gear-carrying shafts, rather than the dynamics of the gear itself. Although investigators have studied whirling of disk carrying shafts for many years, it was not until the 1960s that the influence of the constraint imposed by gears on the whirling of geared shafts was considered in rotor dynamics problem.

Mitchell an Mellen (1975) presented experimental data indicating the torsional lateral coupling in a geared high-speed rotor system. They pointed out that mathematical models based on uncoupled lateral-torsional effects fail to provide the necessary information for proper design of high performance machinery.

Daws and Mitchell (1983) analyzed gear coupled rotors by developing a three-dimensional model in which variable mesh stiffness was considered as a time-varying three dimensional tensor.

Iida et al. have published series of papers between 1980 and 1986 on the coupled torsional-transverse vibrations of geared rotors. In their early work, a two shaft-two gear system was analyzed by assuming that one of the shafts was rigid, and the response to gear eccentricities and mass unbalance was determined.

Hagiwara et al. (1981) used a simple model to study the vibration of geared shafts due to unbalanced and run-out errors. The flexibility of shafts was considered using discrete stiffness values. A constant mesh stiffness was assumed, and backlash and tooth separation were not considered in the analysis.

Iwatsubo et al. (1984) studied the rotor dynamics problem of the geared shafts by including a constant mesh stiffness and the forcing due to unbalanced mass but by neglecting the tooth profile error and backlash. The transfer matrix method was employed in the solution and free and forced vibration analyses were made.

1.2.5 Models for Torsional Vibrations

The models in the third and fourth groups consider the flexibility of gear teeth by including constant or variable mesh stiffness in the model. However there is also a group of studies in which the flexibility of gear teeth is neglected and a pure torsional model of geared system is constructed by using torsionally flexible shafts connected by rigid gears.

1.2.6 Studies on Solution Techniques and Backlash

Tomlinson and Lam (1984) analyzed the forced frequency response characteristics of systems that can be considered to exhibit single or normal mode characteristics and which incorporate spatially localized clearance-type non-linearities by using both analytical and digital simulation technique methods.

14

Comparin and Singh (1990) studied the frequency response characteristics of a multi-degree-of-freedom system with clearances. The method of harmonic balance is used to develop approximate analytical solutions for the undamped equations of the motion of a multi degree of freedom system composed of three coupled non-linear oscillators.

Sinha and Wu (1991) suggested a new efficient numerical scheme for the stability analysis of linear systems with periodic parameters. The approach is based on the idea that the state vector and periodic matrix of the system can be expanded in terms of Chebyshev polynomials over the principal period. Such an expansion reduces the original problem to a set of linear algebraic equations from which the solution in the interval of one period can be obtained.

Kujath and Liu (1992) studied a class of dynamic multi degrees of freedom systems with time varying parameters.

Padmanabhan and Singh (1992) dealt specifically with the issue of dynamic interactions between resonances. They used harmonic balance method, digital solutions and analog computer simulations to investigate a two degrees of freedom system under mean load, when subjected to sinusoidal excitations. The existence of harmonic, periodic and chaotic solution is demonstrated using digital simulation.

Blankenship and Singh (1995a) examined a class of viscosity damped mechanical oscillators having spatially periodic stiffness and displacement excitation functions that are exponentially modulated by the instantaneous vibratory displacement of the inertial element.

Blankenship and Singh (1995b) examined mechanical system exhibiting combined parametric excitation and clearance type non-linearity by analytical methods and did experiments to explain complex behavior that is

15

commonly observed in the steady state forced response of rotating machinery. They considered a specific case of a preloaded mechanical oscillator having a periodically time-varying stiffness function and subject to a symmetric backlash. A generalized solution methodology is proposed based on the harmonic balance method.

Padmanabhan and Singh (1995a) applied parametric continuation scheme based on the shooting method to overcome the problem that is associated with harmonic balance method or Galerkin schemes, piecewise linear techniques, analog simulation and/or direct numerical integration technique (digital simulation).

Padmanabhan and Singh (1995b) proposed to utilize the technique of parametric continuation to study the steady state response and global dynamics of two degrees of freedom piecewise non-linear system with backlash or multi-valued springs and impact damping.

In 1996, Kim (1996) developed a modified FPA (Fixed Point Algorithm) to analyze quasi-periodic responses of strongly non-linear dynamical systems with multi inputs.

Perret and Liaudet (1996) proposed an original method to compute the steady state forced response of linear systems with periodically varying parameters under external excitation. The procedure is based on the modal approach with developments in the frequency domain.

Kahraman and Blankenship (1996) investigated the steady state response of a system with clearance subject to parametric and external forcing excitation by analytically considering a mechanical oscillator with time-varying stiffness and a dead zone type clearance non-linearity. A generalized multiple term harmonic balance procedure is used.

Pilipchuk (1996) formulated a special saw-tooth temporal transformation technique that is simple enough to allow analytical computation of strongly non-linear free and forced dynamic responses, but at the same time, it can be applied to the analysis of general classes of non-linear problems.

1.3 Scope of Thesis

In this thesis, firstly some of the basic gear dynamics models and related softwares (Table 1.1) are studied. The most advanced model, Non-linear Geared Rotor Dynamics, is modified further to include the following features.

Pre and post-processor are written for the program. Emphasis is placed on user-friendliness of the program. Therefore a new interface is written in VB 5.0 to NLGRD v1.0 in which the graphical drawing of the rotor gear system is formed while the user adds new elements to the system. Thus any user-error is tried to be minimized. Having completed the analysis, user can see the results graphically without terminating the interface.

The analysis of the program is extended and the software is modified to calculate the reaction forces at bearings and make the modal analysis of the corresponding linear rotor gear system.

The model is verified by carrying out some case studies and by comparing the results with available experiment results and the results of other theoretical models. As an example case, the experimental set up of Kubo is used.

The effects of several parameters such as mean load, module, center distance are studied by varying the parameters of Kubo's system to investigate their effects on the dynamic to static load ratio. Parabolic and linear profile modifications are applied to spur gears, and the effects of these profile

17

modifications are studied. Lastly, tooth separation is studied in depth, and effects of backlash and damping ratio on separation are investigated.

Table 1.1 Selected studies

NAME	MODEL PROPERTIES	INPUTS	OUTPUTS	CASE STUDIES
DYTE H.N. Özgüven D.R. Houser 1988 OSU	• sdof Non-linear model • Variable mesh stiffness and mesh damping • Approximate method - constant mesh stiffness • Backlash • Gear errors, profile modifications • DF = maximum dynamic Root stress / maximum static Root stress • Use STEP* output file • The method can be applied to low/high contact gears • Tooth separation and tooth impact are considered • Digital simulation technique is used to simulate the system	• STEP output file • Mesh stiffness and damping for the approximate case • Gear and pinion inertias • Gear and Pinion pitch diameters • Static load	• Dynamic transmission error • Dynamic to static load ratio (DSLR) • Dynamic factors (DF) in terms of stress	• DSLR is compared with Kubo's for three different set of data • STE and approximate methods are compared • It is concluded that non-linearity of mesh stiffness can be approximately included in the analysis by using a constant mesh stiffness with a displacement excitation at the mesh point which represents the loaded STE.

* STEP stands for Static Transmission Error Program

19

Table 1.1 (continued)

NONLINEAR DYNAMICS OF A SPUR GEAR PAIR
 	
A. Kahraman
R. Singh
1989
OSU
	• 2-dof non-linear semi-definite model
	• Backlash
	• Time invariant mesh stiffness and damping
	• Fundamental excitation frequency of internal displacement and external torque fluctuations are considered.
	• Equation is solved
	  1. Numerically-Digital Simulation (5th-6th order variable step RK numerical integration method (DVERK of IMSL)
	  2. Analytically - HBM
	• Mathematical expressions are developed for
	  1. No impact
	  2. Single-Sided impact
	  3. Double-Sided impact
		• Rotary inertias of the gear and pinion
		• Base diameters of gear and pinion
		• Mesh stiffness and damping
		• Mean load
		• Alternating force
		• Initial conditions
		• Amplitude of internal displacement excitation
			• DSLR
			• Dynamic transmission error
			• Domains of attraction
			• Time history
			• Phase plane plots of steady state solution
				• Solve equations numerically to resolve various modeling issues such as
				  1. Multiple solutions
				  2. Resonances
				  3. Chaos
				• Compare analytical solution and Digital simulation
				• Perform parametric studies in order to understand the effects of
				  1. Mean load
				  2. Alternating force
				  3. Mesh damping ratio
				  4. Ratio of mean load to alternating force

Table 1.1 (continued)

DYTEM
H.N.Ozguven
1990
METU
	• 6-dof non-linear semidefinite model (four rotations and two translations)
	• Employs the digital simulation technique for the solution (5 th order RK with adaptive step size)
	
	• Model includes
	  1. 2 spur gears
	  2. 2 Shafts
	  3. 2 Inertias (load & prime mover)
	• Considered factors
	  1. Time varying mash stiffness
	  2. Damping (linear viscous)
	  3. Separation of teeth
	  4. Backlash
	  5. Single & double-sided impacts
	  6. Various gear errors & profile modifications
	• Use STEP output file
	• Transverse vibrations are considered along the line of action
	• Digital simulation technique
		• STEP output file
		• Backlash
		• Torsional compliance and damping (linear viscous) of shafts
		• Transverse compliance and damping of bearings
		• Inertias of load and prime mover
			• Dynamic tooth and mesh forces
			• Dynamic factors for pinion and gear (root stress)
			• Dynamic transmission error
			• Dynamic bearing forces
			• Torsion of shafts
				• Effect of lateral-torsional vibration coupling on dynamic tooth forces and dynamic transmission error
				• DYTE and DYTEM are compared for Kubo's test experiment values.
				• Effects of bearing and shaft properties on gear dynamics are studied.(Kubo's parameters)
				• Approximate method (constant mesh stiffness) is also studied

21

Table 1.1 (continued)

NONLINEAR DYNAMICS OF A GEARED ROTOR-BEARING SYSTEMS WITH MULTIPLE CLEARANCES
 	
A. Kahraman
R. Singh
1990
OSU
	• 3-dof Non-linear model
	• Gear mesh is described by a displacement function and viscous damping. Time invariant.
	• Friction forces are assumed to be negligible
	• Shafts and bearings are modeled by non-linear springs defined by force-displacement functions
	• System is assumed to be symmetric about the plane of gears
	• Both fundamental frequency of low-frequency excitation due to torque fluctuations and high frequency excitation due to the static transmission error are considered
	• Linear model corresponding to 3-dof model is constructed and solved numerically
	• 2-dof model is constructed and solved analytically by Harmonic Balance Method.
	• The effects of prime mover and load inertias are not considered
		• Gear masses and inertias
		• Base circle diameters
		• Mean gear mesh force
		• Radial preload on bearings
		• Alternating gear mesh force
		• Amplitude of static transmission error
		Gear mesh and bearing stiffness and backlash
			• Dynamic transmission error
			• Phase plane plots
				• Interactions between gear mesh non-linearity and bearing non-linearity is studied
				• Internal and external excitations are compared.
				• Parametric studies
				  1. Non linear gear mesh, linear bearings
				  2. No gear backlash non-linear bearings

22

Table 1.1 (continued)

| INTERACTIONS BETWEEN TIME-VARYING MESH STIFFNESS AND CLEARANCE NONLINEARITES IN A GEARED SYSTEM

A. Kahraman
R. Singh
1990
OSU | • Non-linear model
• sdof with time varying mesh stiffness
• 3-dof model
• Damping matrix is assumed to be constant
• Mass matrix is time invariant
• The gear mesh is described by a non-linear displacement function with time-varying stiffness and linear viscous damping
• This paper extends the sdof and mdof model by introducing time-varying mesh stiffness
• The STE and mesh stiffness is predicted by an elastic spur gear model
• Digital simulation technique is used | • Gear inertias
• Gear masses
• Base circle diameters
• Mean gear mesh force
• Alternating gear mesh force
• External radial preloads on bearings | • DSLR
• Dynamic transmission error | • Linear time-varying system is solved analytically by Method of scales
• Non-linear time-varying system is studied
• Non-linear time varying mesh damping proportional to mesh stiffness case is considered |

23

Table 1.1 (continued)

HGRD				

Mete Kesan H. N Ozguven 1992 METU	• Finite Element Model
	• Linear model
	• Calculates only steady state response
	• Improved model of GRD
	• Helical and spur gears
	• Constant mesh stiffness
	• damping values
	• Effect of variable mesh stiffness is included in the form of STE
	• Higher harmonics are considered in FFT transform
	• Use LDP output file
	• Considers tooth errors and mounting errors
	• Flexible rotors on flexible bearings
	• Axial dof is included in the finite element model of bearings for helical gears
	• Eigenvalue problem is solved by Sequential Threshold Jacobi method
		• Axial load on rotor
		• Material and geometric properties of disks, bearings, rotors (damping is included)
		• Gear mesh stiffness & damping
		• Number of natural frequencies wanted
		• Forced response (Y/N)
		• Geometric eccentricities of gears
		• Mass unbalance of gears
		• Average force transmitted
			• Free vibration analysis
			• Forced response
			  1. Critical speeds
			  2. The whirling orbit at a specified node
			  3. Deflections at a specified node point
			  4. Acceleration at a specified node
			  5. DSLR at the mesh
				• Compared with DYTE for DSLR
				• Effect of higher harmonics is studied
				• Natural frequencies are compared with Kubo's
				• Effect of some system parameters on dynamics of helical gears are studied
				  1. Transverse bearing stiffness
				  2. Axial bearing stiffness
				  3. Torsional shaft compliance
				  4. Helix angle
				  5. Face width
				• Variation of STE with face width

Table 1.1 (continued)

NLGRD version 1.0 R. Maliha H. N. Özgüven 1994 METU			

• Finite Element Model
• Non-linear model
• Backlash is included in gear mesh interface
• Calculates only steady state response
• Be able analyze only spur gears
• Constant mesh stiffness and damping values are used.
• Effect of variable mesh stiffness is included in the form of STE. STE can be either approximated as a rectangular wave or can be read from LDP output file.
• Higher harmonics are considered in FFT
• Flexible rotors on flexible bearings.
• Considers tooth errors and mounting errors
	• Axial load on rotor
	• Material and geometric properties of disks, bearings, rotors (damping is included)
	• Gear mesh stiffness and damping
	• LDP/RECTANGULAR wave approximation
	• Relaxation factors
	• Eccentricity
		• Forced response
		• DSLR
		• Dynamic transmission error
			• NLGRD is compared with linear models GRD and HGRD
			• NLGRD is compared with DYTE
			• Multi-solution is obtained at ½ design load
			• Compared with Kubo's and Munro's experiment
			• Parametric study
			  1. Rectangular wave approximation and DFT technique is compared
			  2. Effect of bearing properties.
			  3. Effect of backlash non-linearity Effect of amplitude of STE
			  4. Interaction of backlash and bearing stiffness
			  5. Interactions of backlash and STE

25

CHAPTER II

DYNAMIC MODEL OF GEAR MESH INTERFACE

2.1 Introduction

The study of gear dynamics is essential to the design of quite and reliable power transmission products exhibiting high torque-to-weight ratios and acceptable levels of gear noise. Critical to every gear dynamic analysis is the expression used to quantify the vibratory source strength and force coupling associated with the gear mesh interface. Virtually all gear dynamic models consider a scalar expression for the force generated within the gear mesh and consider mostly kinematic transmission error and variation in the mesh stiffness as the primary sources of noise and vibration.

In this chapter, a recently developed dynamic model for a gear mesh (Kahraman and Singh, 1991), which is also used in this study, is explained. Gear bodies are assumed to be rigid except for the elastic compliance of meshing gear teeth as it is the case in most recent models.

2.2 Problem Formulation

2.2.1 Coordinate Systems and Vector Notation

The cylindrical element shown in Figure 2.1 represents a typical gear body. Two Cartesians coordinate systems are shown. The non-rotating

26
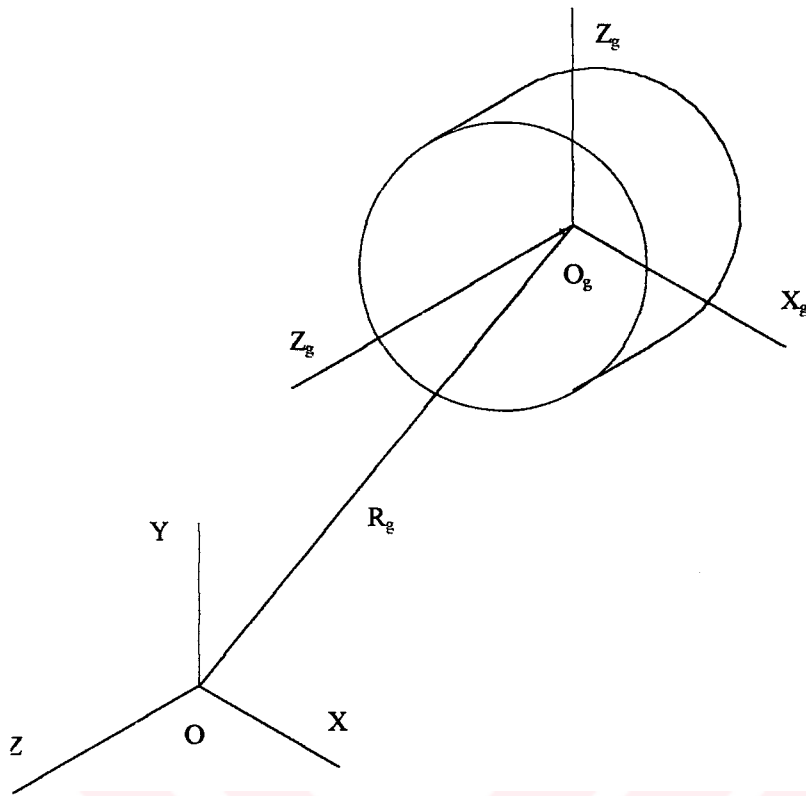
Figure 2.1 : Coordinate system

geometric reference frame (X_g, Y_g, Z_g) is used to describe the position and orientation of gear body with the intended rotational motion $\theta_g(t)$ occurring about the Z_g axis. The mean location and orientation of the geometric frame with respect to the inertial frame (X,Y,Z) are described by time-invariant global position vector $\bar{R}_g$ and angular misalignment vector $\bar{\Theta}_g$ that respectively represent the translation of the origin O_g and the rotational orientation of the (X_g, Y_g, Z_g) frame with respect to the inertial frame.

$$R_g(t) = \bar{R}_g + R_{gm}(t) \tag{2.1}$$

$$\Theta_g(t) = \bar{\Theta}_g + \Theta_{gm}(t) \tag{2.2}$$

27

where $R_{gm}(t)$ and $\Theta_{gm}(t)$ are time varying components of the respective vectors from their mean location.

Thus the displacement vector of the gear body is denoted by

$$q_g(t) = \left\{ R_g^T(t) \quad \Theta_g^T(t) \right\}^T \tag{2.3}$$

Furthermore the coordinate vector can be written as the sum of a time-invariant vector which describes the mean position of the gear and a time-varying vibratory coordinate vector which describes the deviation of gear body from its ideal position defined by

$$q_g(t) = \bar{q}_g + q_{gm}(t) \tag{2.4}$$

$$\bar{q}_g = \left\{ \bar{R}_g^T \quad \bar{\Theta}_g^T \right\}^T \tag{2.5}$$

$$q_{gm}(t) = \left\{ R_{gm}^T(t) \quad \Theta_{gm}^T(t) \right\}^T \tag{2.6}$$

2.2.2 Dynamic Mesh Force Concept

The translational forces acting on gear as a result of its meshing with pinion are denoted by mesh force vector $F^{gp}(t)$ having three components. Any moments acting on the gear are denoted by mesh moment vector $T^{gp}(t)$.

The generalized force vector is

$$Q^{gp}(t) = \left\{ F^{gp^T}(t) \quad T^{gp^T}(t) \right\}^T \tag{2.7}$$

The transmitted gear mesh force is decomposed into static component due to the mean transmitted load and a vibratory component which arises due to the meshing action.

28

$$Q^{gp}(t) = \bar{Q}^{gp} + Q_m{}^{gp}(t) \tag{2.8}$$

Further $Q_m^{gp}(t)$ is written as the sum of conservative or elastic forces and dissipative forces.

$$Q_m{}^{gp}(t) = Q_{me}^{gp}(t) + Q_{md}^{gp}(t) \tag{2.9}$$

Vibratory elastic deformations of mating gear teeth give rise to $Q_{me}^{gp}(t)$. A Hookean expression for $Q_{me}^{gp}(t)$ is assumed in the form

$$Q_{me}^{gp}(t) = -K^{gp}(t)\left[\delta_m^{gp}(t)\right]^n \tag{2.10}$$

where $K^{gp}(t)$ is a mesh stiffness matrix $\delta_m^{gp}(t)$ is a vector of equivalent displacements and n is an exponent. In this study n is taken as 1.

The vibratory displacement vector $\delta_m^{gp}(t)$ is separated into two distinct components; $\delta_q^{gp}(t)$ due to gear body displacement $q^g(t)$ and $q^p(t)$, and $\delta_e^{gp}(t)$ due to deviations of gear tooth profiles from perfect conjugate form over some finite regions of contact; such tooth errors or deviations may be described by a generic error function say $e^{gp}(t)$

$$\delta_m^{gp}(t) = \delta_q^{gp}(t) - \delta_e^{gp}(t) \tag{2.11}$$

Then the expression for Q_{me}^{gp} becomes

$$Q_{me}^{gp}(t) = -K^{gp}(t)\delta_q^{gp}(t) + K^{gp}(t)\delta_e^{gp}(t) \tag{2.12}$$

The term $-K^{gp}(t)\delta_q^{gp}(t)$ may be viewed as a source of parametric excitation and force coupling in the dynamic equation of motion and $K^{gp}(t)\delta_e^{gp}(t)$ as an external forcing excitation. In general

$$K^{gp}(t) = K^{gp}(t)\left[Q^{gp}(t) \quad q^g(t) \quad q^p(t) \quad e^{gp}(t)\right] \tag{2.13}$$

29

$$e^{gp}(t) = e^{gp}(t)\left[Q^{gp}(t) \quad q^{g}(t) \quad q^{p}(t) \quad e^{gp}(t)\right] \tag{2.14}$$

Hence explicit computation of $K^{gp}(t)$ and $e^{gp}(t)$ independent of a complete dynamic analysis is impossible.

2.2.3 Motion Analysis

Displacement vector $q_m^i(t) = q_m^i(t;\theta^*) = q_{mo}^i(\theta^*) + q_{mg}^i(t)$ may be further expanded in terms of spatially varying nominal component $q_{mo}^i(\theta^*)$ and a time-varying dynamic component $q_{mg}^i(t)$. The motion described by $q_{mo}^i(\theta^*)$ includes system misalignment effects and deflections due to static loading or mean transmitted torque as the system is rotated by angle θ^*. Under quasi-static condition as Ω^* approaches zero

$$\lim_{\Omega^* \to 0} q_m^i(t) = q_{mo}^i(\theta_o^*) \tag{2.15}$$

where

$$\lim_{\Omega^* \to 0} \theta^* = \theta_o^* \tag{2.16}$$

Hence, $q_{mo}^i(\theta^*)$ may be determined from a quasi-static or low frequency analysis, or even measured experimentally under quasi-static loaded conditions. Under operating conditions when $\Omega^* > 0, q_{mo}^i(\theta^*)$ and other spatially varying parameters, such as the gear mesh stiffness and kinematic transmission error, give rise to dynamic forces and moments which result in dynamic displacement $q_{mg}^i(t)$ about the instantaneous nominal position $q_{mo}^i(t)$

2.3 Backlash Non-linearity

Many mechanical system exhibit non-linearities that are often non-analytical and non-differentiable. One typical example is the clearance non-

30

linearity that can be used to describe backlash in a gear pair, preset or preload in springs and a bilinear dry friction clutch.

Clearances exist in many complex mechanical systems either by design, due to manufacturing errors and wear, or as a result of mechanical failures. Vibration of a translational or rotational system with clearances can result in relative motion across the clearance space and impacting between the components. Repeated impacts, may lead to excessive noise, large dynamic loads, and large changes in the dynamic stiffness.

Previous studies have shown that the dynamic behavior of a system with discontinuous non-linearities is quite different from a system with continuous non-linearities.

The gear backlash non-linearity is essentially a discontinuous and non differentiable function and it represents a strong non-linear interaction in the governing differential equation. In this study, the gear mesh of a spur gear pair is represented by a non-linear spring and a linear damper. The non-linear spring can be modeled by a dead space function with backlash of 2b, and a time-invariant mesh stiffness k_h when in contact. For a relative displacement p, the non-linear displacement function for gear mesh stiffness $f_h(p)$ is defined as

$$f_h(p) = \begin{cases} 0 & \text{for} & |p| < b \\ k_h p & \text{for} & |p| \geq b \end{cases} \qquad (2.17)$$

The graphical illustration of this formula is shown in Figure 2.2.

As shown in Figure 2.3 there are three possible cases :

- **No impact** : The tooth separation is not observed in a geared system if the displacement q(t) lies in the region q(t)>1 all the time where $q(t) = \dfrac{p}{b}$

$$|q_m + q_a| > 1 \quad \text{and} \quad |q_m - q_a| > 1 \qquad (2.18)$$

31

where q_m and q_a are the mean and alternating part of the relative displacement which is normalized with respect to backlash.
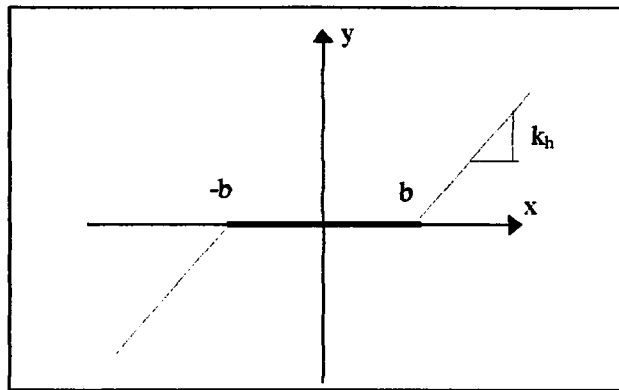

Figure 2.2 : Backlash non-linearity

- **Single-sided impact** : Mathematically, the single-sided impacts (tooth separation without back collision) are observed if

$$q_m + q_a > 1 \quad \text{and} \quad \left| q_m - q_a \right| < 1 \qquad (2.19)$$

- **Double-sided impact** : Double-sided impact exists if q_m and q_a are such that the following conditions are satisfied

$$q_a > \left| 1 - q_m \right| \quad \text{and} \quad q_a > \left| 1 + q_m \right| \qquad (2.20)$$

The non-linearity can be regarded as an amplitude dependent stiffness. The non-linearity is hardening if the stiffness is increasing with alternating displacement, and softening if it is decreasing with alternating displacement. The hardening or softening nature of the clearance nonlinearity depends on the mean deflection and on whether the system is undergoing double or single-sided vibro-impacts (the system is linear for the no-impact case). For the case of single-sided impacts, if the mean deflection is in non zero stiffness stage; as alternating displacement increases the time spent in the
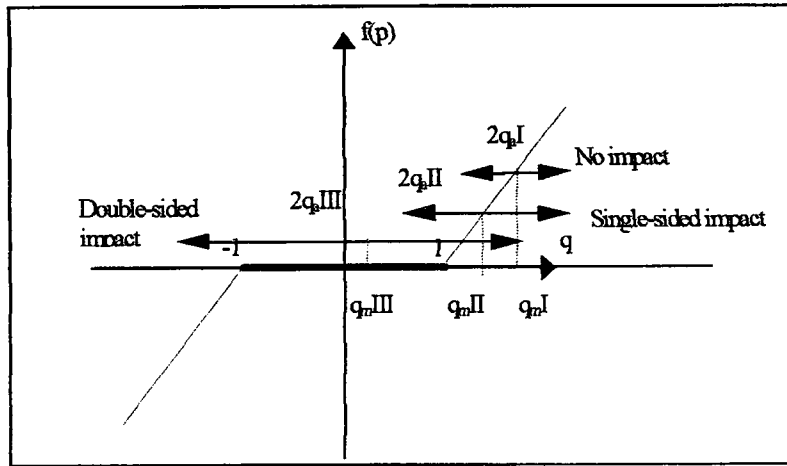
32

Figure 2.3 : No impact, single-sided and double-sided regions

backlash region increases, thereby reducing the average stiffness (softening effects). If however, the mean deflection is within the backlash region, the average stiffness increases, as alternating displacement increases, for both double and single-sided vibro-impacts, leading to hardening effect (Padmanabhan and Singh, 1992).

2.4 Mesh Compliance and LDP

There are several formulas to compute mesh compliance and STE in the literature. K.Y. Yoon and et. al. (1996) reported one of them in a recent article. The drawing of the tooth model is given in Figure 2.4

The compliance of the tooth is computed at all points of contacts during a mesh cycle in the undeformed configuration. The following assumptions are made for this purpose:

1. The tooth deflects as a cantilever beam due to bending and shear loads

2. The tooth base is assumed to be rigid

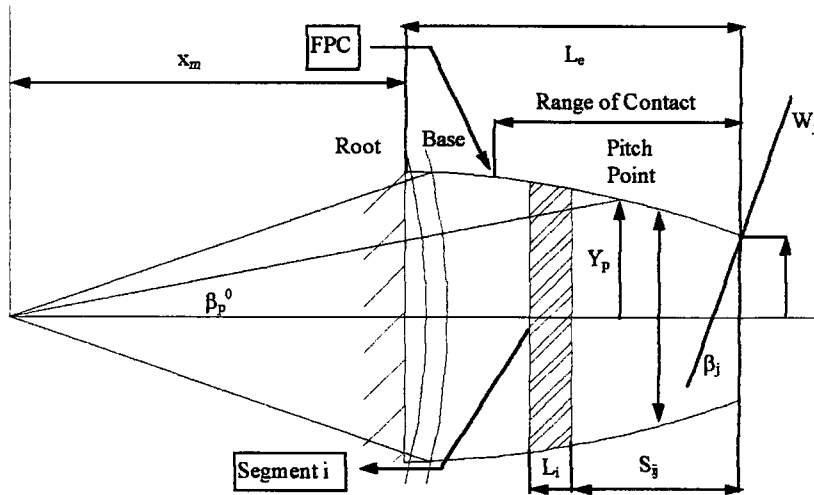3. The deflection due to contact forces are assumed to be Hertzian

33

Figure 2.4 : Tooth model

For the purpose of computation, the range of contact is divided into a series of transverse segments of rectangular cross-section as indicated in figure. A typical segment is indicated by the index i. The total deflection of the point of load application can be found by summing the contributions of individual segments where each segment is considered to be a cantilever beam by itself. The deflections due to the transverse force D_{t_i} and bending moment D_{m_i} induced on segment i by the applied load W_j can be expressed as (Cornell,1981)

$$D_{t_i} = \frac{W_j \cos(\beta_j)}{6EI_i}\left(2L_i^3 + 3L_i^2 S_{ij}\right) \tag{2.21}$$

$$D_{m_i} = \frac{W_j\left(S_{ij} \cos(\beta_j) - y_j \sin(\beta_j)\right)}{2EI_i}\left(L_i^2 + 2L_i S_{ij}\right) \tag{2.22}$$

where

E=Young's modulus of elasticity

34

I_i =second moment of inertia of the segment

W_j =normal load at the point of contact

S_{ij} =moment arm of load W_j for the segment

L_i =thickness of the tooth segment

β_j =pressure angle at the point of contact

and the subscript j denotes the current point of contact.

The shear deformation of the tooth due to segment i can be written as (Cornell,1981)

$$D_{s_i} = \frac{1.2 W_j L_i \cos(\beta j)}{GA_i} \tag{2.23}$$

where G is the shear modulus of elasticity. Thus the total deflection of the tooth at the point of load application along the direction of applied load (normal to the profile), D_{b_i} can be expressed as :

$$D_{b_j} = \sum_{i=1}^{n}\left(D_{t_i} + D_{m_i} + D_{s_i}\right) \tag{2.24}$$

The total compliance coefficient due to tooth bending as cantilever beam for the jth contact, Q_{b_j}, can be defined as

$$Q_{b_j} = \frac{D_{b_j}}{W_j} \tag{2.25}$$

Although the root of the tooth (cantilever beam) was assumed to be fixed (rigid) in deriving the equations, the base of the tooth will have some flexibility due to the elasticity of the tooth support material and the fillet geometry. In addition the load at the contact point W_i was considered to be a

statically applied load in deriving equations. In reality, the problem has to be treated as a Hertzian contact stress problem. Hence a more accurate estimate of the total tooth compliance at point j can be obtained by adding to Q_{b_j}, the compliances due to the base and the Hertzian stress;

$$Q_j = Q_{b_j} + Q_{t_j} + Q_h \qquad (2.26)$$

where the base compliance Q_{t_j} and the Hertzian compliance Q_h are given in Cornell(1981). The total static transmission error at point j , T.E.$_j$ is generally is defined to be the sum of the contributions due to the applied load and the profile modification used for the tooth:

$$T.E._j = T.E._{w_j} + T.E._{p_j} \qquad (2.27)$$

where T.E.$_{w_j}$ and T.E.$_{p_j}$ denote the transmission error due to applied load and profile modifications, respectively. The static transmission error and the shared tooth load for a low -contact-ratio (less than 2) gear pair can be found from the following equations (Cornell 1981).

$$Q_j^a W_j^a + (E_t)_j^a = (E_m)_j^a \qquad (2.28)$$

$$Q_j^b W_j^b + (E_t)_j^b = (E_m)_j^b + (E_t)_j^{ab} \qquad (2.29)$$

$$W_j^a + W_j^b = W_N \qquad (2.30)$$

$$(E_t)_j^a = (E_t)_j^b \qquad (2.31)$$

where E_t, E_m, E_s represent the static transmission error, the profile modification error and the tooth spacing error, respectively. The subscript j represents the contact point on the tooth profile, and the subscript a and b represents the leading and the lagging tooth pairs (Yoon et al., 1996).

36

NLGRD uses LDP (Load Distribution Program) which was developed at Ohio State University, to find mesh compliance and STE in loaded helical and spur gears

2.4.1 How LDP Works

The Load Distribution Program (LDP) is a computer program for predicting the load distribution across the zone of contact for a single pair of spur or helical gears. The gears may have an internal or an external mesh and be mounted on shafts between centers or overhung. The model assumes the load distribution to be a function of the elasticity of gear system and errors or modifications on the gear teeth. Below is a list of effects that the program considers in its calculations.

Elasticity(Elastic Deformations)
- Bending deflection of gear bodies and supporting shafts
- Flexibility of bearings and housings
- Torsional deflection of gear bodies
- Bending of teeth in contact
- Local contact deflections

Errors and Modifications (Initial Separation)
- Shaft misalignment
- Involute error
- Lead error
- Tooth spacing error

2.4.2 Elastic Deformation Calculations

The following assumptions are made in calculating the elastic deflections in LDP:

1. The total elastic deformation is the sum of the individual elastic deformations

37

2. The elastic deformations are small, thus tooth contact is assumed to be on the line of contact

3. The gear bodies and supporting shafts behave as solid cylinders for the purpose of determining the bending and torsional deformations

2.5 Static Transmission Error

The periodic displacement excitation acts along the line of action and taken as the loaded static transmission error. The period of the displacement excitation is given by $\Omega_h = N_p \Omega_p$ where N_p is the number of teeth on pinion and Ω_p is the rotational speed of pinion. A typical loaded transmission error is shown Figure 2.5.

Although the transmission error is periodic it is not harmonic, which is not suitable for modal analysis. However, periodic functions can be defined in terms of harmonic sine waves, by using Fourier series.

Now consider a function $f(t)$ which has a period T, then the fundamental frequency is $\omega = 2\pi/T$. Such a function may be represented by Fourier series of the form :

$$f(t) = \sum_{m=0}^{\infty} (a_m \cos(m\omega t) + b_m \sin(m\omega t)) \qquad (2.32)$$

In this study, STE is approximated by the highest n harmonics. A typical STE which is approximated by Fourier harmonics, is shown in Figure 2.6. These harmonics can be found by two methods :

Rectangular wave approximation : The periodic STE is taken as a rectangular wave with an amplitude of the periodic transmission error (Maliha, 1994). The coefficients a_m and b_m of such a rectangular wave can be calculate analytically as :
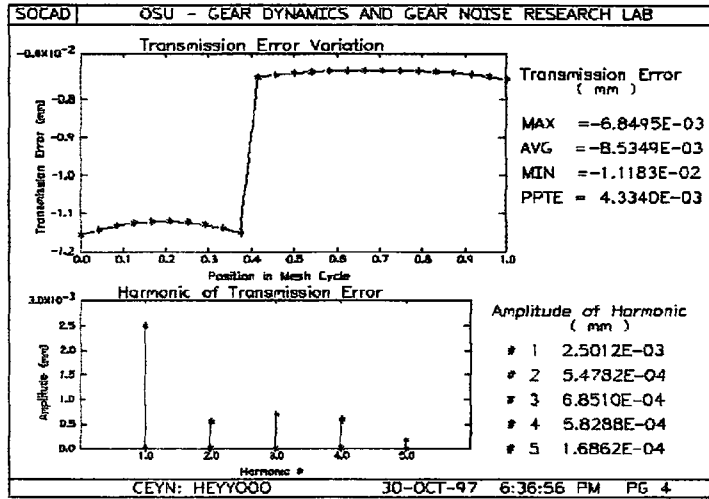
38

Figure 2.5 : Static transmission error graph

$$a_m = \frac{-e_t}{m\pi}\left\{\left[3 - \cos(m\omega y)\right]\sin(m\omega \frac{x}{2}) - \sin(m\omega y)\cos(m\omega \frac{x}{2})\right\} \qquad (2.33)$$

$$b_m = \frac{-e_t}{m\pi}\left\{\left[\cos(m\pi y) - 1\right]\cos(m\pi \frac{x}{2}) - \sin(m\pi y)\sin(m\pi \frac{x}{2})\right\} \qquad (2.34)$$

where x+y/y is the gear contact ratio, e_t is the amplitude of the STE function. Then the highest n coefficients are taken to represent the STE function.

2. **DFT (Discrete Fourier Transform Method)** : The expression for Fourier coefficients in DFT is given as

$$(a_m + jb_m) = \frac{1}{N}\sum_{r=0}^{N-1}x_r e^{\frac{-j(2\pi mr)}{N}} \qquad (2.35)$$

where (N+1) and x_r are the number and the amplitude of discrete data points, respectively. It should be noted that the maximum calculated (m) should be less than N/2 to prevent aliasing.
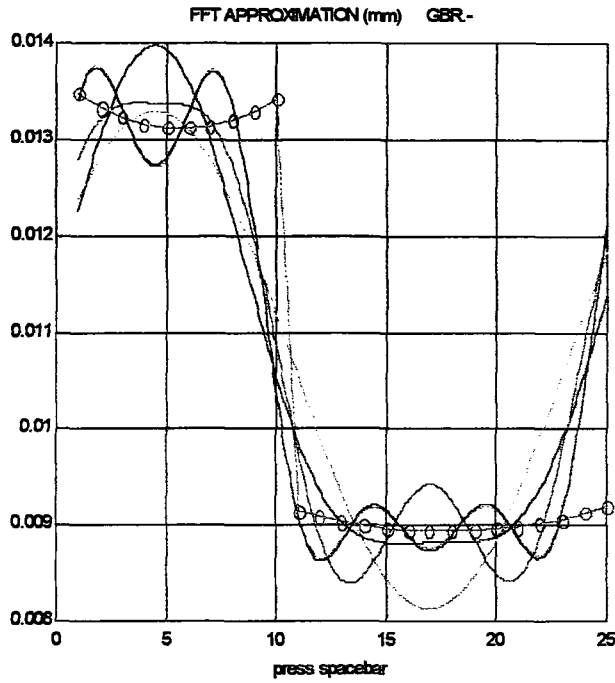
39

Figure 2.6 : FFT approximation of STE

2.6 Formulation of Spur Gear Mesh

A typical spur gear mesh that is shown in Figure 2.7 is represented by a pair of rigid disks which are coupled by a non-linear displacement function f_h and a viscous damping coefficient C_m along the pressure line which is tangent to the base circles of the gears. Friction forces at the mesh point can be assumed to be negligible. Thus the transverse vibrations along the pressure line are uncoupled from the vibration in the direction perpendicular to the pressure line. The damping coefficient can be assumed to be time-invariant. The effect of tooth separation is considered but no tooth impact is assumed. (Maliha, 1994; Kahraman et al. 1991).

The relative displacement p along the pressure line can be defined as

$$p = y_p + r_p\theta_p + \varepsilon_p\sin\theta_p - y_g - r_g\theta_g - \varepsilon_g\sin\theta_g - e_t(t) \qquad (2.36)$$
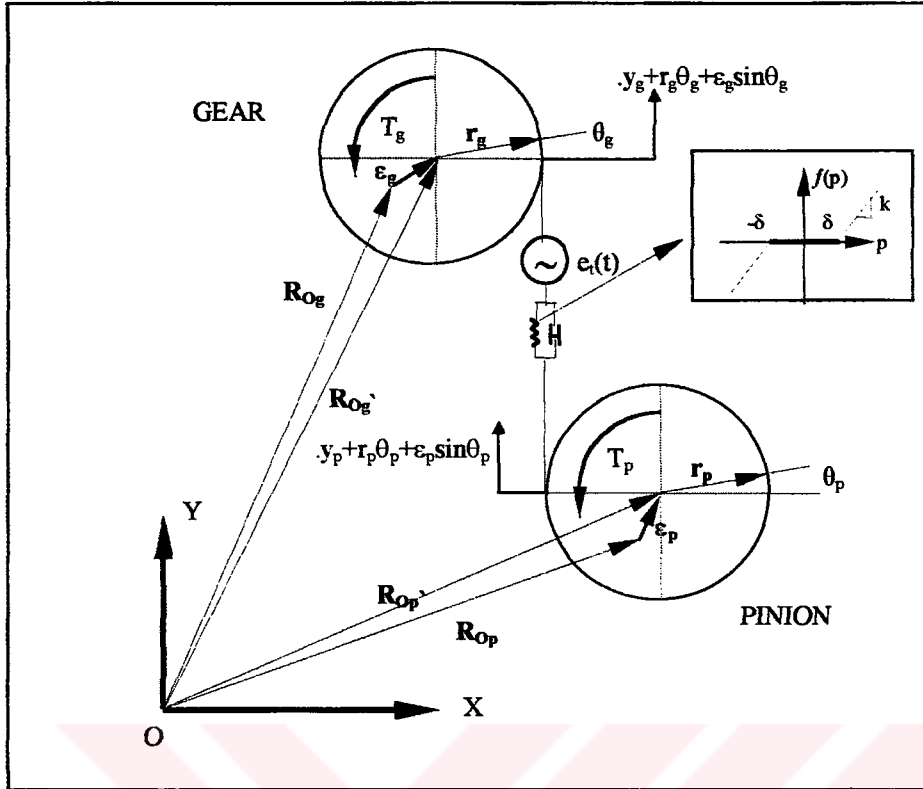
40

Figure 2.7: Dynamic mesh interface model

where θ_p and θ_g are the total angular rotations, r_p and r_g are the base circle radii and ε_p and ε_g are the geometric eccentricities of driving and driven gears, respectively. $e_t(t)$ is the static transmission error which is approximated by

$$e_t(t) = \sum_{m=1}^{n} a_m \cos(mN_p\Omega_p t) + jb_m \sin(mN_p\Omega_p t) \tag{2.37}$$

Dynamic transmission error DTE is defined as :

$$DTE = y_p + r_p\theta_p - y_g - r_g\theta_g \tag{2.38}$$

Total angular positions θ_p and θ_g are given by

$$\theta_p = \Omega_p t + \theta_{pa}(t) \tag{2.39}$$

41

$$\theta_g = \Omega_g t + \theta_{ga}(t) \qquad (2.40)$$

Substituting Equation 2.39 and Equation 2.40 into Equation 2.36 and noting that

$$\theta_p >> \theta_{pa} \qquad (2.41)$$

$$\theta_g >> \theta_{ga} \qquad (2.42)$$

$$r >> \varepsilon \qquad (2.43)$$

the relative displacement p and velocity $\overset{*}{p}$ reduce to

$$p = y_p + r_p \theta_p + \varepsilon_p \sin(\Omega_p t) - y_g - r_g \theta_g - \varepsilon_g \sin(\Omega_g t) - e_t(t) \qquad (2.44)$$

$$\overset{*}{p} = \overset{*}{y}_p + r_p \overset{*}{\theta}_p + \varepsilon_p \Omega_p \cos(\Omega_p t) - \overset{*}{y}_g - r_g \overset{*}{\theta}_g - \varepsilon_g \Omega_g \cos(\Omega_g t) - \overset{*}{e}_t(t) \qquad (2.45)$$

The mesh forces in the y direction along the pressure line can be written as :

$$W_1 = C_m \overset{*}{p} + k_h(p) f_p(p) \qquad (2.46)$$

$$W_2 = -W_1 \qquad (2.47)$$

where W_1 and W_2 are the mesh forces at the driving and driven gear locations, respectively, and $f_h(p)$ is the gear backlash non-linear force-displacement function. k_h is the mesh stiffness and C_m is the viscous mesh damping which can be expressed in terms of equivalent mass m_{cl} and viscous damping coefficient C_m as:

$$C_m = 2m_{cl}\omega_n\zeta \qquad (2.48)$$
$$\qquad (2.45)$$

where

$$\omega_n = \sqrt{k_h/m_{cl}} \qquad (2.49)$$

42

Equations of motions of the meshing gears, on the other hand, can be written as :

$$I_p \, \ddot{\theta}_p + W_1 \left[r_p + \varepsilon_p \cos(\Omega_p t) \right] = T_p \qquad (2.50)$$

$$I_g \, \ddot{\theta}_g - W_1 \left[r_g + \varepsilon_g \cos(\Omega_g t) \right] = -T_g \qquad (2.51)$$

The eccentricity term is included in the relative displacement formulae however it can safely be omitted with respect to gear radius term for the sake of simplicity, which implies that change in the moment arm is neglected. This leads to *time-invariant equivalent mesh inertia*. Thus, the spur gear mesh interface is modeled by a linear time invariant system.

A term in the force equation is neglected which means that a second-order coupling term is ignored whereas it is kept in the displacement equation. This idea is basically identical to the very basic assumption used by several investigators : *using a constant mesh stiffness while representing the change in the gear mesh stiffness as a periodic displacement excitation at the mesh point along the line of action.*

$$I_p \, \ddot{\theta}_p + W_1 r_p = T_p \qquad (2.52)$$

$$I_g \, \ddot{\theta}_g + W_1 r_g = -T_g \qquad (2.53)$$

The equations can be combined to give the following equation

$$m_{cl} (r_p \, \ddot{\theta}_p - r_g \, \ddot{\theta}_g) + W_1 = W \qquad (2.54)$$

where equivalent mass m_{cl} and the load W are

$$m_{cl} = \frac{I_p I_g}{r_p^2 I_g + r_g^2 I_g} \qquad (2.55)$$

$$W = m_{cl} (T_p + T_g) \qquad (2.56)$$

43

In Equation 2.54, substituting for $(r_p \ddot{\theta}_p - r_g \ddot{\theta}_g)$ gives

$$m_{cl}\left[\ddot{p} - \ddot{y}_p + \ddot{y}_g + \varepsilon_p \Omega_p^{\ 2} \sin(\Omega_p t) - \varepsilon_g \Omega_g^{\ 2} \sin(\Omega_g t) + \ddot{e}_t(t)\right] + W_1 = W \quad (2.57)$$

Substituting W_1 in Equation 2.56 and rearranging in matrix form

$$\begin{bmatrix} m_{cl} & m_{cl} & m_{cl} \\ 0 & m_p & 0 \\ 0 & 0 & m_g \end{bmatrix} \begin{bmatrix} \ddot{p} \\ \ddot{y}_p \\ \ddot{y}_g \end{bmatrix} + \begin{bmatrix} C_m & 0 & 0 \\ C_m & 0 & 0 \\ C_m & 0 & 0 \end{bmatrix} \begin{bmatrix} \dot{p} \\ \dot{y}_p \\ \dot{y}_g \end{bmatrix} + \begin{bmatrix} k_h f(p) \\ k_h f(p) \\ k_h f(p) \end{bmatrix} = \begin{bmatrix} f_h \\ 0 \\ 0 \end{bmatrix} \quad (2.58)$$

where the total excitation force is given by

$$f_h = W + m_{cl}\left[-\ddot{e}_t - \varepsilon_p \Omega_p^{\ 2} \sin(\Omega_p t) + \varepsilon_g \Omega_g^{\ 2} \sin(\Omega_g t)\right] \quad (2.59)$$

As a final step, after the mass, stiffness and damping matrices are formed for each shaft by assembling the elementary matrices, the gear mesh interface is inserted in to the equations to couple the uncoupled equations of separate shafts.

CHAPTER III

SOLUTION TECHNIQUE

3.1 Forced Periodic Response

The equation of motion of an axisymmetric non-linear geared rotor in which the non-linearities are involved only in elastic part of the system and damping is assumed to be linear, can be written by adding a term $\{N\}$, expressing the non-linear behavior of the system, to the linear differential equations of motion. (Genta and Bona, 1990)

$$[M]\{\ddot{x}\} + [C]\{\dot{x}\} + [K]\{x\} + \{N\} = \{F_n\} + \{F\} \qquad (3.1)$$

It is well known that it is not possible to separate the study of the free behavior of the system from that of the response to forced vibration such as unbalance or the deformation under static loads. An approximate solution of Equation 3.1 can be of the type

$$\{x\} = \{X_n\} + \{X_0\}e^{i\omega t} + \sum_{k=1}^{n} \{X_k\}e^{i\lambda_k t} \qquad (3.2)$$

This is an approximate solution, since it takes into account only the fundamental harmonics of the response which is certainly non harmonic.

Static forces will also be neglected, which is obviously an approximation and it can limit the application of the present approach in some cases.

It can be assumed that the system response is periodic when the external forcing is periodic. A solution of the type of Equation 3.1 is consequently assumed as

$$\{x\} = \{X\}e^{i\omega t} \qquad (3.3)$$

Owing to the axial symmetry of the system, Equation 3.3 certainly expresses an exact solution of Equation 3.1, even if solution is not the only possible one and is not necessarily stable. If the considerations of Tondl are intuitively generalized to system with many degrees of freedom (Tondl, 1976), such a solution can be considered to be the governing one, at least up to the threshold of instability of the linearized system.

In fact Kahraman et al. (1990) studied non-linear single degree of freedom spur gear model and has shown that the steady state response of the system is strongly dependent on the initial conditions and system properties even in some cases it is not possible to get a deterministic steady state response, indeed the response is chaotic, especially for lightly loaded systems with low damping.

Equation 3.3 allows one to transform the non-linear differential Equation 3.1 into the non-linear algebraic equation.

$$\left[-(m\omega)^2[M] + j(m\omega)[C] + j[H] + [K]\right]\{X\}_m + \{N\} = \{F\}_m \qquad (3.4)$$

Equation 3.4 can be solved directly by using an iterative technique, which is generally very difficult.

As often the number of degrees of freedom directly involved in the non-linearities is small, condensation techniques can be used to simplify the solution. If the number of the degrees of the freedom after condensation is greater than two, the iterative solution is a difficult task. Moreover, the

46

condensation has to be performed for each value of the speed, and this leads to long and costly computation.

In this problem non-linearity is associated only with three degrees of freedom of the dynamic gear mesh interface since shafts and bearings models are linear. Maliha (1994) has expressed these three non-linearities associated with the dynamic gear mesh interface as follows :

$$\{N\} = \left\{ \begin{array}{c} k_h f_h(p) \\ k_h f_h(p) \\ -k_h f_h(p) \end{array} \right\}$$

(3.5)

In his work he used the formulation and solution technique developed by Budak and Özgüven (1990,1993) and extended by Tanrıkulu and Özgüven (1993).

Re-expressing the non-linear function $f_h(p)$ by using the describing function

$$f_h(p) = \sum_{m=0}^{\infty} v_m(A) P_m e^{im\varphi}$$

(3.6)

$$f_h(p) = \left(\frac{1}{\pi P_0} \int_0^\pi f_h(p) d\varphi \right) P_0 + \sum_{m=1}^{\infty} \left(\frac{2}{\pi P_m} \int_0^\pi f_h(p) \sin(m\varphi) d\varphi \right) P_m e^{im\varphi}$$

(3.7)

$$\{N\} = \{G\}_m e^{jm\psi}$$

(3.8)

where

$$\{G\}_m = \left\{ \begin{array}{c} v_m(A) \\ v_m(A) \\ -v_m(A) \end{array} \right\} k_h P_m = [\Delta]_m \left\{ \begin{array}{c} P \\ Y_g \\ Y_p \end{array} \right\}_m e^{jm\psi}$$

(3.9)

and

$$[\Delta]_m = \begin{bmatrix} k_h v_m & 0 & 0 \\ k_h v_m & 0 & 0 \\ -k_h v_m & 0 & 0 \end{bmatrix}$$ (3.10)

Then

$$\left[-(m\omega)^2[M] + j(m\omega)[C] + j[H] + [K] + [\Delta]_m\right]\{X\}_m = \{F\}_m$$ (3.11)

and

$$\{X\}_m = [\alpha]_m\{F\}_m$$ (3.12)

where $[\alpha]_m$ is the response level dependent quasi-linear receptance matrix of the system at frequency $m\omega$ and can be expressed as

$$[\alpha]_m = \left[-(m\omega)^2[M] + j(m\omega)[C] + j[H] + [K] + [\Delta]_m\right]^{-1}$$ (3.13)

The quasi-linear receptance matrix is a function of frequency $m\omega$, the linear and non-linear coefficient matrices of the system, and all the harmonics response components

3.2 Solution Technique

The quasi-linear theory presented above converts a set of differential equations into a set of non-linear complex algebraic equations. To reduce the computational time one can separate the non-linear equations from the linear ones. After the linear equations are separated from the non-linear ones, the number of non-linear equations left is three. Then perform the iteration only for the non-linear set of equations and solve the linear set directly as follows:

48

Equation 3.12, can be first rearranged as :

$$[\beta]_m \{X\}_m + \{G\}_m = \{F\}_m \tag{3.14}$$

Then Equation 3.14, can be written as

$$\begin{bmatrix} [\beta_{11}] & [\beta_{12}] \\ [\beta_{21}] & [\beta_{22}] \end{bmatrix} \begin{Bmatrix} \{X_1\} \\ \{X_2\} \end{Bmatrix} + \begin{Bmatrix} \{G_1\} \\ \{0\} \end{Bmatrix} = \begin{Bmatrix} \{F_1\} \\ \{F_2\} \end{Bmatrix} \tag{3.15}$$

$$[\beta_{11}]\{X_1\} + [\beta_{12}]\{X_2\} + \{G_1\} = \{F_1\} \tag{3.16}$$

$$[\beta_{21}]\{X_1\} + [\beta_{22}]\{X_2\} = \{F_2\} \tag{3.17}$$

Solving Equation 3.17, for $\{X_2\}$ yields

$$\{X_2\} = [\beta_{22}]^{-1} \left[\{F_2\} - [\beta_{21}]\{X_1\} \right] \tag{3.18}$$

Substituting Equation 3.18 in Equation 3.16 and noting that $\{G_1\} = [\Delta_{11}]\{X_1\}$ give

$$\{X_1\} = \left[[\beta_{11}] + [\Delta_{11}] - [\beta_{12}][\beta_{22}]^{-1}[\beta_{21}] \right]^{-1} \left\{ \{F_1\} - [\beta_{12}][\beta_{22}]^{-1}\{F_2\} \right\} \tag{3.19}$$

As shown in Equation 3.19, the right hand side contains the non-linear matrix $[\Delta_{11}]$ which depends on the unknown vector $\{X_1\}$ and thus it should be recalculated in each iteration step in the solution process. It should be noted that by using this technique, the size of non-linear algebraic problem is reduced to the number of coordinates associated with non-linearity matrix. This implies that only the limited number of coordinates rather than all coordinates, are updated in the iteration procedure which reduces the computational time considerably.

49

Note that $\{F_2\} = 0$ since there is no external force on the system other then the mesh force. Then the non-linear set of equations can be arranged as

$$\{X_1\} = \left[[\gamma] + [\Delta_{11}] \right]^{-1} \{F_1\}$$ (3.20)

where

$$[\gamma] = \left[[\beta_{11}] - [\beta_{12}][\beta_{22}]^{-1}[\beta_{21}] \right]$$ (3.21)

Equation 3.20 represents $3(n+1)$ set of non-linear equations and have to be solved simultaneously. The coupling terms are functions of vectors $\{X_1\}_0, \{X_1\}_1, \dots \{X_1\}_n$ They must be found by iteration as $[\Delta_{11}]$ includes the elements of $\{X_1\}$ and in each iteration they should be substituted in non-linear coupling terms to form the non-linearity matrix $[\Delta_{11}]$. The linear response is used to form the non-linearity matrix in the first trial. The iteration is continued until the required accuracy is achieved. To reduce the computational time required to solve the problem the following procedure is implemented. (See Figure 3.1)

- The $3(n+1)$ set of equations are decomposed into $n+1$ set of equations having 3 unknowns in 3 equations (i.e. the vector $\{X_1\}_i$)

- Initially, each vector $\{X_1\}_i$ is calculated independently by inverting the matrix $\left[[\gamma]_i + [\Delta_{11}]_i \right]$ (of order 3), where $[\Delta_{11}]_i$ is evaluated by neglecting the non-linear terms in the first trial

- After solving for the whole set of vectors $\{X_1\}$ (i.e. solving (n+1) system of equations), the non-linear terms in matrix $[\Delta_{11}]$ are evaluated using the computed vector $\{X_1\}$

- The previous steps are repeated using the new evaluated non-linearity matrix $[\Delta_{11}]$ in each iteration until attaining a convergence for the whole vector $\{X_1\}$

The following iteration scheme is used at a particular frequency (See Figure 3.2)

1. The quasi-linear receptance matrix $[\alpha]$ is formed for the m-th harmonic

2. The non-linear matrix $[[\gamma]+[\Delta]]$ is calculated from $[\alpha]$

3. The internal excitation vector $[F_1]$ is calculated for the m-th harmonic

4. Steps 1-3 are repeated for m=0,1,2.....n, to form $[\gamma]_0, [\gamma]_1, ... [\gamma]_n$ and $\{F_1\}_0, \{F_1\}_1, ... \{F_1\}_n$

5. The complex displacement amplitude vectors $\{X_1\}_0, \{X_1\}_1, ... \{X_1\}_n$ are calculated using the linear receptance matrices $[\gamma]_0, [\gamma]_1, ... [\gamma]_n$. Note that for this case $[\Delta_{11}]_0, [\Delta_{11}]_1, ... [\Delta_{11}]_n$ matrices are assumed to be zero (linear case).

6. The non-linear coupling matrices $[\Delta_{11}]_0, [\Delta_{11}]_1, ... [\Delta_{11}]_n$ are determined by using the new $\{X_1\}_0, \{X_1\}_1, ... \{X_1\}_n$ vectors

51

7. The complex displacement amplitude vectors at the next iteration step are determined using the non-linear part of quasi-linear receptance matrices. Since the system is highly non-linear, the new vectors are determined by applying a relaxation factor.

8. The iteration is continued until the displacement root mean square error drops below a certain limit.

Figure 3.3 shows the flow of the NLGRD code .

SET OF DIFFERENTIAL EQN'S
3*(n+1) Eqn's
$D_1 X_1 = F_1(x)$
$D_2 X_1^1 = F^1_2(x)$
$D_3 X_1^1 = F^2_3(x)$
.
.
.
$D_1 X_n = F_{3(n+1)-2}(x)$
$D_2 X_n^1 = F^{3(n+1)-1}(x)$
$D_3 X_n^1 = F_{3(n+1)}(x)$

Group Eqn's

$D_1 X_1 = F_1(x)$
$D_2 X_1^1 = F^1_2(x)$
$D_3 X_1^1 = F^2_3(x)$

.
.
.

$D_1 X_n = F_{3(n+1)-2}(x)$
$D_2 X_n^1 = F^{3(n+1)-1}(x)$
$D_3 X_n^1 = F_{3(n+1)}(x)$

START

YES

Evaluate [γ] by neglecting
Non-linear terms

NO

Calculate X by inverting
[γ+Δ]

Evaluate [Δ] by using the
computed X

NO

Calculate X by inverting
[γ+Δ]

Check
convergence of
X

YES

Proceed to the
next frequency

Figure 3.1 Solution technique

53
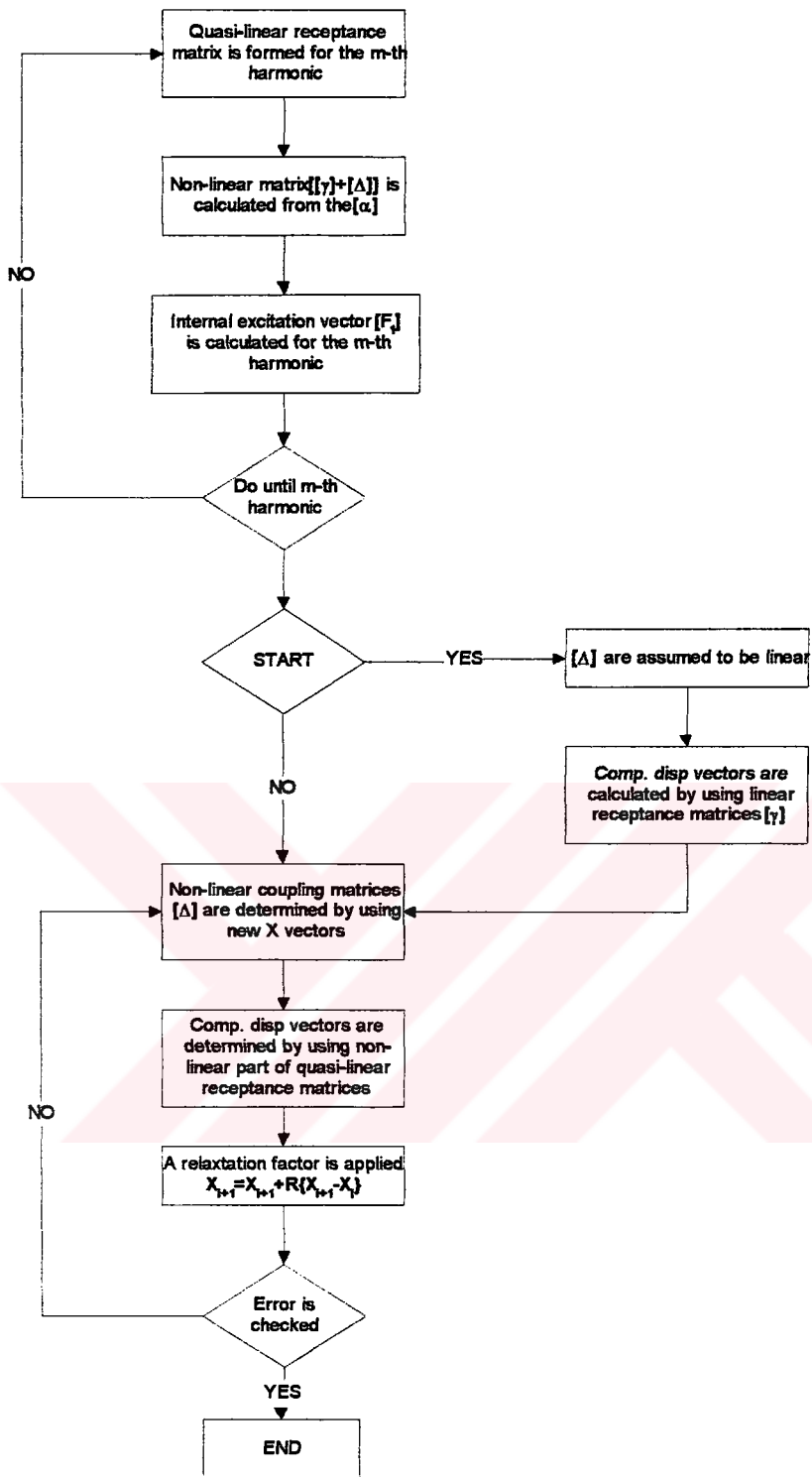
Figure 3.2 : Iteration scheme used at a particular frequency

54

MAIN
Control and drive the excution of subroutines

MASTER
Control input and output of NLGRD

ASSEMB
Form and assemble elemantal matrices for the first and second shaft

SOLUTION

INFORC/FORCE
Calculate Fourier coefficients

Form linear receptance matrices corresponding to excitation frequencies

MATDIV
Separate set of linear equations to be added to non-linear set of equations

GRMESH
Calculate gear mesh non-linear and linear coupling equations and add them to the separated linear set of equations

Find displacement vectors

GRMESH
Calculate DF values (Delta matrix) and add them to the separated set of non-linear equations

Find displacement vectors

Del(Disp)<Error

DYNF
Calculates DSLR and DTE

END

Figure 3.3 : Flowchart of the original program

55

CHAPTER IV

USER INTERFACE

4.1 Introduction

NLGRD user interface - pre-processor and post-processor - is written in VB 5.0. The emphasis is placed on user-friendliness. The graphical drawing of the geared rotor system is formed while the user add new items to the system. Thus any user dependent error is minimized. The program is capable of making more than one analysis at the same time. The user interface, Visual Geared Rotors (VGR), could prepare input file for both NLGRD and LDP version 10.1

There are four basic items in the program:

- Bearing elements

- Weight elements

- Rotor elements

- Gear elements

Every time user clicks one of these buttons, NLGRD interface loads a new item on the CAD form.

Material, geometric and other types of data can be entered by just double clicking the items.

Beside these elements there are:

- Stop button

- Move button

- Delete Button

The main window of NLGRD interface is shown in Figure 4.1. Having formed the system, user can make analysis by clicking the **processor button**.

4.2 Pre-processor

Connectivity of the system is formed while the user is clicking the basic item buttons. Position of the items are irrelevant to connectivity. Therefore items must be loaded from *left to right, top to buttom*. So user must first construct the first shaft from left to right, then click **stop button,** then start constructing the second shaft and click **stop button** again when finished. The construction of typical geared rotor system is shown in Figure 4.2.

Loaded items can be dragged anywhere on the screen after clicking the **move button.**

Geometric properties of the items can be defined on screen after **stretch button** is clicked or first double clicking the item then entering the geometric properties through data windows.

4.2.1 Bearing Element

When the bearing button shown in Figure 4.1 is clicked a new bearing element is loaded on the CAD window. In order to enter bearing stiffness and hysteric damping constants the user must double click the bearing element. Figure 4.3 is displayed immediately after double click.

57
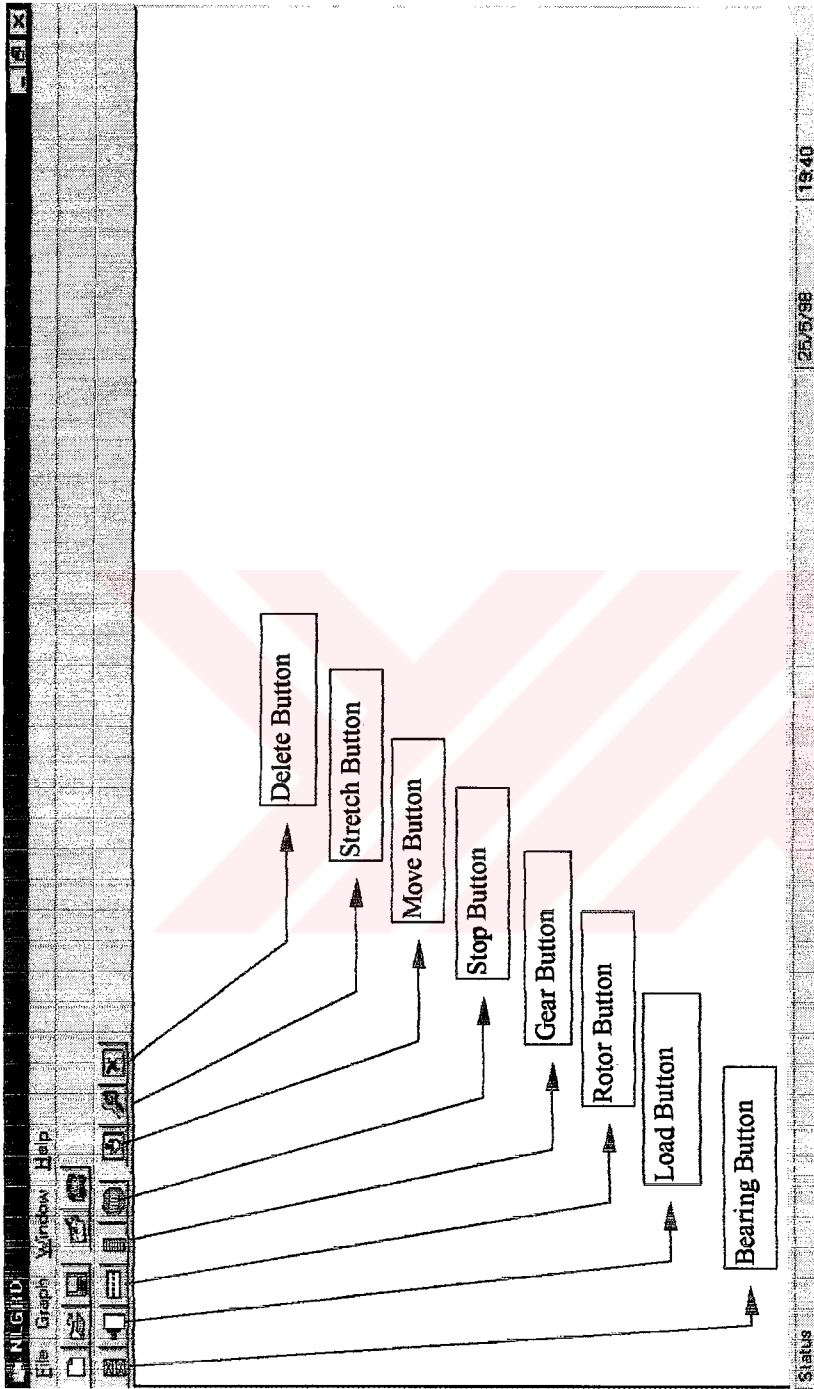
Figure 4.1 Main window of user interface

58
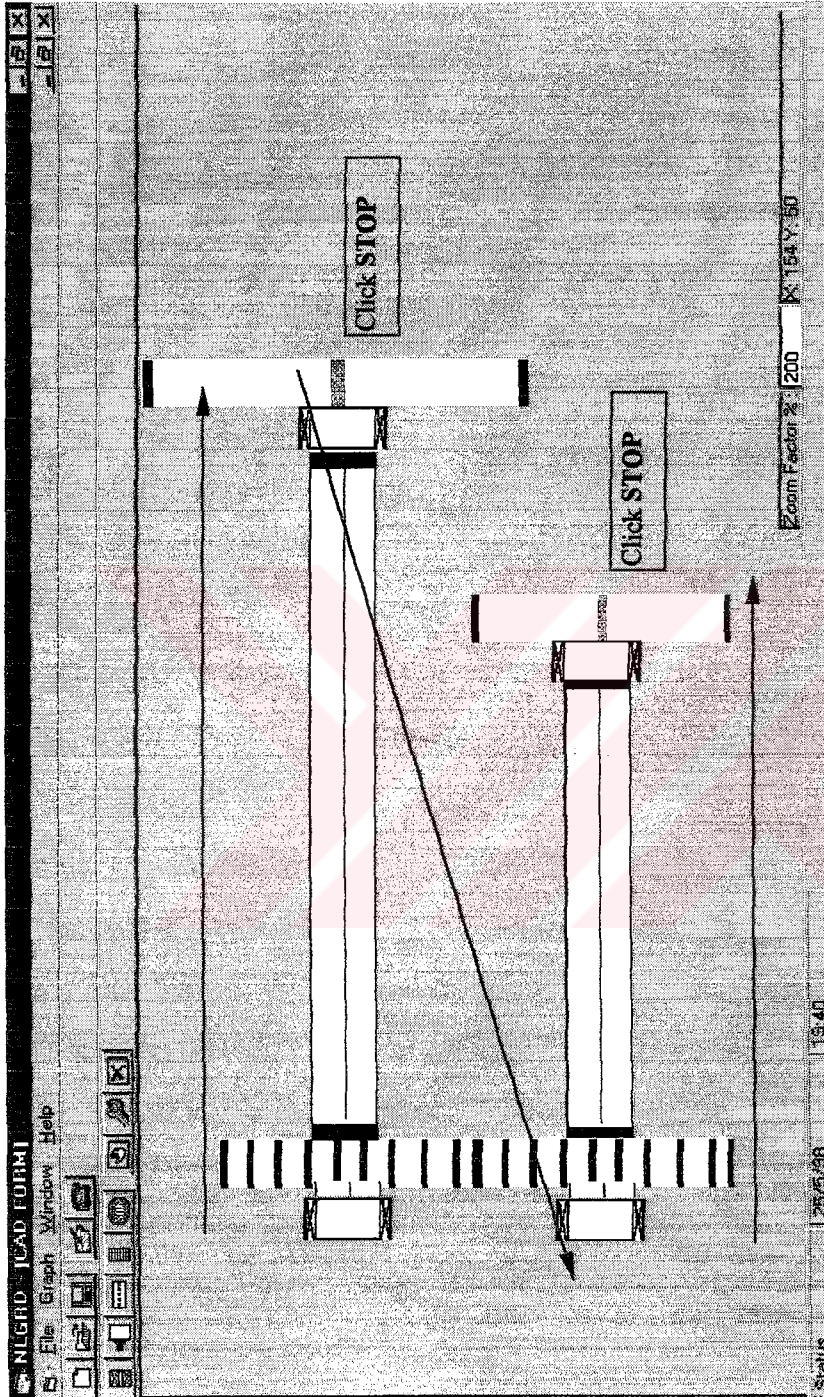
Figure 4.2 : Pre-processor, assembly of geared rotors

Figure 4.3 Bearing data window

Figure 4.4 Weight data window

4.2.2 Weight Element

When the weight button shown in Figure 4.1 is clicked, a new weight element (e.g. flywheel) is loaded on the CAD window. As soon as the user double clicks the weight element, Figure 4.4 is displayed on the screen. User can enter the following NLGRD data:

- diameter

- width

60

- density

through this window.

Figure 4.5 Rotor data window

4.2.3 Rotor Element

When the rotor element shown in Figure 4.1 is clicked, a new rotor element is loaded on the CAD window. Figure 4.5 is displayed when the user double clicks the rotor elements. User can enter the following NLGRD data :

- outer diameter

- inner diameter

- length

- axial load

through this window. In order to enter material properties of the rotor material button must be clicked. Figure 4.6 is loaded when the material button is clicked. User can enter the following NLGRD data :

- Density

- Modulus of elasticity (NLGRD and LDP)

- Shear modulus of elasticity

- Viscous damping coefficient

- Hysteric damping coefficient

through this window.

User can reach misalignment and shaft dimensions window through rotor data window. When the user clicks the misalignment button Figure 4.7 is displayed. User can enter the following LDP data :

- Misalignment at X=0

- Misalignment slope

When the user clicks the shaft dimension button, Figure 4.8 is displayed. User can enter the following LDP data :

- Outer, inner diameter and length of shaft

  - Before pinion

  - After pinion

Figure 4.6 Shaft material data window

Figure 4.7 Misalignment data window

- Before gear

- After gear

- Gear and pinion hub diameter

LDP can only take into account single shaft before and after the gear pair therefore equivalent shaft dimensions must be entered.
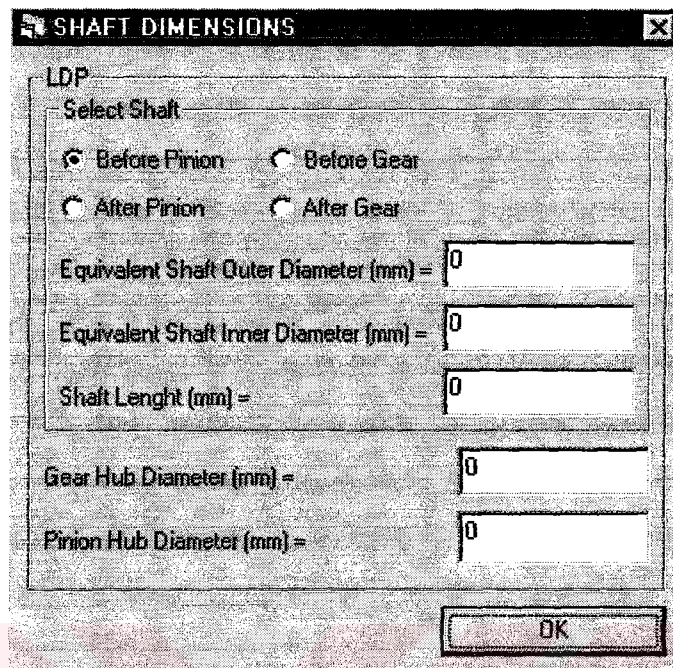
Figure 4.8 Shaft dimensions data window

4.2.4 Gear Element

When the gear button shown in Figure 4.1 clicked, a new gear element is loaded on the CAD window. Figure 4.9 is displayed when the user double clicks the gear element. User can enter the following NLGRD data :

- Pitch diameter

- Face width

- Density

through this window. Three new windows can be reached through Figure 4.9. When the user clicks mesh data button Figure 4.10 is displayed. User can enter

- Number of teeth

64

- Viscous damping coefficient

- Backlash

- Static load

- Eccentricity

through this window.

When the user clicks STE button, Figure 4.11 is displayed. User can enter the following NLGRD data :

- Contact ratio

- Amplitude of STE

- Average mesh stiffness

- Name of STE file

User can choose either LDP output file or rectangular wave approximation. User must enter contact ratio, amplitude of STE and average mesh stiffness unless he chooses the STE file option. By clicking data button user can reach Figure 4.12. This windows controls the flow of the NLGRD processor. User can enter the following NLGRD parameters shown in Figure 4.12 :

Number of FFT Terms : The number of harmonics used in the approximation of STE. The maximum number of harmonics is five.

Starting angular speed (rpm) : The simulation starts at this rpm.

Upper Limit of angular speed (rpm) : The simulation ends at this rpm.

Increment : Speed increment between successive simulation.

Figure 4.9 Gear data window

Figure 4.10 Gear mesh data window
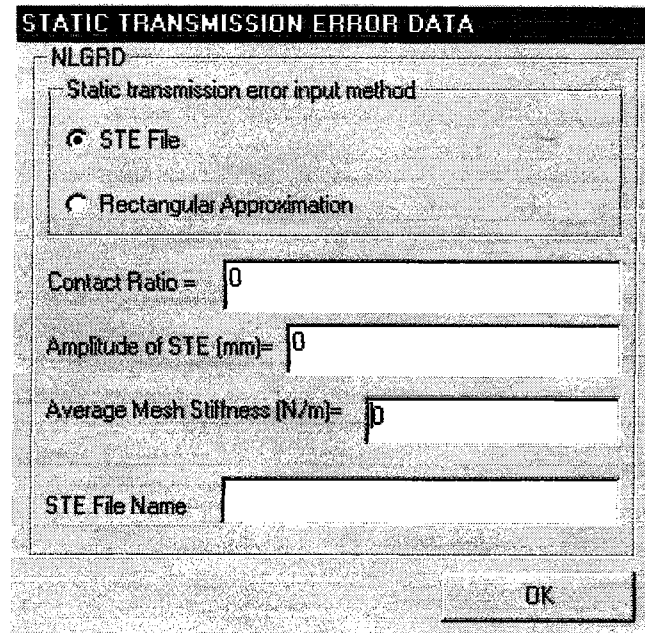
Figure 4.11 Static transmission error data window

Tolerance : It controls the error limit (Recommended : 0.01)

Relaxation Factor : The result of NLGRD is modified by a weighted average of the results of the previous and present iterations. (Recommended : Relaxation factor 1 = 0.001, Relaxation factor 2 = 0.13)

When the user clicks gear geometry button, Figure 4.13 is displayed. User can enter the following LDP data :

- Number of teeth

- module

- Generating pressure angle

- Helix angle

- Outer diameter

Figure 4.12 Data window

- Root diameter

- Center distance

- Input torque

- Location of the output torque relative to input torque

- Type of gear mesh (External / Internal)

When the user click the tooth data button, Figure 4.14 is displayed. User can enter the following LDP data :

68

LDP

Teeth Number = | 0 | ☐ Use the same teeth number in NLGRD

Module (mm) = | 0 | ☐ Calculate module using the pitch diameter in NLGRD

Generating Pressure Angle (deg) = | 20 |

Helix Angle (deg) = | 0 |

Outside Diameter (mm) = | 0 |

Root Diameter (mm) = | 0 |

Center Distance (mm) = | 0 |

Input Torque (Nm) = | 0 |

Locate the position of output torque relative to input torque
◉ Same
○ Opposite

External / Internal Gear
◉ External Gear
○ Internal Gear

OK

Figure 4.13 Gear geometry data window

- Starting tooth number

- Face width

- If backlash is choosen

  - Amplitude of backlash

  - Percentage of backlash attributed to pinion

- If tooth thickness is choosen

  - Tooth thickness

- Diameter at which tooth thickness measured

When the user clicks the tooth model button, Figure 4.15 is displayed. User must choose the model of the tooth (Flat/Tapered). If he choose tapered tooth model he must decide on the type of calculation method (manual/automatic). If he choose manual method, he must enter the following parameters :

- Tooth thickness at tip

- Tooth thickness at root

Beside these, user must enter the following constants :

- Plate bending exaggeration factor

- Tooth base rotation factor

- Hertz exaggeration factor

When the user click gear material button, Figure 4.16 is displayed. User can enter the following LDP data :

- Young's modulus

- Poisson's ratio

When the "use the same material" check box is checked, both gear and pinion has the same material properties.

When the user clicks the lead data button, Figure 4.17 is displayed. User can enter the following LDP profile modification data :

- Straight modification on X=0 side

- Parabolic modification on X=0 side

Figure 4.14 Tooth data window

Figure 4.15 Tooth model data window

Figure 4.16 Gear material data window

- Beginning position on X=0 side

- Straight modification on X=F side

- Parabolic modification on X=F side

- Beginning position on X=F side

- Circular modification on X=0,F side

- Lead angle error

When the user click involute data button, Figure 4.18 is displayed. User can enter following LDP profile modification data :

- Roll angle at start of tip modification

- Parabolic tip modification magnitude

- Straight tip modification magnitude

- Roll angle at start of root modification

- Parabolic root modification magnitude

- Straight root modification magnitude

- Circular modification at tip and root

- Pressure angle error

When the user clicks the program control button, Figure 4.19 is displayed. This window controls the flow of LDP. User can enter the following LDP data :

- Beginning position constant

- Ending position constant

73

- Number of positions to analyze

- Multiplier for number of points across face

- Include shaft effects in transmission error calculation ? (Yes/No)

- How profile modifications are entered ?

- Interactive

PINION LEAD MODIFICATION

LDP

Gear Side X=0

Straight Modification on X=0 Side (mm) = 0

Parabolic Modification on X=0 Side (mm) = 0

Beginning Position on X=0 Side (mm) = 0

Gear Side X=F

Straight Modification on X=F Side (mm) = 0

Parabolic Modification on X=F Side (mm) = 0

Beginning Position on X=F Side (mm) = 0

Circular Modification on X=0,F Side (mm) = 0

Lead Angle Error (mm) = 0

OK

Figure 4.17 Lead modification data window
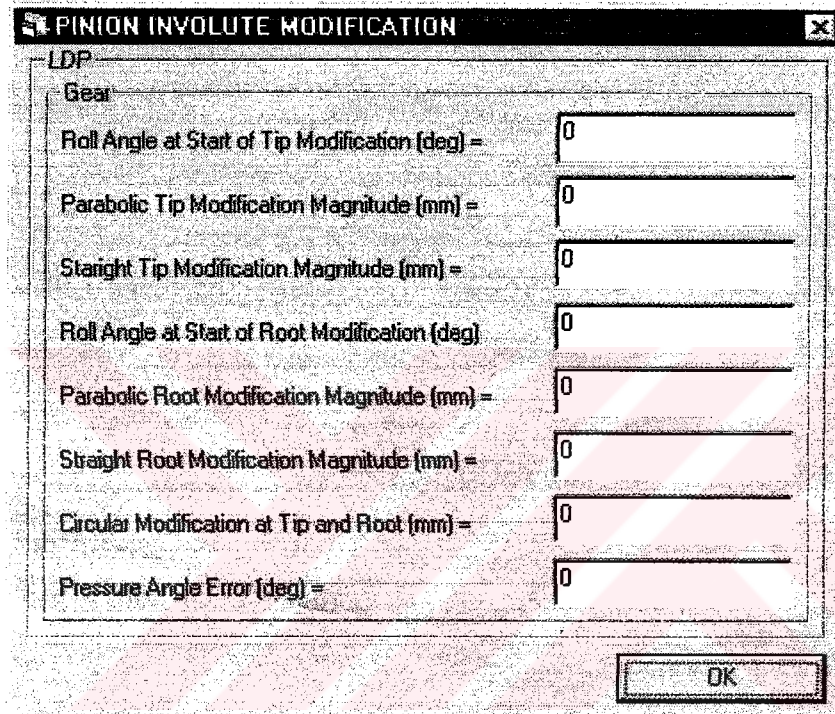
Figure 4.18 Involute modification data window

Figure 4.19 Program control data window

76

- Files

- Both

- Not at all

- Are there spacing errors ? (Yes/No)

- Create dynamic analysis file ? (Yes/No)

- Use off line action of model ? (Yes/No)

- Perform varying torque analysis ? (Yes/No)

- Perform multi/single torque analysis ?

- Which shaft use gfiles ?

  - Pinion shaft

  - Gear shaft

  - Both pinion and gear shaft

  - None of them

When the user clicks title and filenames button, Figure 4.20 is displayed. User can enter the filenames necessary for LDP. These are :

- Program identity title

- Output file name

- File name for detailed pinion data (when tooth spacing option is checked)

- File name for detailed gear data (when tooth spacing option is checked)

77

- File name for torque values (when varying torque analysis is checked)

- File name for pinion shaft (when the pinion shaft use gfiles)

- File name for gear shaft (when gear shaft use gfiles)

- Position constants (number of positions to be printed)

- Do you want detail in output file (Yes/No)

4.3 Post-processor

After NLGRD version 2.0 analyses the system, results can be seen through user interface graphically. The post-processor window is shown in Figure 4.21. User can control the graph window by changing parameters of control window. X and Y-axis variable, X and Y-axis scale can be changed. The user can take the advantage of seeing both the results and the model of the system at the same time.
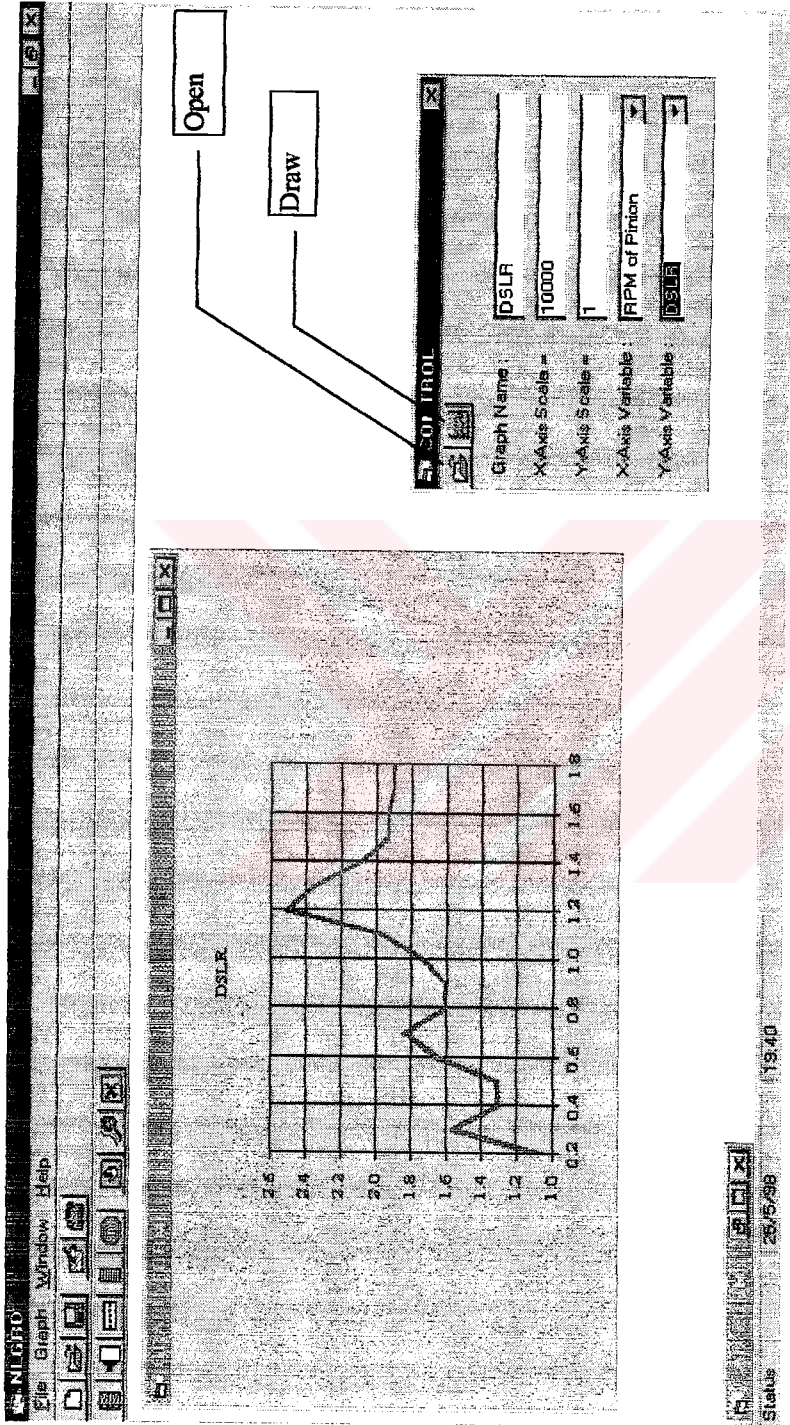
Figure 4.20 Title and filenames data window

Figure 4.21 : Post-processor window

80

CHAPTER V

CASE STUDIES

5.1 Introduction

In this chapter several case studies are carried out. Firstly, the numerical results obtained by using NLGRD are compared with those of the experimental studies available in literature. Then the Kubo's setup is used to study the effect of several system parameters on system response; namely the effects of mean load, module, center distance, parabolic and linear modifications on DSLR, bearing forces, STE and mesh stiffness are investigated. Finally, empirical relations are suggested between DSLR and module, and between DSLR and amount of profile modifications.

5.2 Case Study I : Verification by Experimental Results - Munro's Experimental Setup

Munro used a four-square test rig, which is shown in Figure 5.1, to measure dynamic transmission error of a spur gear pair. High precision spur gears with manufacturing errors much smaller than tooth deflections were selected. Pinion and gear were identical with 32 teeth, face width of 12.7 mm and diametral pitch of 4. Tooth profile modifications were applied to obtain a minimum (but not zero) static transmission error at design load (DL) of 3780 N. Other components of the set-up including shafts, bearings and casing
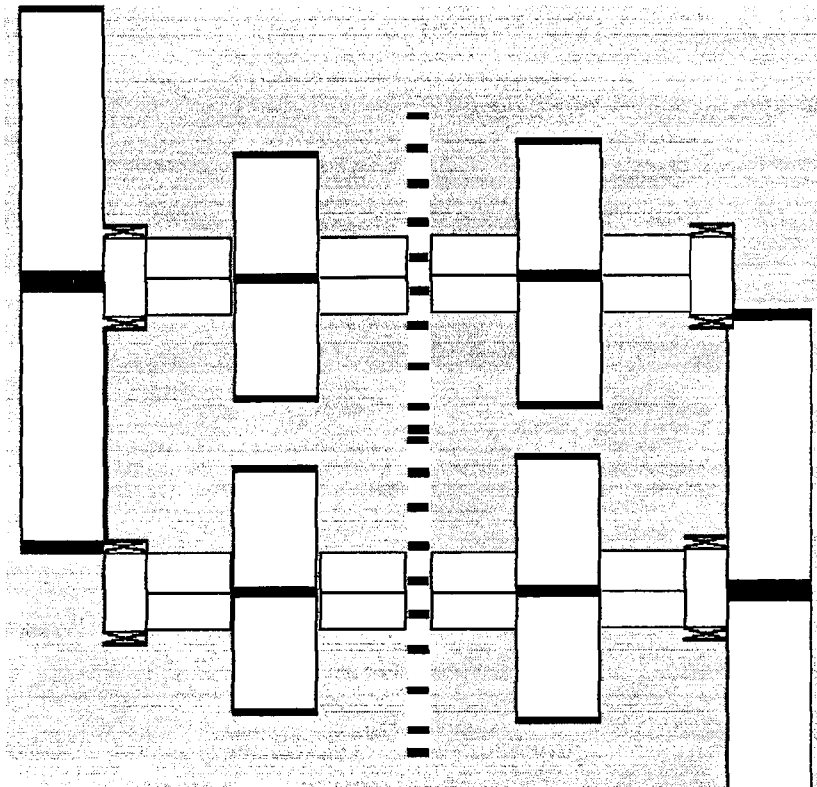
81

Figure 5.1 Munro's test rig

were made as rigid as possible. Dynamic transmission error was measured for a range of gear mesh excitation frequencies under different mean loads. Some of the key parameters were not specified by Munro. For example, it was stated that some additional inertias were added to the gears to shift the primary resonant frequency within the operational speed range, but the specific values of such inertias were not given. It was also reported that the damping ratio varies with load in a random manner. Also backlash was not measured or reported. System parameters used in the following study are given in Table 5.1.

The measured and predicted dynamic transmission error, on a peak to peak basis, at the design load and at ¾, ½ and ¼ of the design load, respectively are compared. The results of Munro's experiment and the results of NLGRD for design load are shown in Figure 5.2. The frequency ratio on the x-axis of Figure 5.2 can be defined as the ratio of rotational speed to torsional

Table 5.1 Parameters of Munro's experiment set-up

Diametral pitch	4
Number of teeth	32/32
Pitch diameter (mm)	204.8
Face width (mm)	12.7
Backlash (mm)	0.12
Contact ratio*	1.60
Mesh stiffness (N/m)	3.44E8
Mesh damping ratio	0.0175
Amplitude of STE (m)	0.1143E-5
Design load (N)	3780
$I_1 = I_3$ (kgm^2)	0.02563
$I_2 = I_4$ (kgm^2)	0.03426
I_L* (kgm^2)	0.67
I_M* (kgm^2)	0.60
Bearing stiffness (N/m)	0.58E9
Bearing damping (Ns/m)	0.58E5
Shaft damping ratio	0.005

♣ Estimated data

Table 5.2 Mesh stiffness and STE for different loads

	Design load	¾ DL	½ DL	¼ DL
Stiffness (N/m)	2.6620E08	2.6352E08	2.5983E8	2.5376E+09
STE (m)	3.1378E-6	2.3924E-6	1.6283E-	8.4383E-7

natural frequency. It is observed in Figure 5.2 that the subharmonic and resonance frequencies are predicted correctly. Although NLGRD predicts the subharmonic peaks which are also reported in the experiment, the amplitude of the predicted main resonance is lower than that of the experiment results. The STE and mesh stiffness which are calculated by LDP for different mean loads are shown in Table 5.2. The profile modifications, which were used in Munro's experiment to give minimum STE, are not modeled in LDP. Damping ratio of the gear mesh, shafts and bearings are estimated. Such slight changes in the critical system parameters can alter the results drastically. Munro has also used some extra flywheels to shift the system resonance frequency. Although these flywheels are modeled through NLGRD, their exact dimensions are not known. Therefore the results of NLGRD are not expected to be in very good agreement
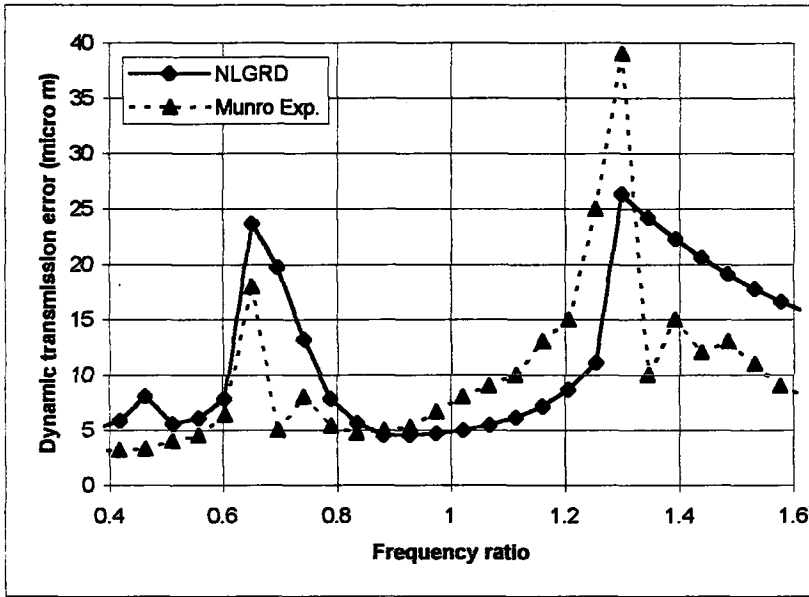
83

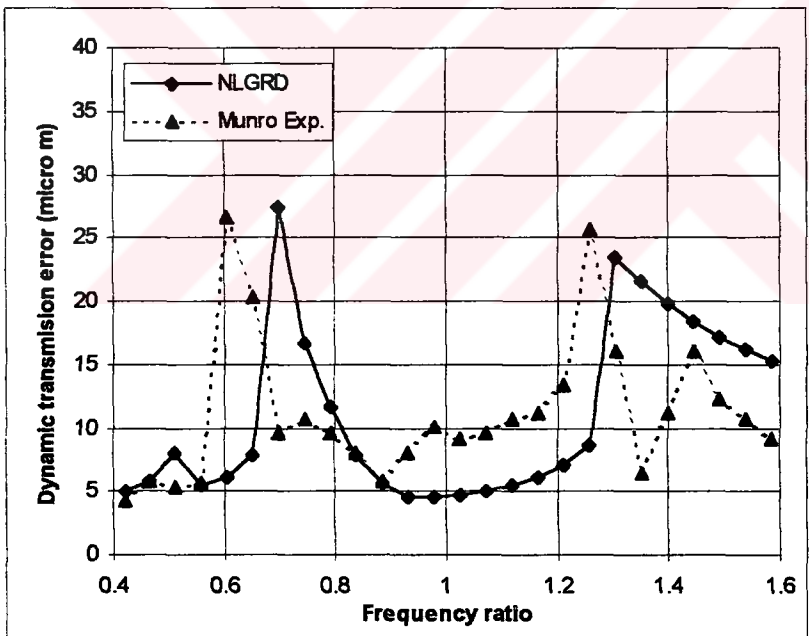Figure 5.2 Comparison of the results of NLGRD with Munro's experimental results at design load (DL)

Figure 5.3 Comparison of the results of NLGRD with Munro's experimental results at ¾ DL

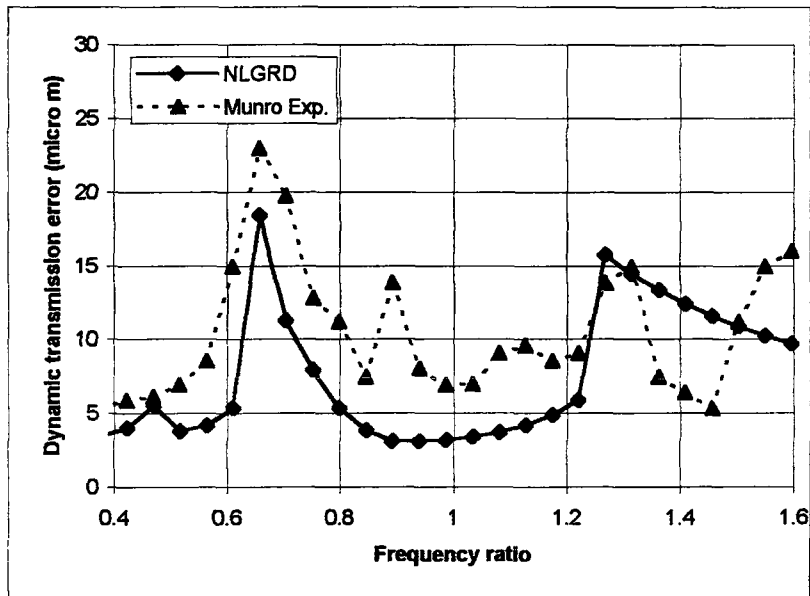Figure 5.4 Comparison of the results of NLGRD with Munro's experimental
results at ½ DL

with Munro's experimental results. Figure 5.3 and Figure 5.4 show the results
of NLGRD and Munro's experimental results for ¾ and ½ design load
respectively. As the design load is decreased, the experimental results in Figure
5.3 and Figure 5.4 start having irregular shapes. Munro has reported
unrepeatable response (probably chaos) at ¼ of the design load. NLGRD
predicts response up to ½ design load and cannot run for the ¼ design load.

The whole trend of the results obtained by NLGRD follow the trend
of Munro's experimental results. The jump at the main resonance and the
subresonance whose frequency is half of the main resonance are predicted
successfully.

5.3 Case Study II : Verification by Experimental Results - Kubo's Experimental Setup

Kubo used a heavily damped ($\xi=0.1$) four-square spur gear test rig
which is shown in Figure 5.5 and measured dynamic factors as the ratio of the

dynamic to static tooth stresses. The experimental set-up was designed to support gear pair with very stiff shafts and bearings. Table 5.3 shows the parameters of Kubo's setup. The parameters shown in Table 5.3, are extracted from Özgüven (1991), and Kahraman and Singh (1991a).

In this study the dynamic factor is defined as the dynamic to static load ratio which is equivalent to the dynamic factor calculated, based on the
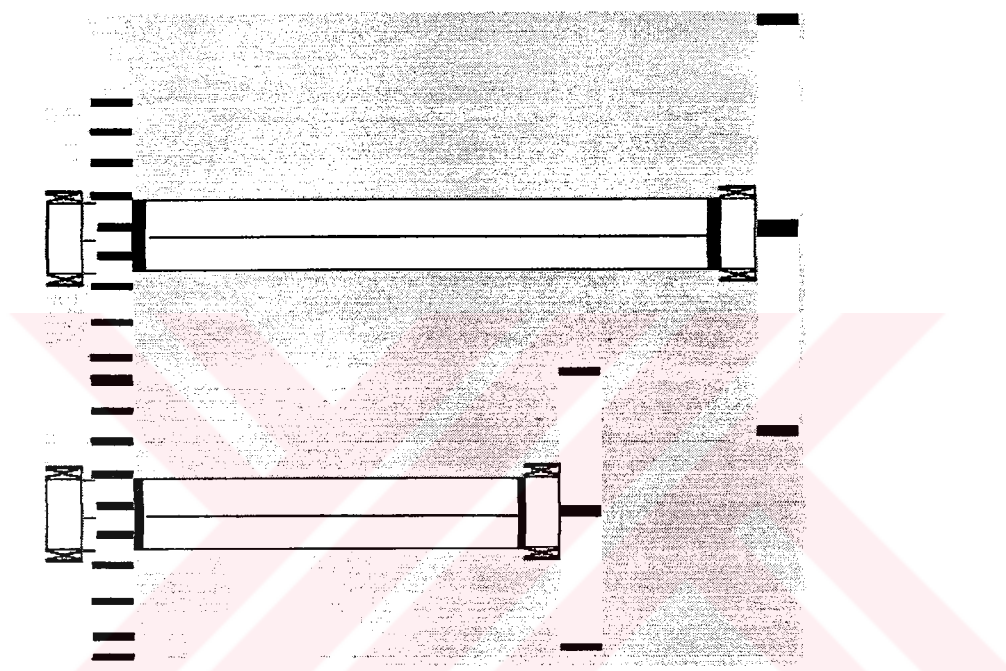

Figure 5.5 Kubo's test rig

stress analysis under the assumption that the change in the moment arm due to changes in the contact point is negligible. Since this assumption is not a valid one, dynamic factors calculated by NLGRD are not expected to match with the experimental values. However the change of dynamic forces with rotating speed can be compared. Comparison of the results of NLGRD and Kubo's experiment results are shown in Figure 5.6. In Figure 5.6 the results of the NLGRD with 1
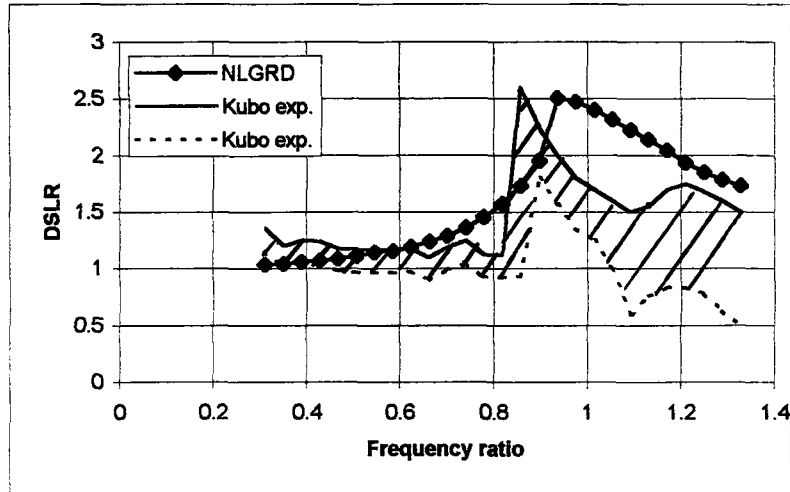
Figure 5.6 Comparison of NLGRD results with Kubo's experimental results

Table 5.3 Parameters of Kubo's setup

Module (mm)	4
Number o teeth	25/25
Base diameter (mm)	94
Outside diameter (mm)	108
Root diameter (mm)	90
Pitch diameter (mm)	100
Face width (mm)	15
Backlash (mm)	0.1
Pressure angle (deg)	20
Contact ratio	1.56
Mesh stiffness (N/m)	0.2587E9
Amplitude of STE (m)	0.2479E-5
Drive and load torques (Nm)	107.9
Static load (N)	2295
I_p (kgm^2)	0.1152E-2
I_g (kgm^2)	0.1152E-2
I_L (kgm^2)	0..1152E-2
I_M (kgm^2)	0.5762E-2
Bearing stiffness (N/m)	0.3503E13
Bearing damping (Ns/m)	0.3503E6
Shaft damping ratio	0.005

harmonic follow the trend of the Kubo's experiment results envelope. It predicts

87

the jump which exists in the experiment. However the predicted main resonance around the jump is observed at a slightly higher frequency.

5.4 Case Study III: Comparison of Results of NLGRD with Those of Other Mathematical Models

Lin et al. (1994) have developed a four degree of freedom torsional model. The equations are linearized by dividing the mesh period into small intervals. Then the solution is obtained by iteration as follows: to start the iteration process, initial values of the angular displacement were obtained by preloading the input shaft with nominal torque carried by the system. Initial values of the angular speed were taken from the nominal operating speed. The calculated values of angular displacement and speed after one mesh period were compared with the assumed initial values. Until the differences between them were smaller than a preset tolerance, the procedure was repeated using the average of the initial and the calculated values as the new initial condition. The data related to this study is given Table 5.4.

The predictions obtained by NLGRD and Lin's model are given in Figure 5.7. It can be observed that, both NLGRD and Lin's model predict the subharmonic peaks at 3000 rpm and 6000 rpm. However Lin's model gives the main resonance at 12000 rpm whereas NLGRD predicts the main resonance at a slightly lower frequency (11000 rpm). The trend observed in both results are comparable. Both models predict the subharmonics at ½, $\frac{1}{3}$ of the main resonance frequency.

Özgüven (1991) has developed a six degree of freedom non-linear gear dynamics model and the program (DYTEM). It is an improved version of the DYTE. The results of NLGRD are also compared with those of DYTEM for the Kubo's gears set.

Table 5.4 Parameters of Lin's gear set

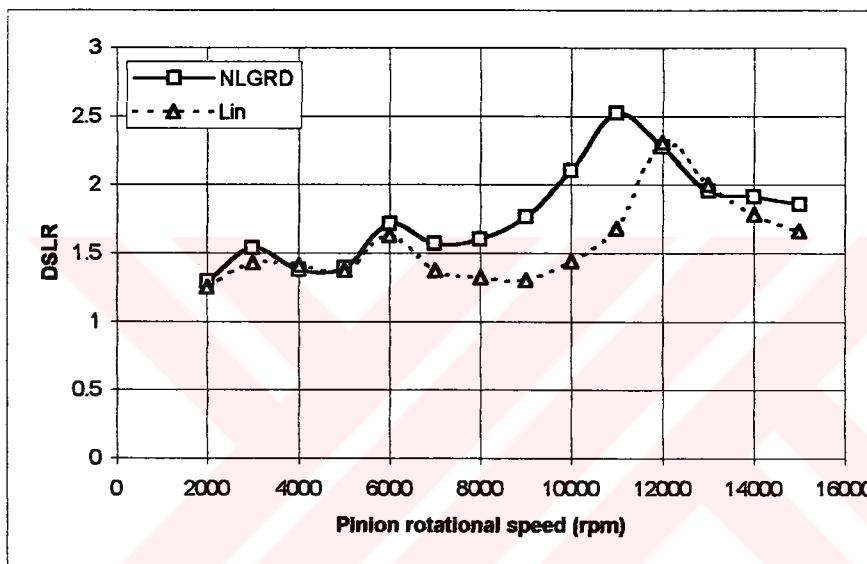| Gear tooth	Standard involute full-depth tooth
Module (mm)	3.18
Pressure angle (deg)	20
Number of teeth	28
Face width (mm)	25.4
Design load (N)	2540
Theoretical contact ratio	1.64

Figure 5.7 Comparison of NLGRD results with Lin's results

Both the results of NLGRD and the results of DYTEM are shown in Figure 5.8. In Figure 5.8 both programs predicted the subharmonics but the DSLR, found by NLGRD, is a little bit higher than the result of DYTEM. The resonance frequency found by NLGRD is 12000 rpm whereas DYTEM predicts it as 11000 rpm. The jump in the results of NLGRD is not as significant as the jump in the results of DYTEM. Generally the results of NLGRD are in good agreement with the results of DYTEM.
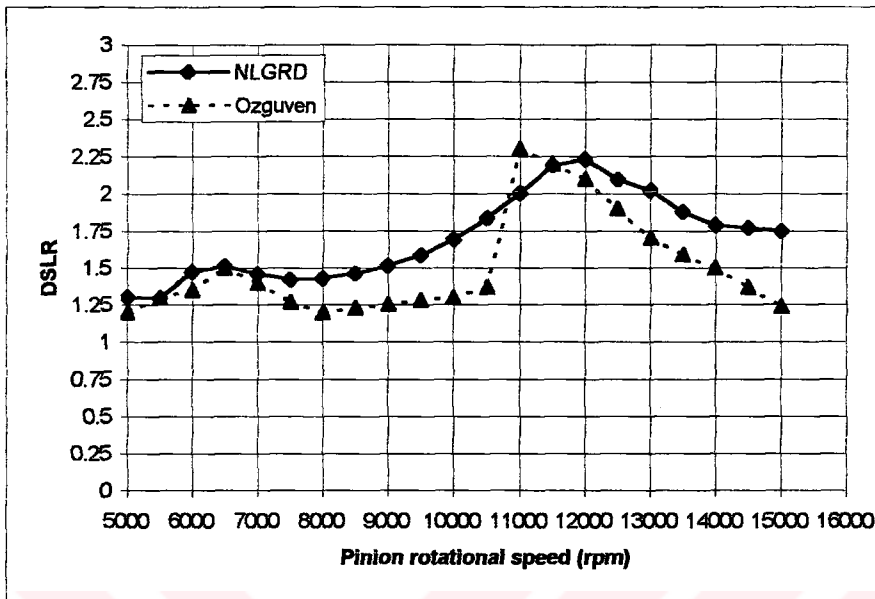
Figure 5.8 Comparison of the results of NLGRD with Özgüven's results

5.5 Case Study IV: Effect of Mean Load

In this part the effects of mean load on DSLR, dynamic transmission error, mesh stiffness and static transmission error are studied. While keeping all the parameters of the Kubo's setup fixed, the mean load is increased to two times of the design load and then three times of the original design load. In Figure 5.9 the results of NLGRD for different mean loads are shown. Figure 5.10 shows the mesh stiffness calculated by LDP for different mean loads. As shown in Figure 5.9 the results for different mean loads almost coincide with each other. This suggests that it will be convenient to use the same DSLR for off design loads. These results do not imply that maximum dynamic force remains constant. Although the DSLR is the same for different mean loads,
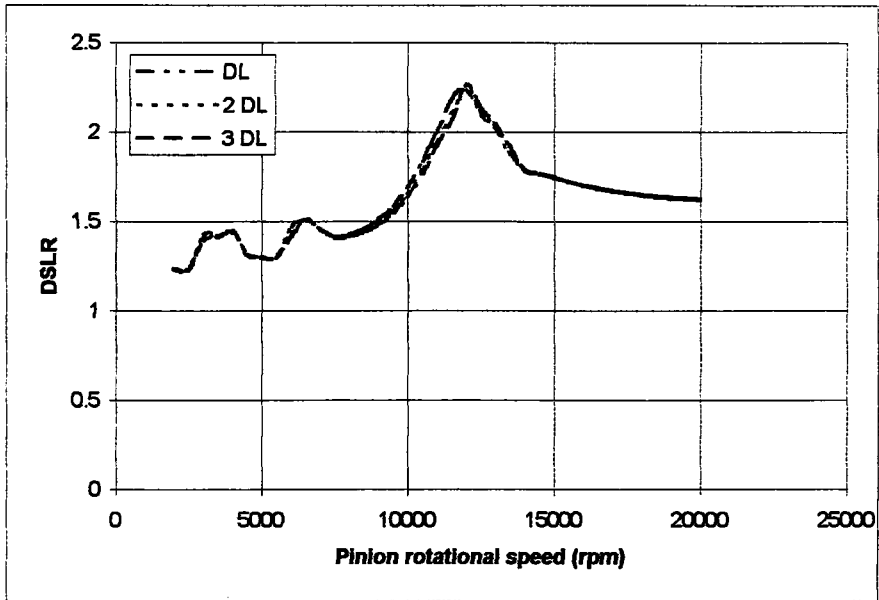
90

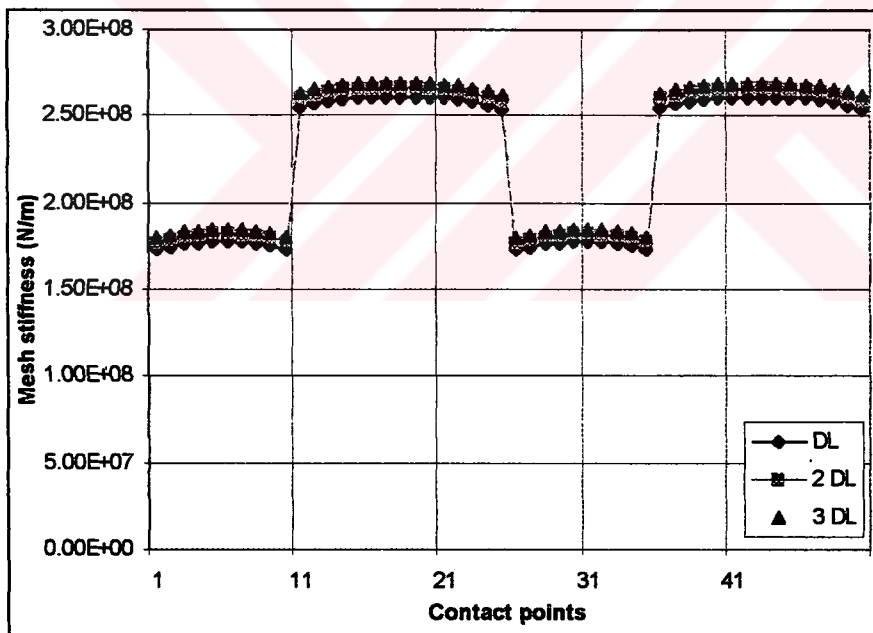Figure 5.9 Effect of mean load on DSLR

Figure 5.10 Effect of mean load on mesh stiffness

91

dynamic forces change, since the mean load is not the same at each case. As it is seen in Figure 5.10 the mesh stiffness tends to increase with the increasing mean load.
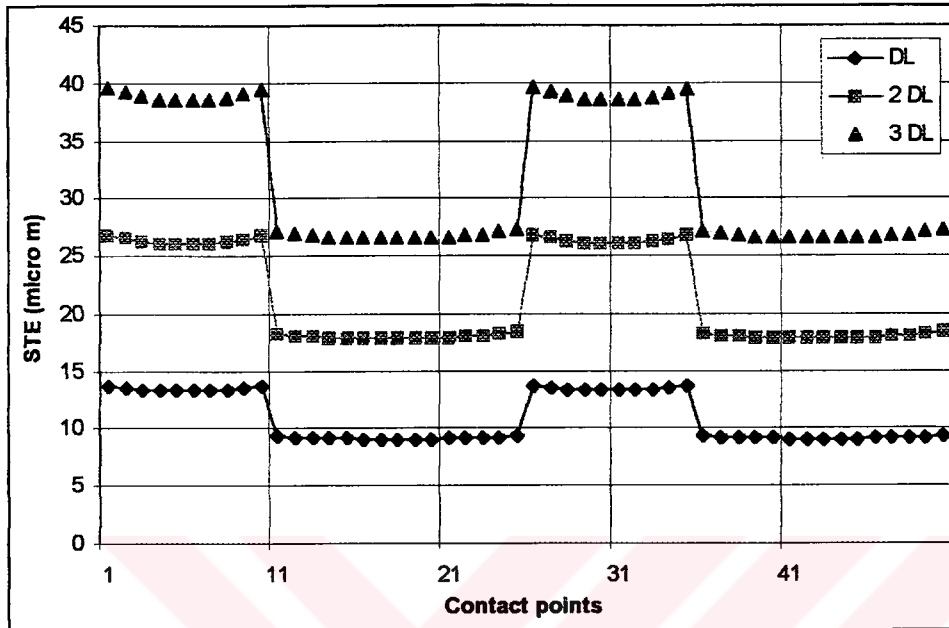

Figure 5.11 Effect of mean load on static transmission error

Static transmission error for different mean loads are plotted in Figure 5.11. It is seen that both single tooth contact and double tooth contact part of the static transmission error graph increase with increasing load. As a result the jump amplitude increases too. STE certainly depends on the deflections of the tooth through the applied load.

Figure 5.12 shows the dynamic transmission error for different mean loads. In Figure 5.12 it is seen that dynamic transmission error increases with increasing mean load. In fact this increase in the amplitude of dynamic transmission error is the effect of mean load through STE. Although the DSLR which is simply the maximum dynamic force over mean load, is the same for different analyses, it is seen that dynamic transmission error which has direct

relation with dynamic forces is not the same. This implies high noise and high dynamic forces when mean load increases.

When the jump magnitudes versus load to design load ratio are plotted in Figure 5.13, it is observed that there is almost a linear relation between jump magnitude and load to design load ratio.

High STE does not always implies high DSLR but the magnitude of the jump in STE causes high dynamic forces. There is a linear relation between load to design load ratio and jump magnitude which is the main cause of dynamic forces. As the mean load is increased, the dynamic force increases as a result of high jump in STE, nevertheless the ratio of dynamic forces to static forces tends to remain constant. It can be said that DSLR is a system property which is determined by the system parameters. It is independent of the applied mean load. The dynamic transmission error also increases with mean load.

5.6 Case Study V: Effect of module

In this part, effect of gear module on DSLR, mesh stiffness and STE are studied. All the parameters of the Kubo's setup other than module is kept the same and module has been changed.

Mesh stiffness which is calculated by LDP for different modules are shown in Figure 5.14. It can be seen in Figure 5.14 that, as the module is increased the mesh stiffness increases for single tooth contact, whereas it decreases for double tooth contact. However the average mesh stiffness remains the same.

In Figure 5.15 STE calculated by LDP for different modules are shown. As it is seen in Figure 5.15 both STE and the magnitude of jump decrease as the module increases. However contact ratio does not change.
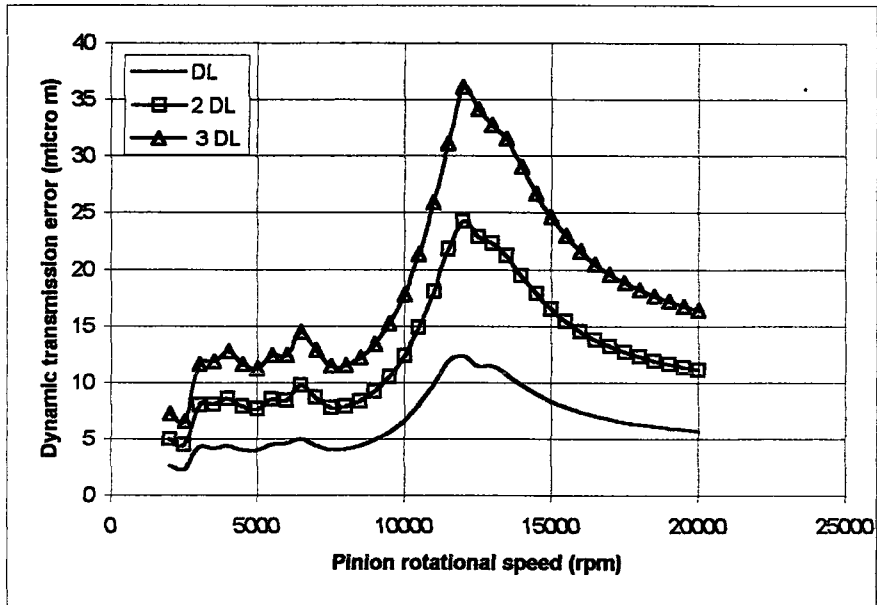
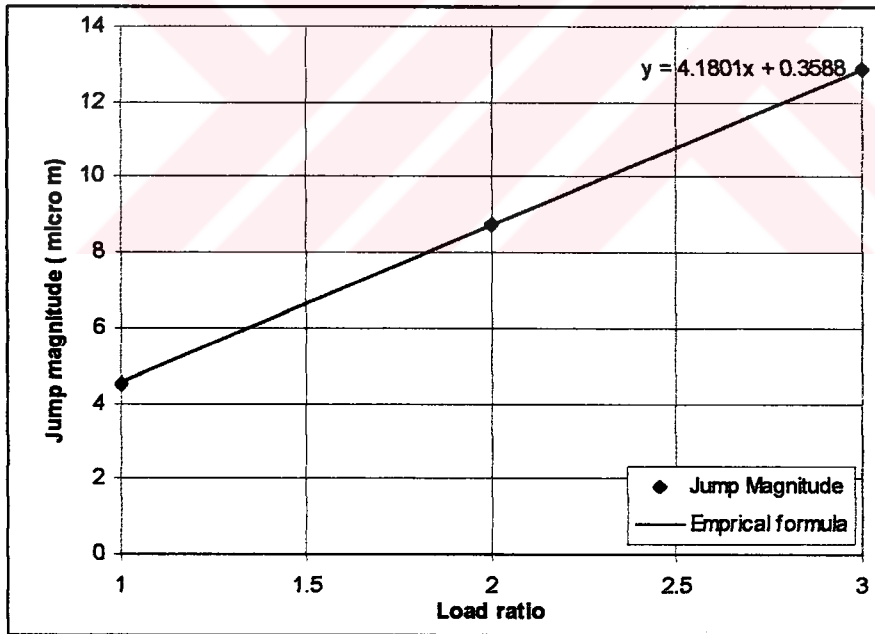Figure 5.12 Effect of mean load on dynamic transmission error

Figure 5.13 Jump amplitude of STE versus Load ratio

94

Frequency response of the system for different modules are plotted on Figure 5.16. It can be that DSLR decreases as the module is increased due to the high STE, and the resonance frequency shifts to lower frequencies since the gear mass increases. The tooth separation becomes more significant at small modules, since the magnitude of jump in the excitation displacement, which is given by the difference between maximum and minimum values of STE, attains larger values for smaller modules.
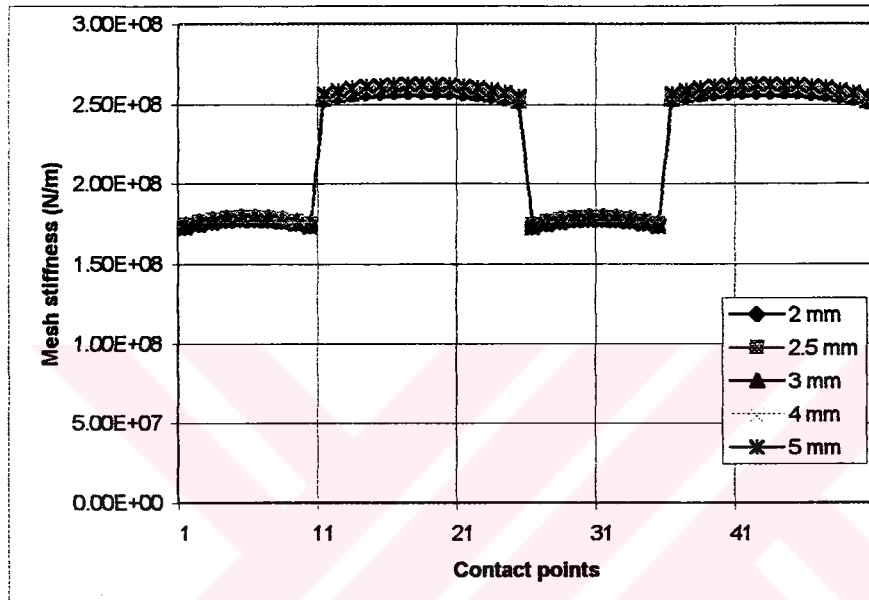

Figure 5.14 Effect of module on mesh stiffness

In Figure 5.17 maximum DSLR versus module is plotted. Logarithmic regression fits the data best. In Figure 5.18 log (Max DSLR) versus log(Module) is plotted, and the equation of the linear regression line is obtained as:

$$\log(Max.DSLR) = -0.3718\log(Module) + 0.5758 \qquad (5.1)$$

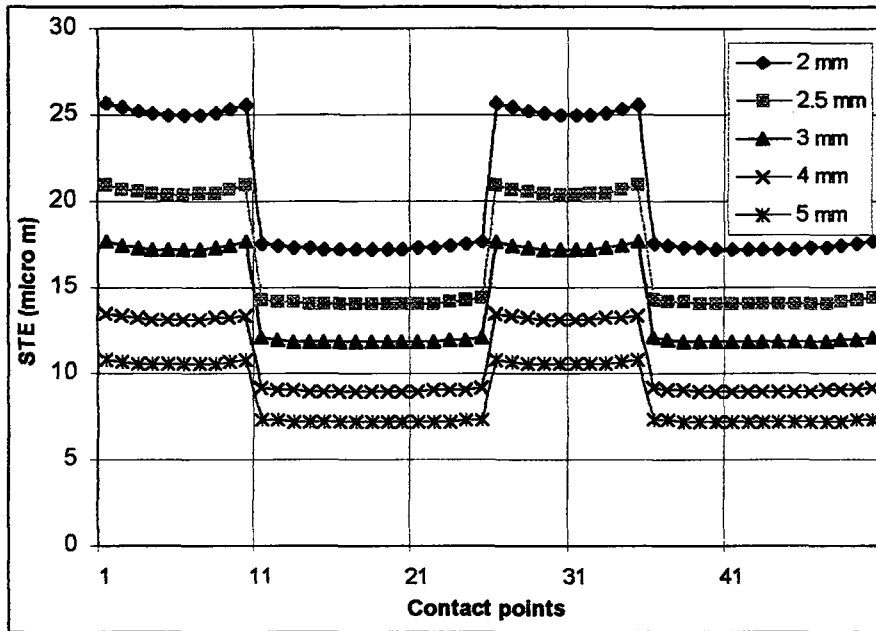In Figure 5.19 Equation 5.1 is plotted for a wide range of modules.

95

Figure 5.15 Effect of module on static transmission error

The marked points show the values calculated by NLGRD. The square ones are used in regression analysis, and the triangles are used to compare with the empirical predictions, which are represented by the continuos line. When module is very large, maximum DSLR approaches to zero. When module is small, amplitudes of Maximum DSLR attains larger values. Table 5.5 shows maximum DSLR calculated by using NLGRD and the empirical equation. The extrapolation is observed to be very successful.

In the second attempt, gear pair is moved to the middle of the second shaft and NLGRD is ran for modules 2, 2.5, 3, 4, 5 mm. The maximum DSLR versus module is plotted in Figure 5.20 and linear regression is made. The equation of the regression is :

$$\log(\text{Max.DSLR}) = -0.4543\log(\text{Module}) + 0.5857 \tag{5.2}$$

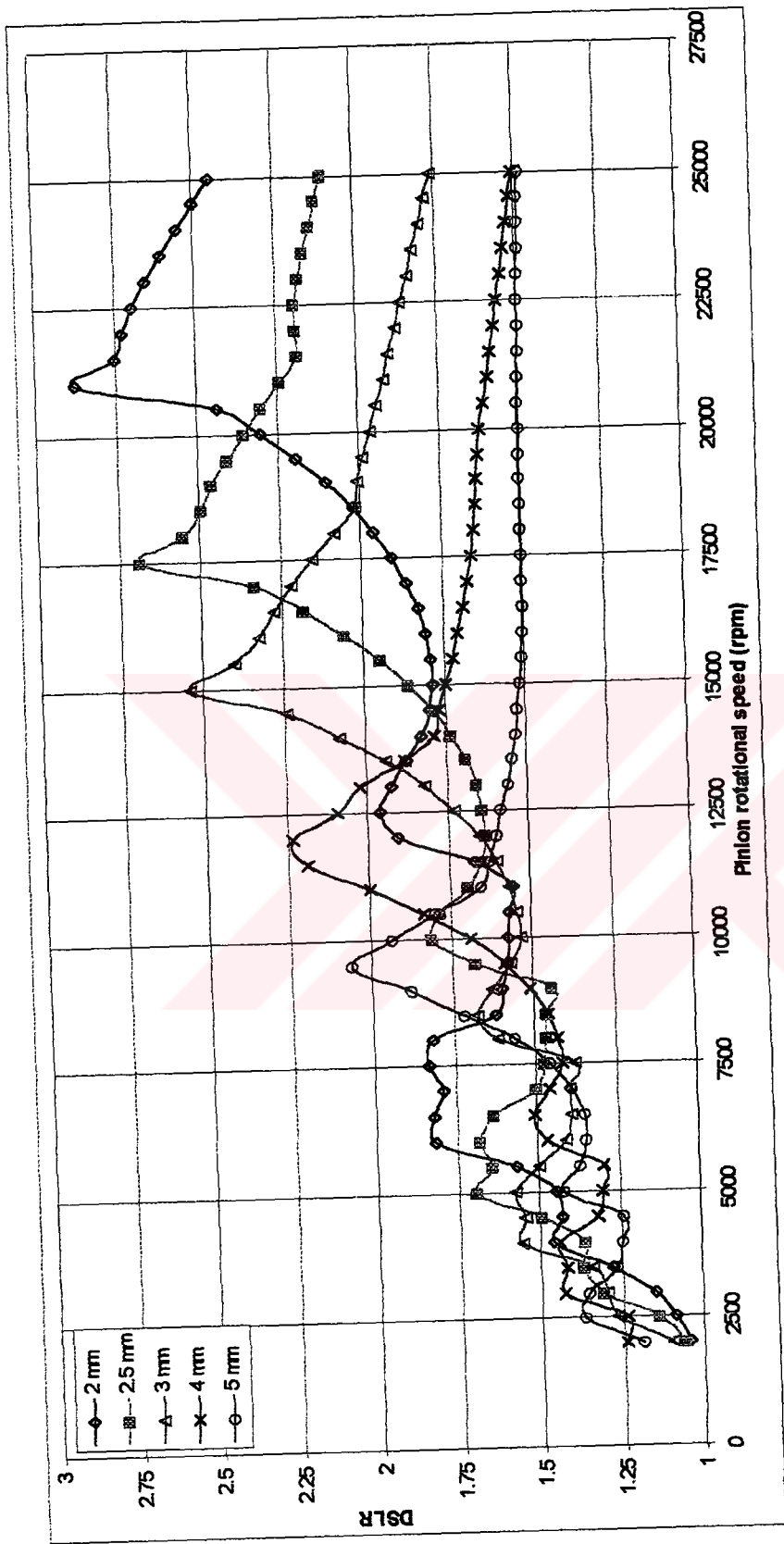In Figure 5.21 Equation 5.2 is plotted for a wide range of modules

Figure 5.16 Effect of gear module on DSLR

97

Table 5.5 Empirical and calculated DSLR

Module (mm)	Max DSLR (NLGRD)	Max. DSLR (Empirical)
10	1.563	1.599
20	1.278	1.244

and compared with the calculated Maximum DSLR. Equation 5.2 is successful in interpolation. It is also successful in extrapolation up to module
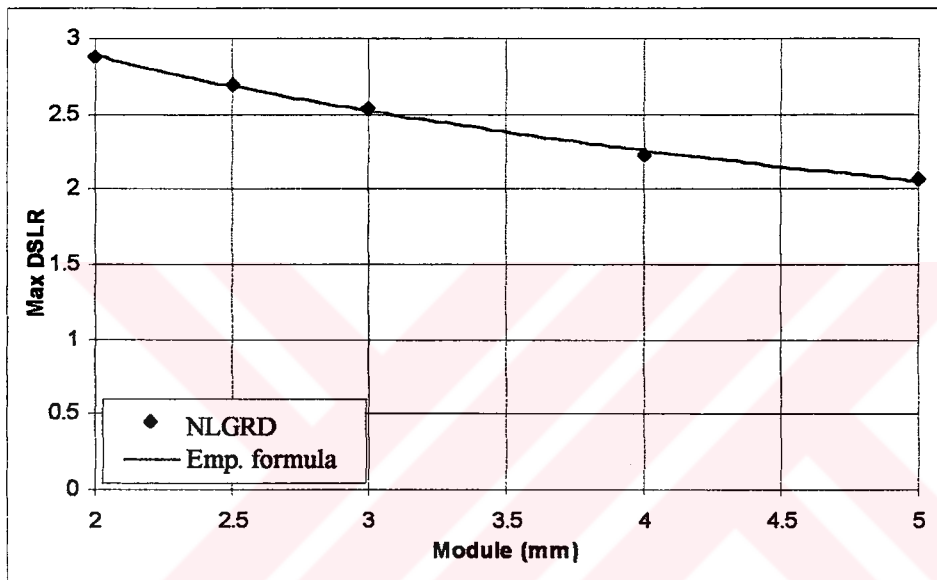

Figure 5.17 Maximum DSLR versus Module graph

10 mm however after 10 mm it is not successful. DSLR falls suddenly under unity for modules larger than 20 mm which seems unlogical.

In order to improve accuracy, the data points 10, 15, 20, 25 mm are included in the regression analysis. In Figure 5.22 it is seen that the data points have a curvature, so a parabolic polynomial is fitted. The new equation is :

$$\log(\text{Max.DSLR}) = 0.1549\log^2(\text{Module}) - 0.6214\log(\text{Module}) + 0.6264 \quad (5.3)$$
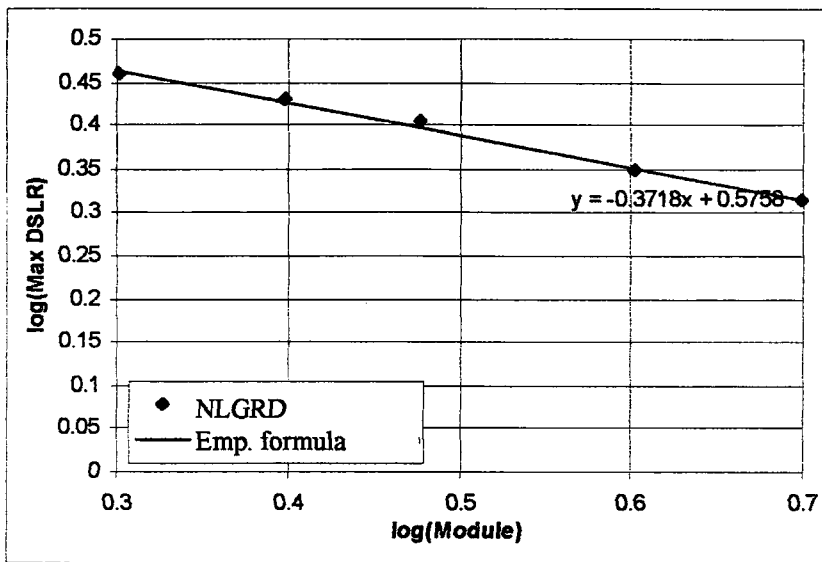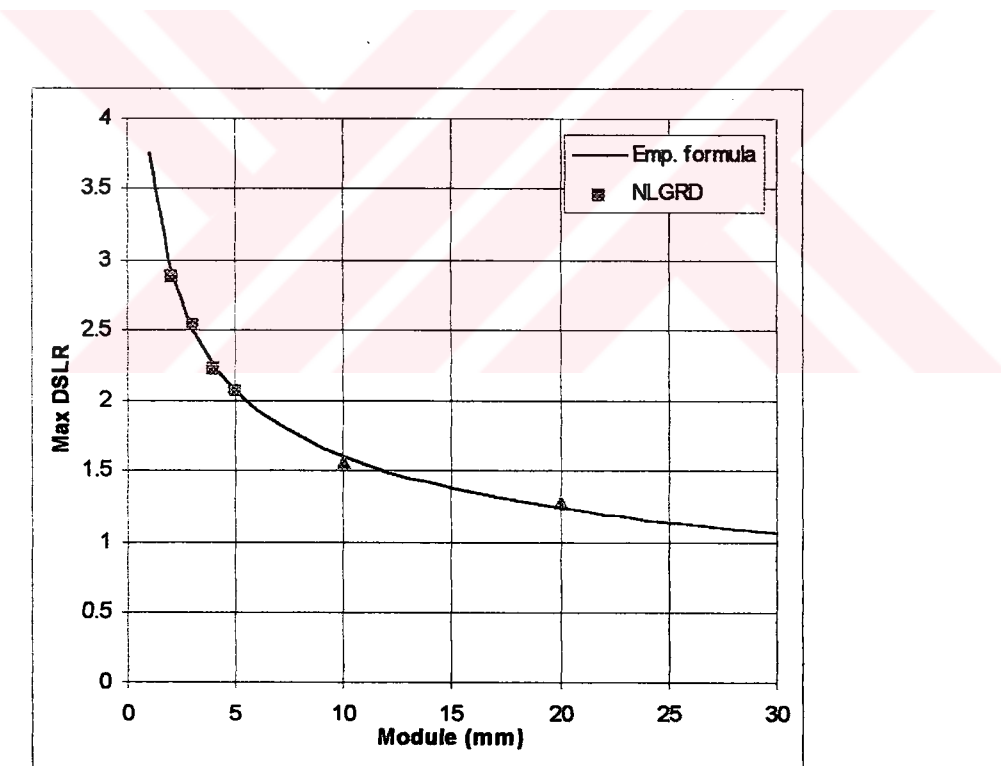
Figure 5.18 log(Max DSLR) versus log(Module) graph

Figure 5.19 Empirical maximum DSLR versus Module graph (■ are used in regression. ▲ are not used in regression)

99

The coefficient of the second order term of Equation 5.3 is significant which justifies using a parabolic equation. Then Equation 5.3 is plotted for a wide range of module values in Figure 5.23. The new data points and higher order regression analysis has improved the trend of the empirical formula at high module values and for high modules empirical formula estimates maximum DSLR values higher than unity which is logical. Table 5.6 shows maximum DSLR calculated by NLGRD and empirical equation results. The error between DSLR calculated by NLGRD and those predicted by Equation 5.3 is very small.

Table 5.6 Empirical and calculated DSLR

Module (mm)	Max DSLR (NLGRD)	Max. DSLR (Empirical)
10	1.409	1.428
15	1.295	1.273
20	1.223	1.188
25	1.139	1.136

When the gear pair is near the bearings, it is seen that there is a logarithmic relation between maximum DSLR and module, and a straight line in log-log scale is able to successfully predict the maximum DSLR at modules other than those used for the regression analysis. But when the gear pair is moved to the middle of the second shaft, and shaft and bearing effects become significant, then a second order curve in log-log scale represents the relation between maximum DSLR and module better.

5.7 Case Study VI: Effect of Center Distance

In this case study the effect of center distance modification on the DSLR, STE and mesh stiffness is studied. Kubo's test rig is used as a model.
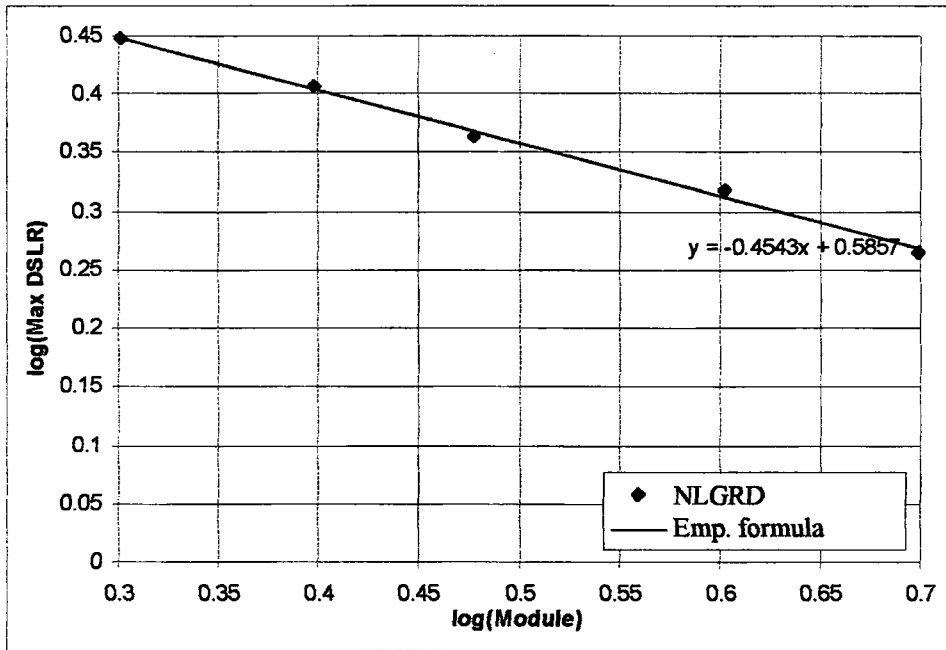
Figure 5.20 log(Max DSLR) versus log(Module) graph
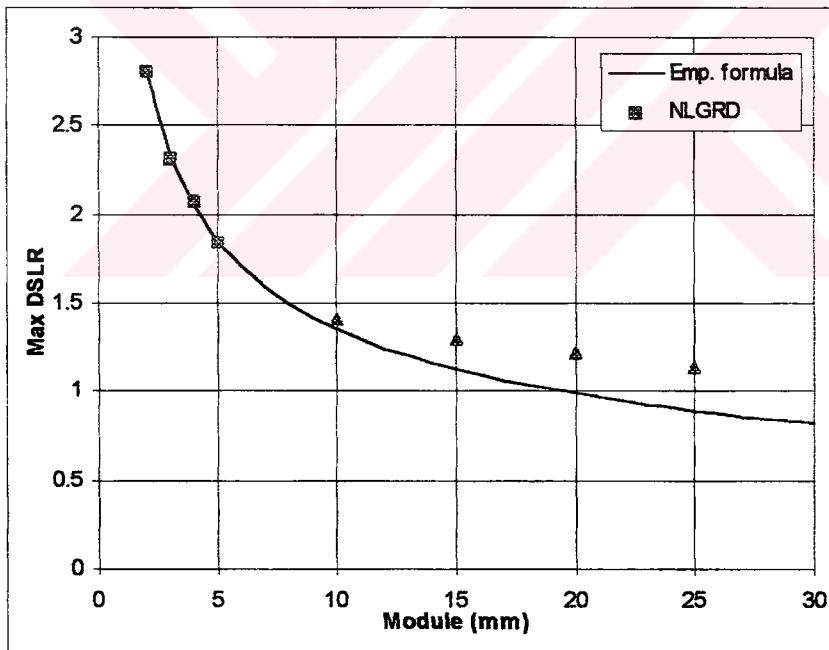

Figure 5.21 Empirical maximum DSLR versus Module graph (■ are used in regression. ▲ are not used in regression)
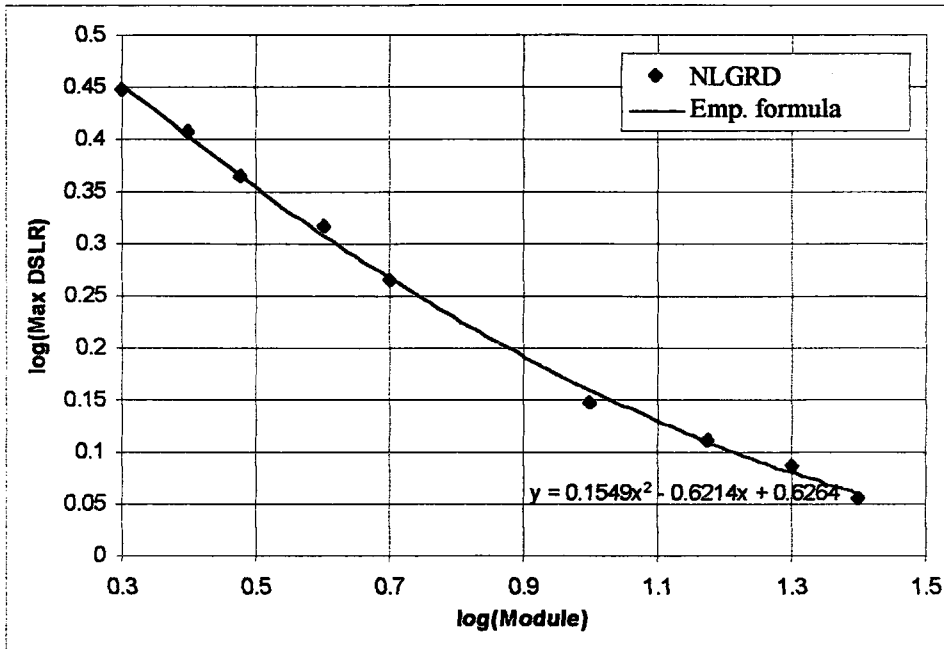
101

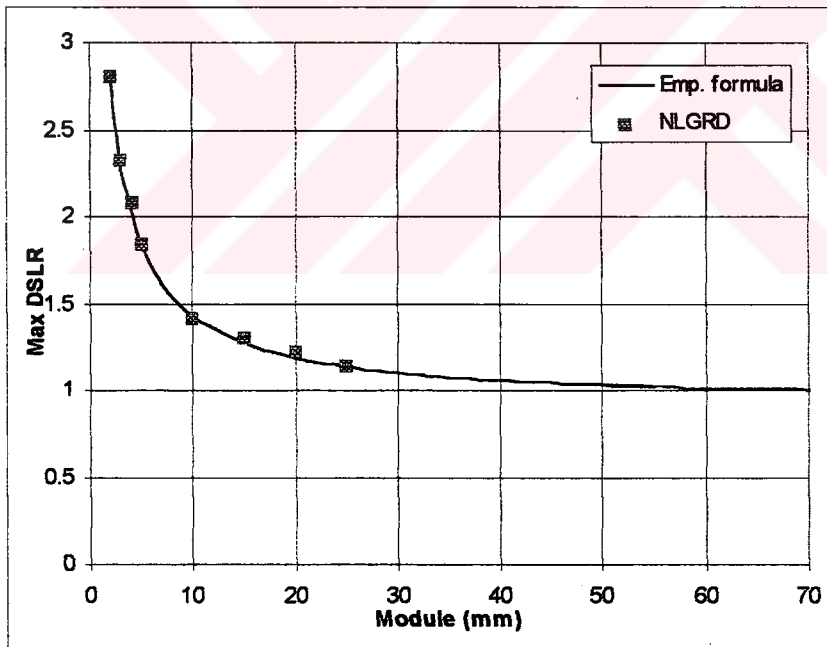Figure 5.22 log(Max DSLR) versus log(Module) graph

Figure 5.23 Empirical maximum DSLR versus Module graph

102

In Figure 5.24 the effect of center distance on mesh stiffness is shown. As it is seen in Figure 5.24, when the center distance increases, the mesh stiffness function assumes curvature and single tooth contact part starts covering the whole mesh period. Thus it reduces the average mesh stiffness. The amplitude of single tooth contact and double tooth contact parts do not change much, though.

Effect of center distance on STE is shown in Figure 5.25. This is the counterpart of the mesh stiffness function. Center distance has the same effect on STE. Figure 5.25 shows that the single tooth contact part of STE starts covering the whole mesh period since the ratio of single tooth contact period to mesh period increases as the center distance increases

Table 5.7 tabulates the theoretical contact ratio and pressure angle for different center distances. Table 5.7 shows that contact ratio decreases as the center distance increases. This validates the results of LDP.

Table 5.8 tabulates the average mesh stiffness, amplitudes of STE and torsional resonance frequency for different center distances. It can be observed from Table 5.8 that average mesh stiffness decreases with increasing center distance. In Figure 5.24, although the amplitudes of single tooth contact and double tooth contact parts of the mesh stiffness do not change. Their period ratio changes, and therefore average mesh stiffness approaches to the amplitude of the single tooth contact part of mesh stiffness function. Since the average mesh stiffness decreases, the torsional resonance frequency decreases too. As the center distance increases, amplitude of STE decreases, therefore the amplitude of vibration is expected to decrease.

Figure 5.26, Figure 5.27 and Figure 5.28 show the FFT approximation of STE for center distances 100 mm, 102 mm and 102.5 mm, respectively. In Figure 5.26 where period of high and low amplitude parts of STE are almost equal, the single harmonic is sufficient to approximate the

general shape of STE. However in Figure 5.27 and Figure 5.28 where the high

Table 5.7 Contact ratio and pressure angle for different center distances

Center distance (mm)	Contact ratio	Pressure angle (deg)
100	1.51	20
100.5	1.40	20.72
101	1.29	21.45
102	1.09	22.84
102.5	1.0	23.5

Table 5.8 Mesh stiffness, STE and resonance for different center distances

Center distance (mm)	Average mesh stiffness (N/m)	Amplitude of STE (m)	Resonance RPM
100	0.2258E9	0.20263E-5	11967.6
100.5	0.21033E9	0.22434E-5	11550.4
101	0.19495E9	0.22091E-5	11120.2
102	0.16809E9	0.14467E-5	10325.7
102.5	0.15282E9	0.87478E-6	9845.4

amplitude and low amplitude parts of STE are not equal, higher harmonics contribute to the shape of approximation. Therefore higher harmonics must be included in the analysis of gear pairs which have low contact ratio. Figure 5.29 and Figure 5.30 show the amplitudes of harmonics of STE and change of DLSR with rotation speed for different center distances, respectively. It can be observed that for center distances 100 mm, 100.5 mm and 101 mm, the amplitudes of the first harmonics are almost the same, therefore in Figure 5.30 the trend of DSLR graph is almost the same around the resonance region which is mainly dominated by the first harmonic of STE. In Figure 5.29, the amplitude of second harmonic of STE for center distance 102 mm is larger than the first harmonic amplitude. This results in a subresonance peak amplitude higher than main resonance peak amplitude, as can be seen in Figure 5.30.

The main effect of the center distance in this example is the

104

changing contact ratio through mesh stiffness function and STE function. As the center distance increases, the contact ratio decreases. This results in small
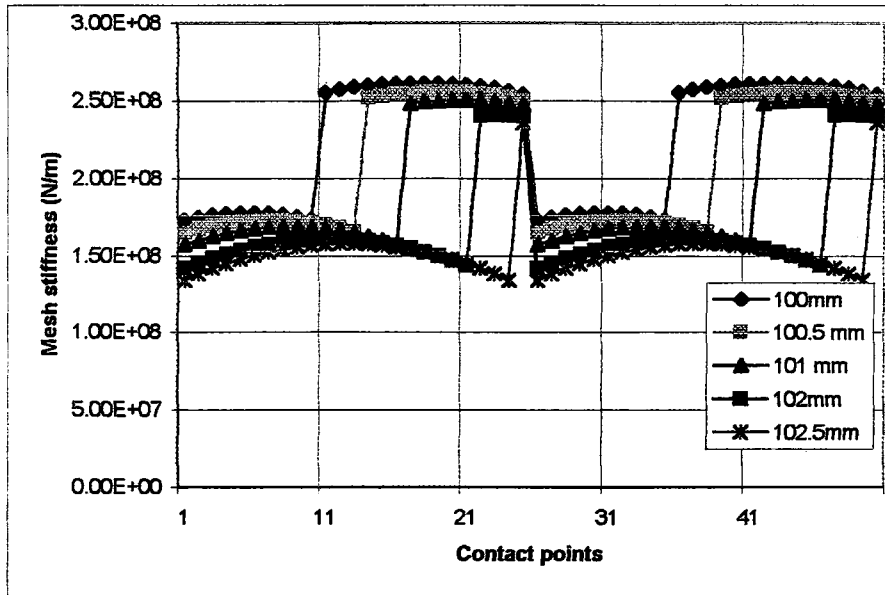

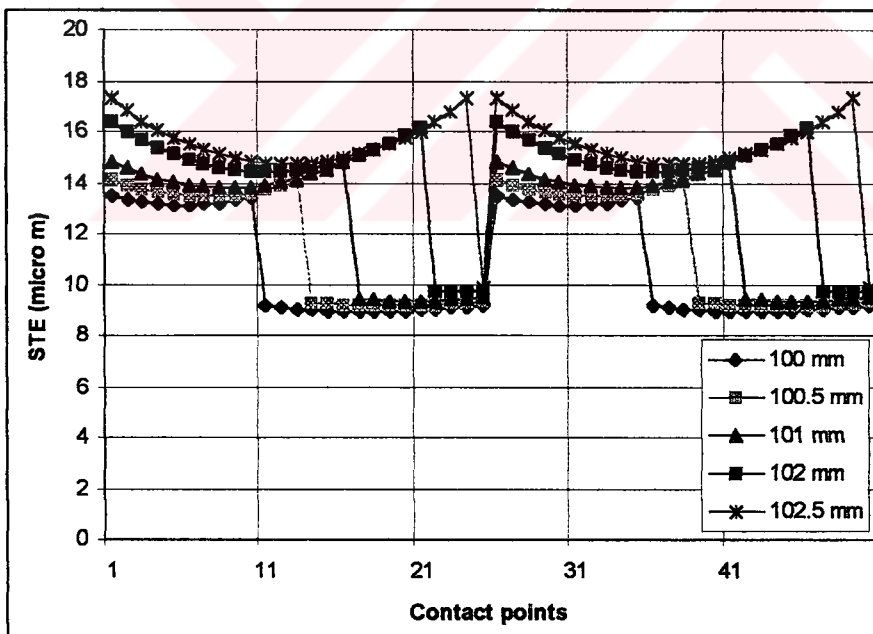Figure 5.24 Effect of center distance modification on mesh stiffness

Figure 5.25 Effect of center distance modification on STE

average mesh stiffness and low STE amplitude. However it is observed that for a specific configuration and a data set up, to a critical value (101 mm in this case) center distance does not effect the frequency response around resonance. At some critical contact ratio (102 mm in this case) at which there exists a sudden impulse in STE function, the amplitudes of higher harmonics can overtake the amplitude of the first harmonic which results in a subresonance peak amplitude higher than the main resonance peak amplitude.

5.8 Case Study VII: Parabolic Profile Modification

The explanation for the change of the static transmission error and mesh stiffness in time lies in the conjugate action of gears. The number of pairs of teeth in contact for a low contact ratio spur gear pair oscillates between one and two. This leads to a sudden increase or decrease in the mesh stiffness hence, results in the variation of the static transmission error. One way to reduce this
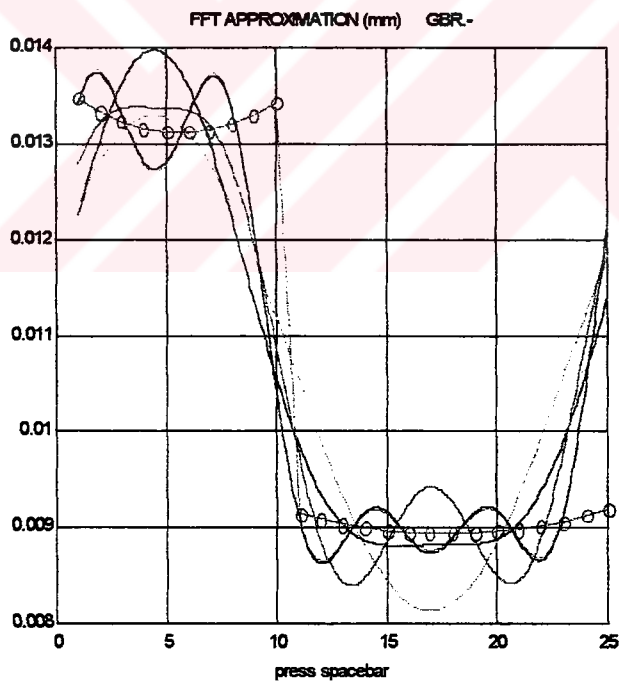
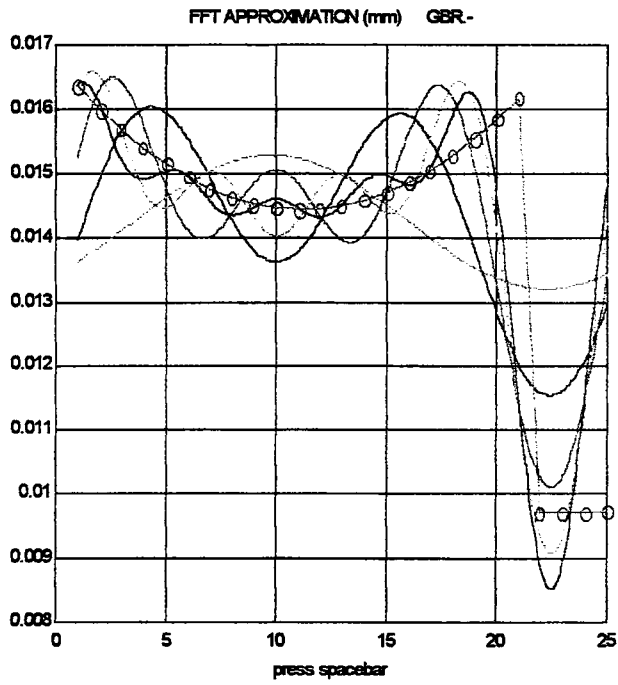Figure 5.26 FFT approximation of STE (center distance = 100 mm)

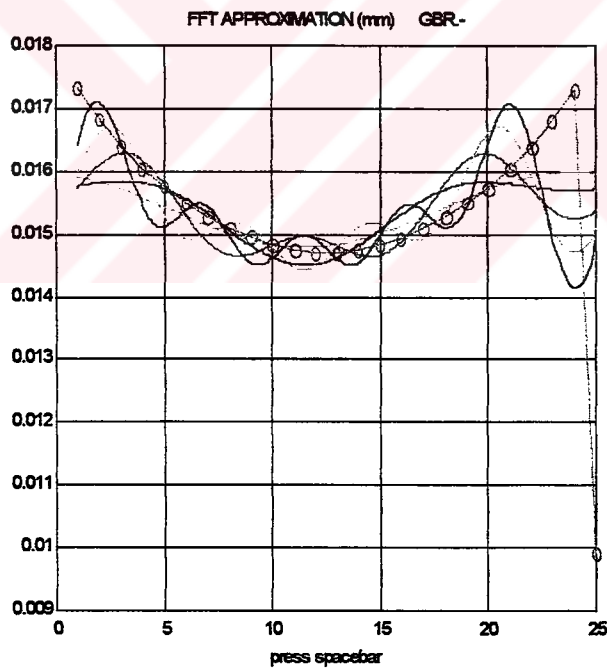Figure 5.27 FFT approximation of STE (center distance = 102 mm)

Figure 5.28 FFT approximation of STE (center distance = 102.5 mm)
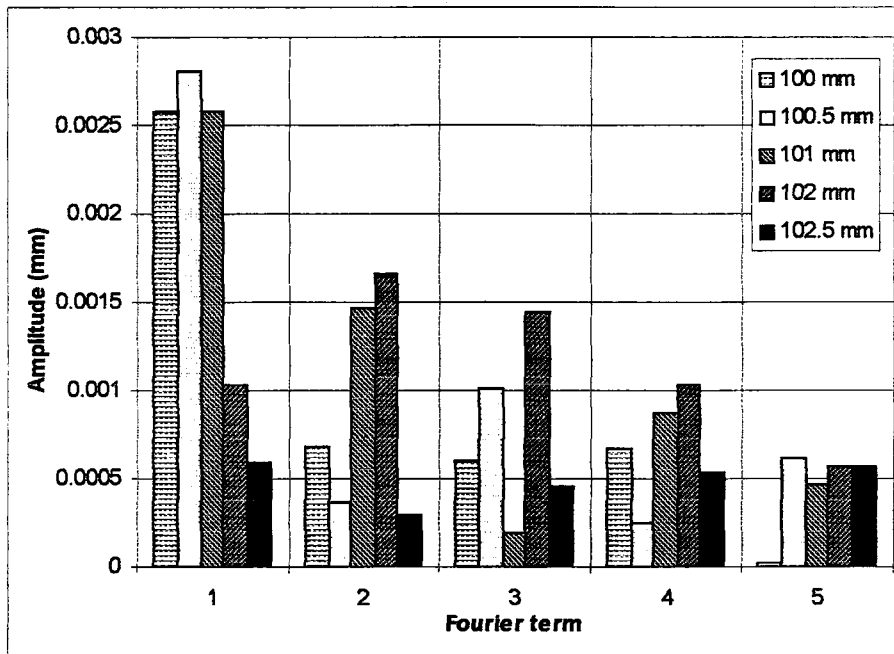
107

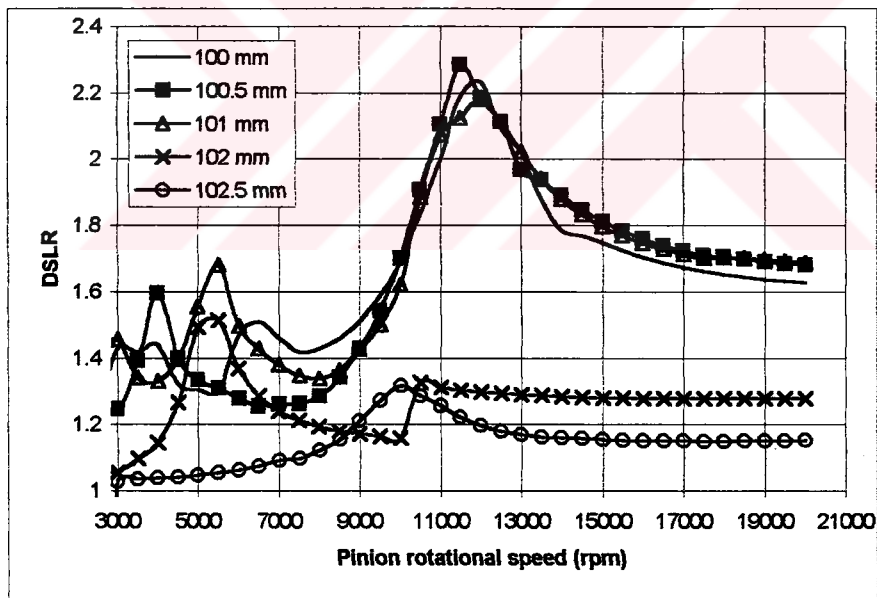Figure 5.29 Amplitudes of STE harmonics of different center distances

Figure 5.30 DSLR for different center distances

variation is to modify the profile of the gear tooth (by relieving the tip/root of gear tooth) such that one tooth starts unloading when the second tooth makes initial contact. This process, called tooth modification, reduces the chance of premature gear tooth impact.

For convenience, the same amount and the same length of profile modifications are assumed to be applied to the tooth tip of both pinion and gear. Since modifying the root of one member has the same effect as modifying the tip of mating member. The amplitude of applied profile modifications used in Kubo's system are listed in Table 5.9

Mesh stiffness functions for different amount of parabolic profile modifications are plotted in Figure 5.31. Figure 5.31 shows that the jump in the mesh stiffness graph takes a more smooth form as the amount of applied profile modification is increased.

Table 5.9 Magnitudes of parabolic modifications

CASE STUDIES	AMOUNT (mm)
No profile modification	0
Case A	0.005
Case B	0.008
Case C	0.01

Figure 5.32 shows the STE for different amount of parabolic profile modifications. It is seen that the lower part of the STE approaches the higher part of STE and takes a curvature form. As a result the main reason of gear vibrations, sudden jump in STE diminishes.

Figure 5.33 and Figure 5.34 show the FFT approximation of STE. These figures suggest that more harmonics are necessary to model the sudden jump in no profile modification case. In Figure 5.34 it is observed that a square wave model of STE is insufficient to simulate the effect of real STE function.

109

Amplitudes of STE harmonics for different amount parabolic profile modifications are plotted in Figure 5.35. Amplitudes of first five harmonics decrease with increasing amount of parabolic profile modification which implies small vibration amplitude.

Figure 5.36 shows the DSLR versus frequency graph. It is seen that application of parabolic profile modification decreases DSLR at all frequencies.

Figure 5.37 shows the dynamic forces on the bearing which is at the left of the first shaft. It shows that dynamic forces follow the same trend of the dynamic mesh forces.

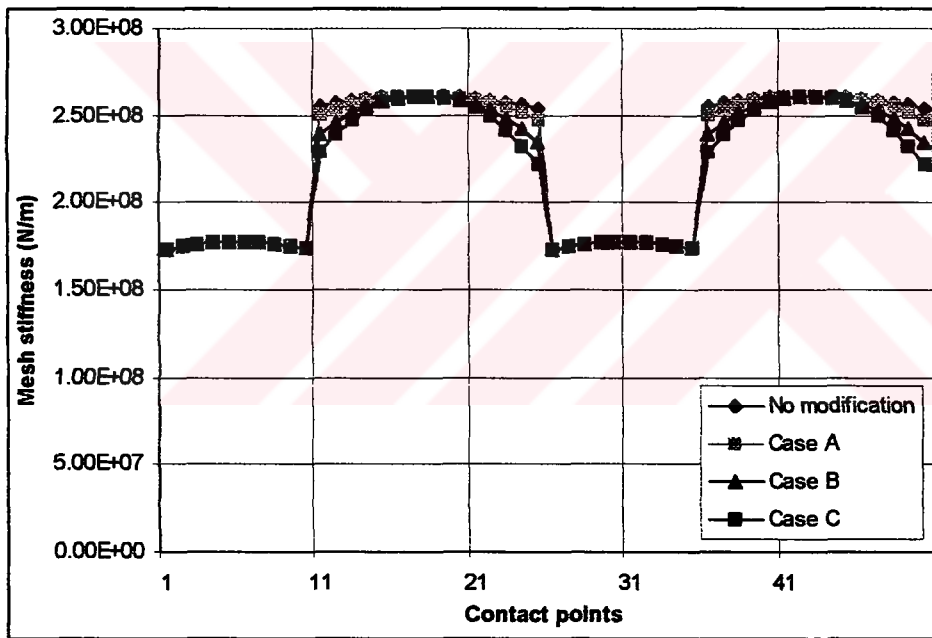Figure 5.38 shows the dynamic forces on the bearing which

Figure 5.31 Effect of parabolic modification on mesh stiffness

Figure 5.38 shows the dynamic forces on the bearing which is at right end of the first shaft. This figure shows that dynamic forces on this bearing decrease at all frequencies as a result of applied modification.

110
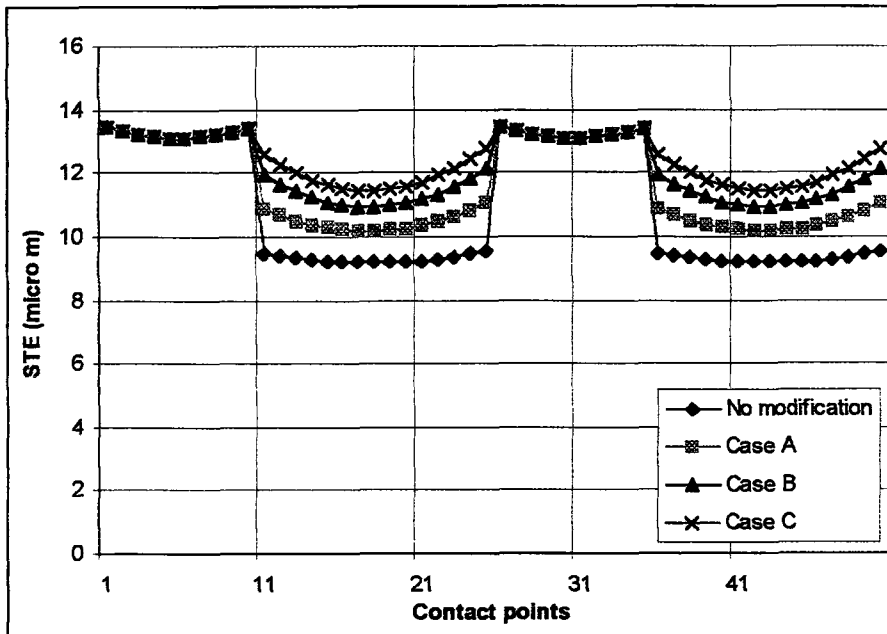
Figure 5.32 Effect of parabolic modification on STE

The maximum DSLR is plotted against the amount of parabolic profile modification in Figure 5.39. Figure 5.39 shows that there is a linear relation between maximum DSLR and the amount of parabolic profile modification within the limits of this study.

Application of parabolic profile modification decreases the DSLR as expected. As the amount of parabolic profile modification is increased both mesh stiffness and STE function start taking a smoother shape so the sudden jump in these graphs diminishes. Therefore the amplitudes of harmonics which directly effect the DSLR graph decrease. It is concluded that using square wave model for STE in case of parabolic profile modification may give wrong results. It is seen that there is a linear relation between the amount of parabolic profile modification and maximum DSLR.

5.9 Case Study VIII: Linear Profile Modification

In this case study the effects of linear profile modification on DSLR, STE, harmonics of STE and mesh stiffness are studied and compared with those of the parabolic profile modification. The amplitudes of the linear profile modifications used are given in Table 5.10

Table 5.10 Magnitudes of linear modifications

CASE STUDIES	AMOUNT (mm)
No profile modification	0
Case A	0.005
Case B	0.007
Case C	0.008
Case D	0.01
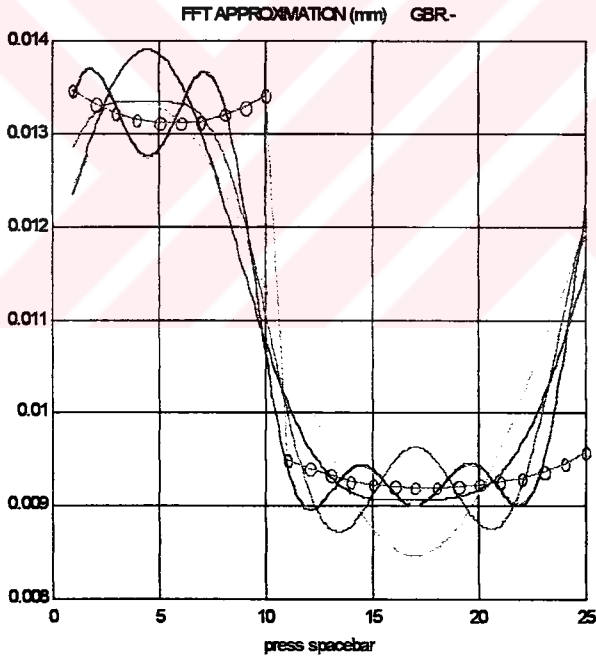
Figure 5.33 FFT approximation of STE (no modification)

Figure 5.34 FFT approximation STE (Case III)

Figure 5.35 Amplitudes of STE harmonics for different modifications

113
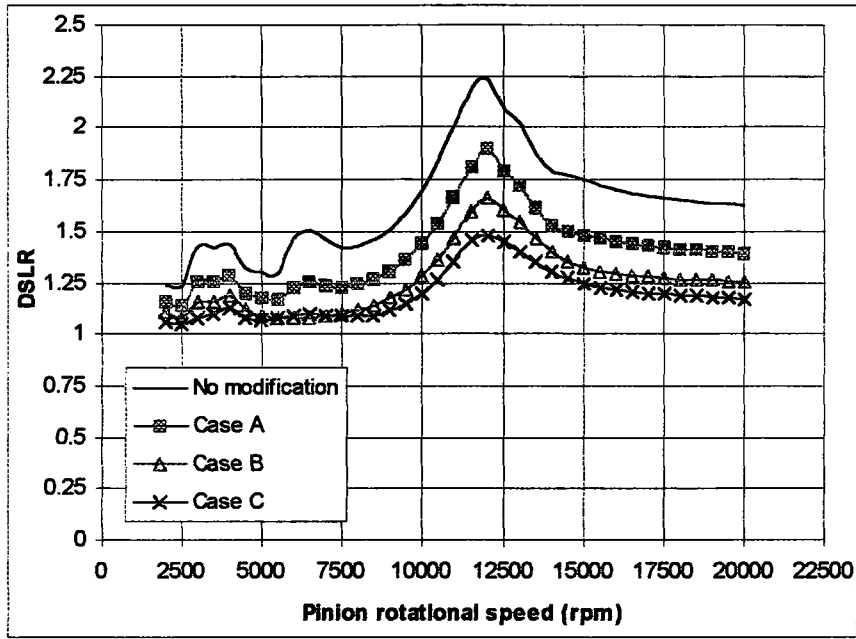
Figure 5.36 DSLR for different parabolic modifications

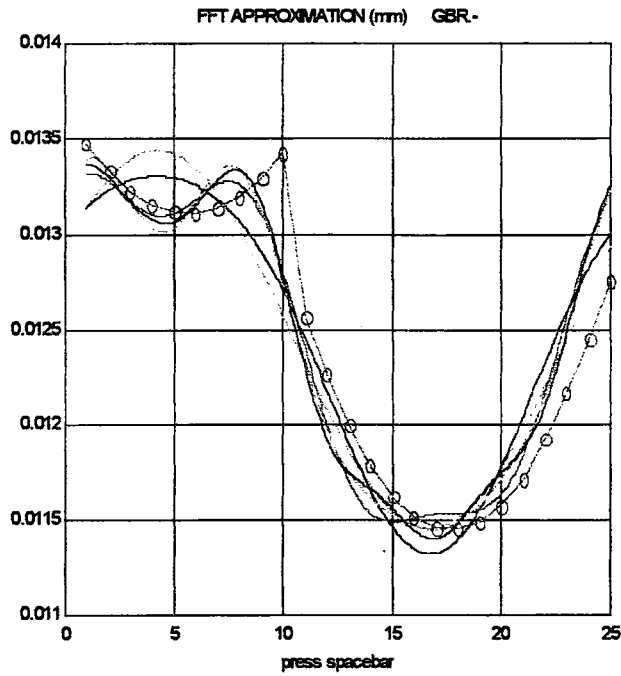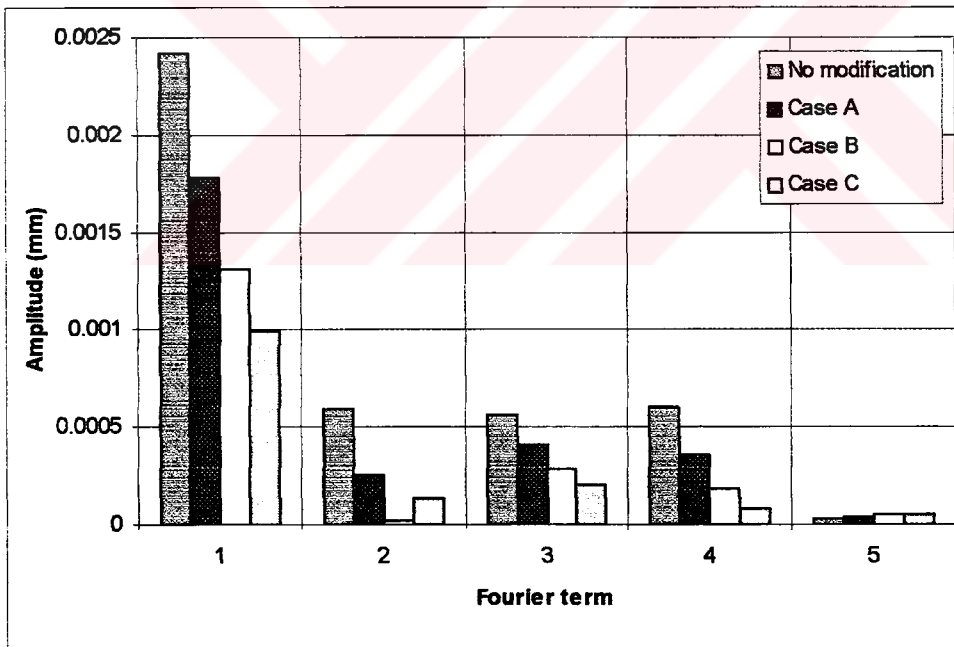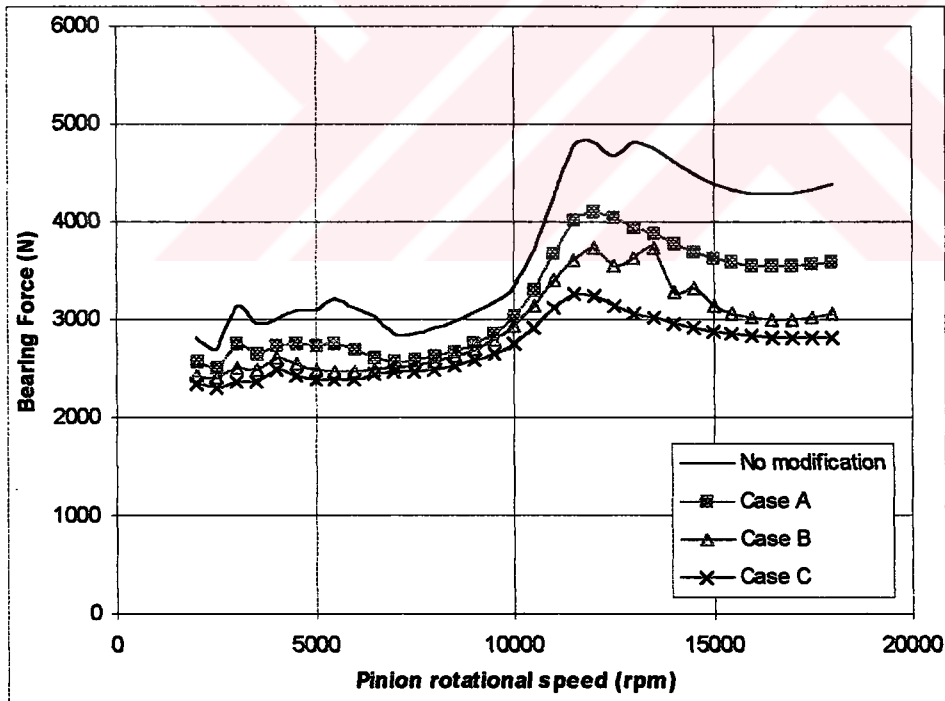Figure 5.37 Effect of parabolic modification on left bearing force

114
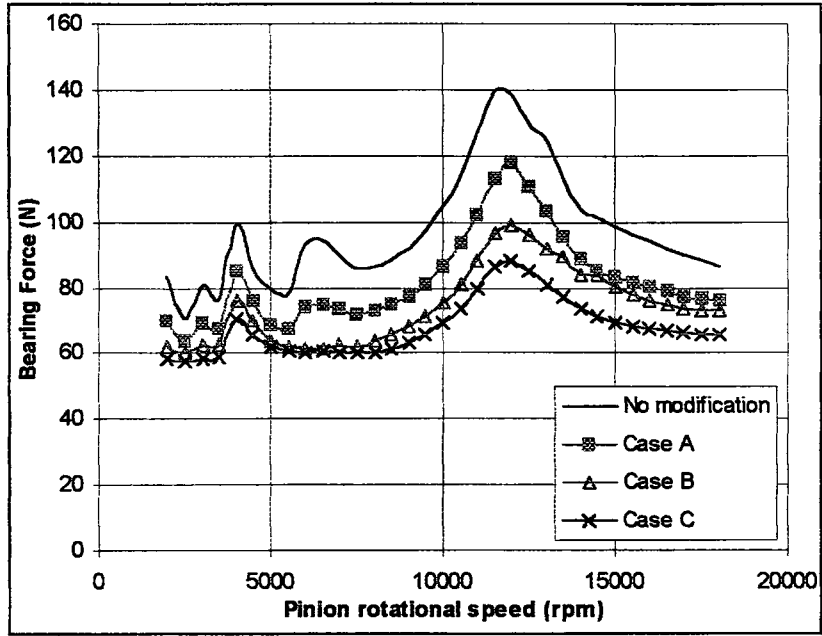
Figure 5.38 Effect of parabolic modification on right bearing force
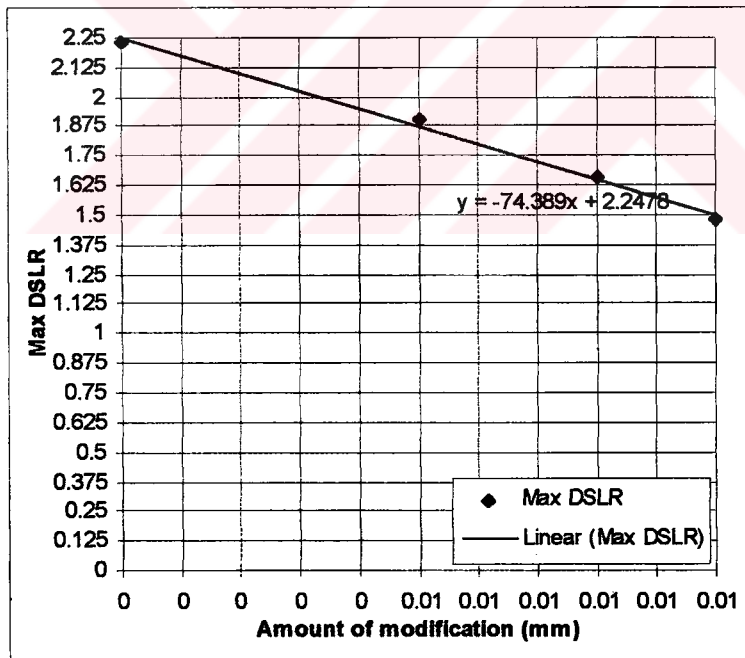
Figure 5.39 Maximum DSLR versus Amount of parabolic modification

115

The mesh stiffness which is calculated by LDP for different amounts of linear profile modifications are shown in Figure 5.40. Figure 5.40 shows that the mesh stiffness function assumes a smooth form as the amount of linear profile modification is increased. Therefore the difference between the maximum and minimum values of the mesh stiffness decreases. Figure 5.41 shows STE which is calculated by LDP for different amounts of linear profile modification. It is seen that as the amount of modification is increased the STE functions becomes a constant line and the jump diminishes. Since the main cause of the gear vibration is the sudden jump in STE it is expected that the amplitude of vibration will decrease.

Figure 5.42 and Figure 5.43 show the amplitude of STE harmonics and DSLR respectively. In Figure 5.42 the amplitudes of all harmonics
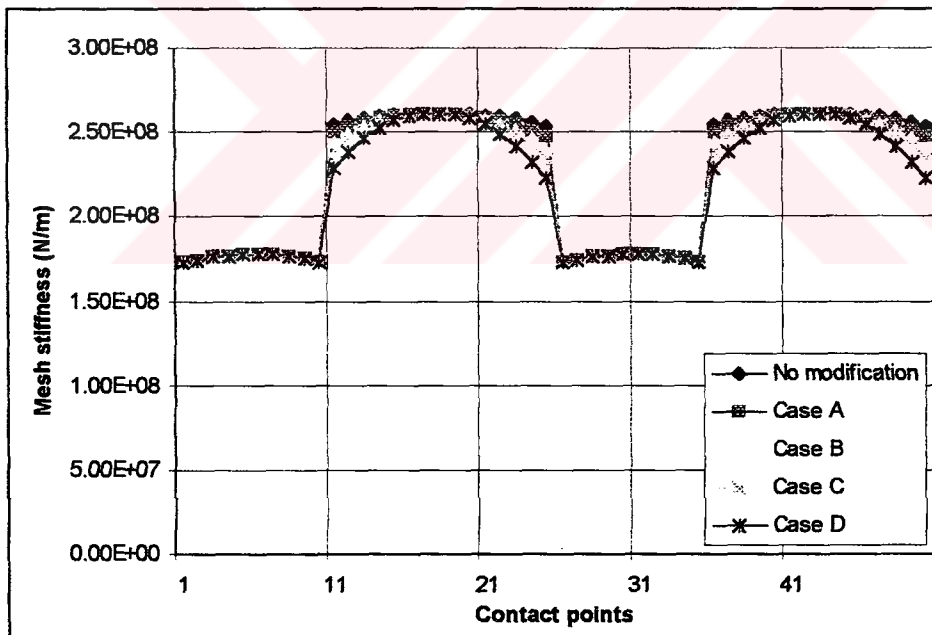
Figure 5.40 Mesh stiffness for different linear profile modifications

116
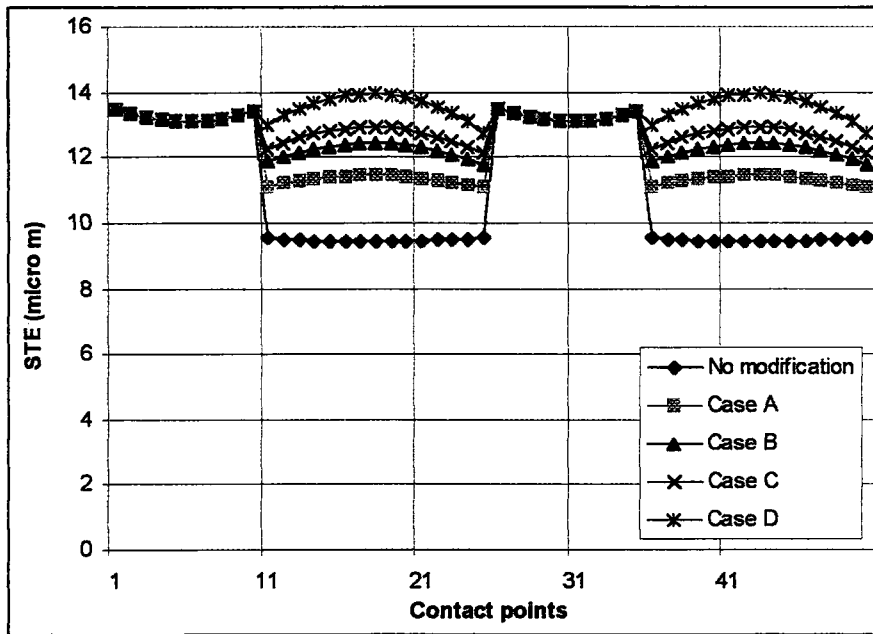
Figure 5.41 STE for different linear profile modifications
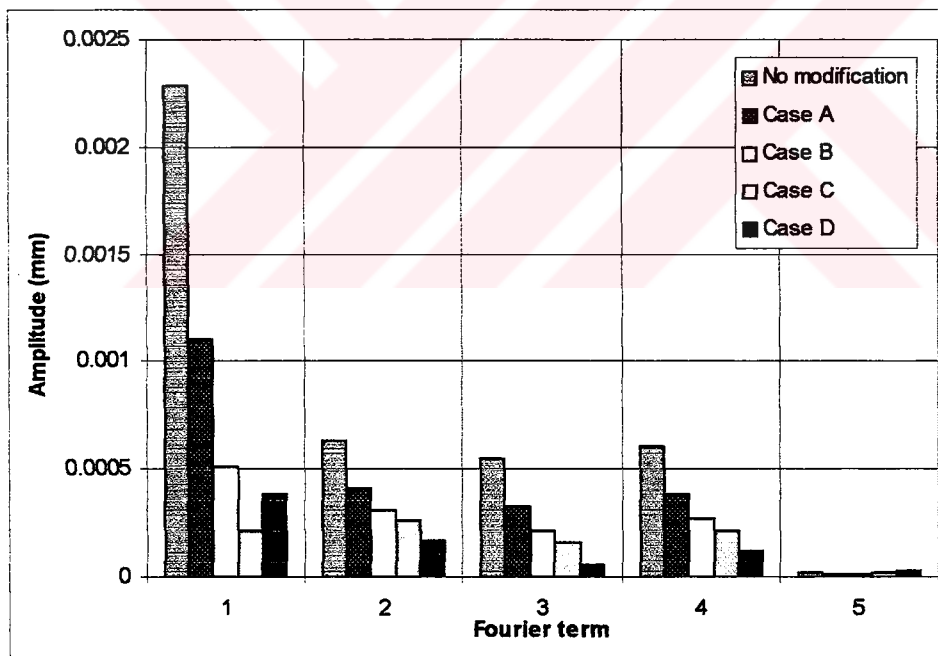
Figure 5.42 Amplitudes of STE harmonics for different linear modifications

117
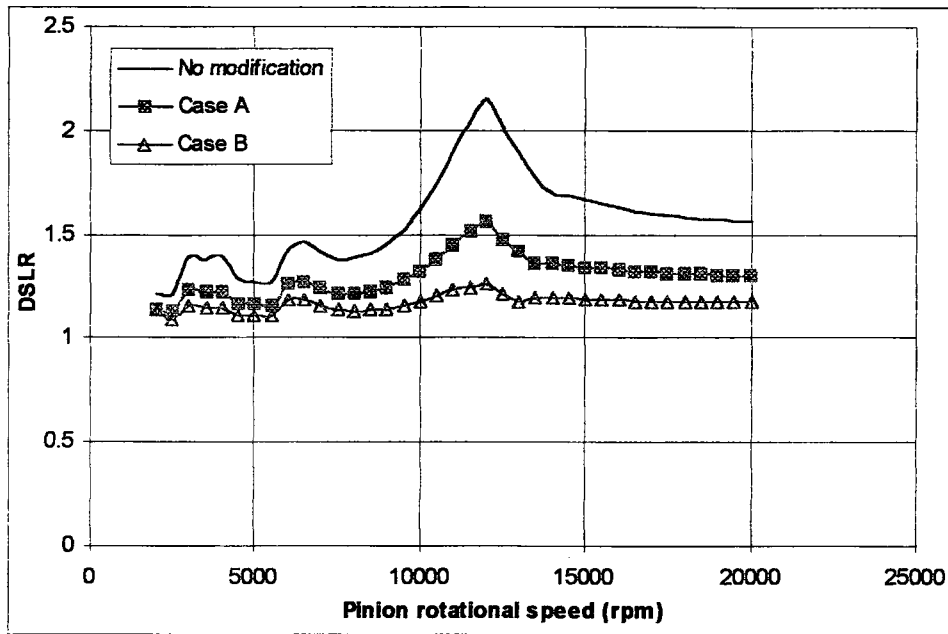
Figure 5.43 DSLR for different linear profile modifications

decreases as a result of linear profile modifications. Figure 5.43 shows that DSLR decreases as the amplitude of linear profile modification is increased.

Figure 5.44 and Figure 5.45 show the dynamic force on the on the left and the right bearings, respectively. It is seen that application of linear profile modification decreases the dynamic forces on both bearings as well.

In Figure 5.46 the maximum DSLR is plotted against the amount of linear profile modification. It is observed that there is a linear relation between the amount of profile modification and Maximum DSLR within the limits of this study.

This case study shows that linear profile modification is effective in reducing both the dynamic mesh force and the dynamic bearing force as it is stated by other authors. Linear profile modification reduces the dynamic mesh force by giving a smooth form to both mesh stiffness and STE.

Figure 5.42 and Figure 5.43 suggest that there is a direct correlation

118

between the magnitudes of STE harmonics and DSLR. Although dynamics of the geared rotor system has important aspects in the analysis, one can approach the problem purely from an excitation point of view in order to decrease the dynamic mesh force.

Comparing Figure 5.43 with Figure 5.36 it can be said that linear profile modifications are more effective in reducing the DSLR than parabolic profile modifications. Both modifications do not change the contact ratio. Figure 5.46 and Figure 5.39 show that the slope of the line giving maximum DSLR is steeper for linear profile modification than for parabolic modification. Therefore it can be concluded that gears with parabolic modifications are much less sensitive to changes in the amount of modification compared to gears with linear modifications. Therefore it is expected that dynamics of parabolic profile modifications of gears would be less affected by manufacturing tolerances.
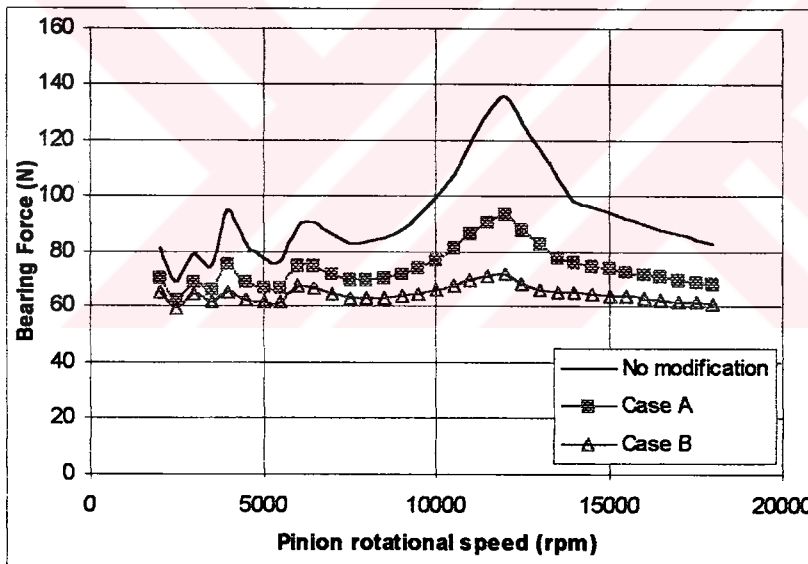
Figure 5.44 Effect of linear modification on left bearing force

5.10 Case Study IX: Tooth Separation

119
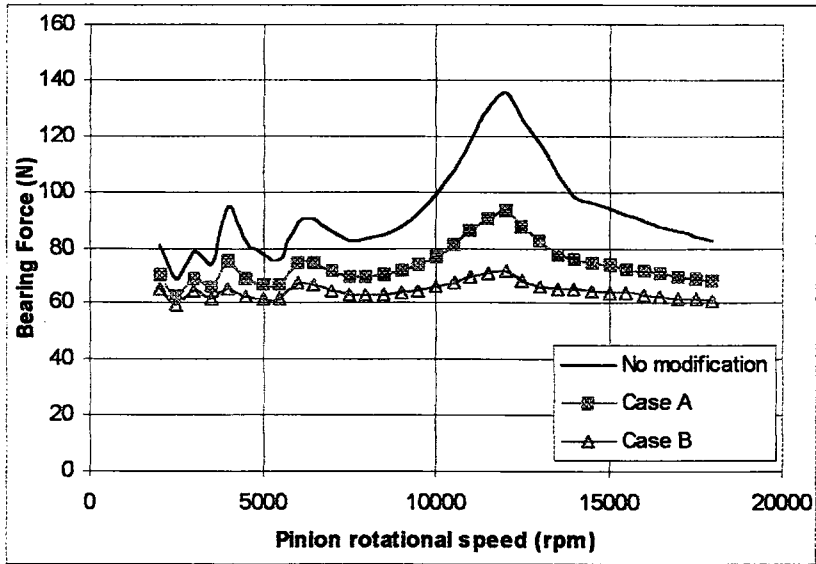
Figure 5.45 Effect of linear modification on right bearing

$y = -126.44x + 2.1647$
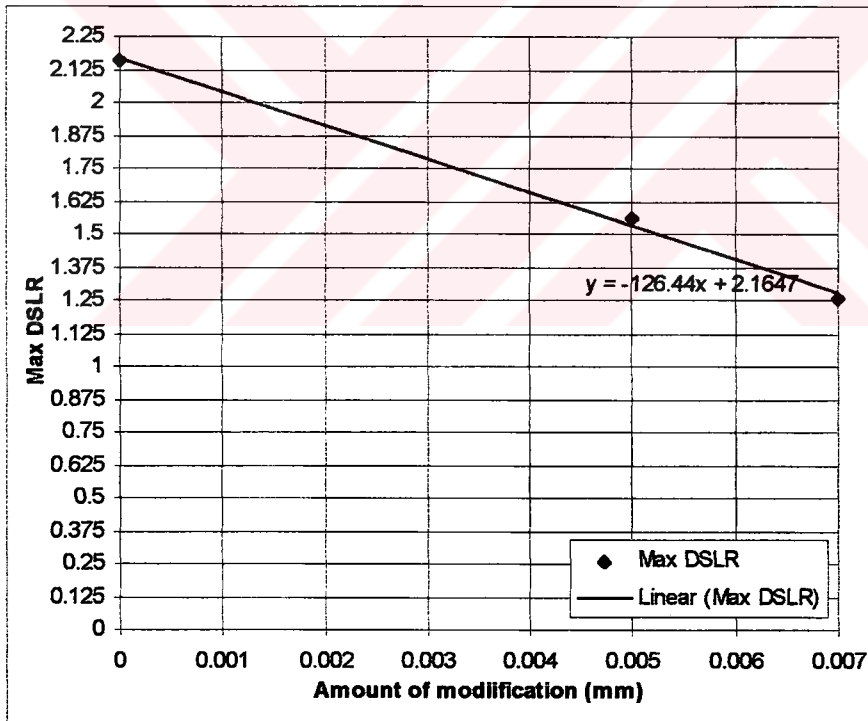
Figure 5.46 Maximum DSLR versus Amount of linear profile modification

120

In this case study tooth separation is studied and several plots giving the change of DSLR and dynamic transmission error with tooth separation are presented.

In this case study the module of the Kubo's setup is reduced to 2 mm since case study VI shows that gears with small modules are more sensitive to tooth separation. The amount of applied backlash is given in Table 5.11

Figure 5.47 and Figure 5.48 show the DSLR for different

Table 5.11 Amount of backlash

CASE STUDIES	AMOUNT (mm)
No backlash	0
Case A	0.005
Case B	0.05
Case C	0.1

backlash amplitudes and damping ratio. In Figure 5.47 when backlash is introduced, resonance frequency shift from 24000 rpm to 20500 rpm and DSLR decreases since the mesh stiffness decreases (as the time spent in backlash region increases, the average mesh stiffness decreases).

Figure 5.47 and Figure 5.48 show that backlash has no effect on DSLR in subharmonic regions where dynamic transmission error is not large enough to cause tooth separation. When the damping ratio is reduced from 0.1 to 0.08 the jump at the resonance becomes more apparent in Figure 5.48. The peak of the system with 0.005 mm backlash (Case A) is larger than the peak of he system with 0.05 mm backlash (Case B).

Figure 5.49 and Figure 5.50 show dynamic transmission error for mesh damping ratio of 0.1 and 0.008 for Case A, respectively. Comparison of Figure 5.49 and Figure 5.50 shows that double sided impact has become more
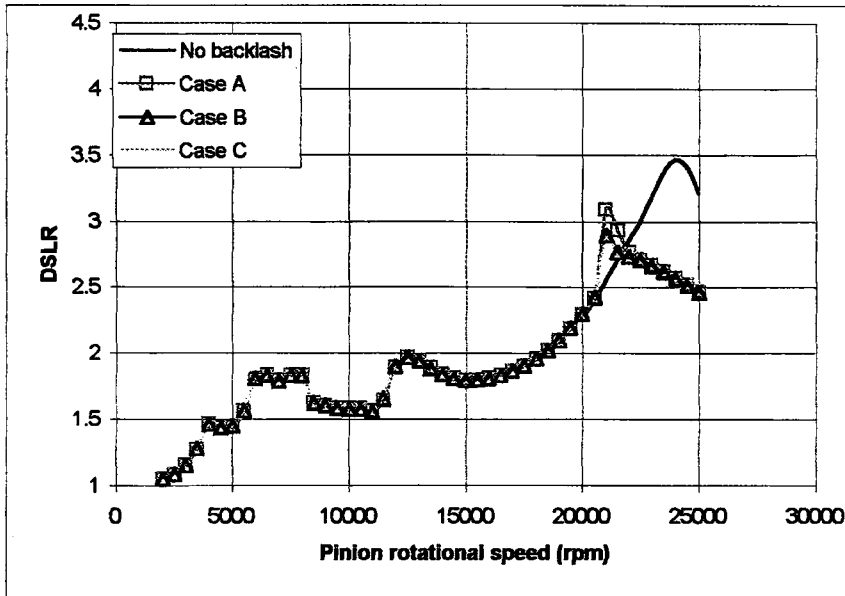
Figure 5.47 DSLR graph (ξ=0.1)
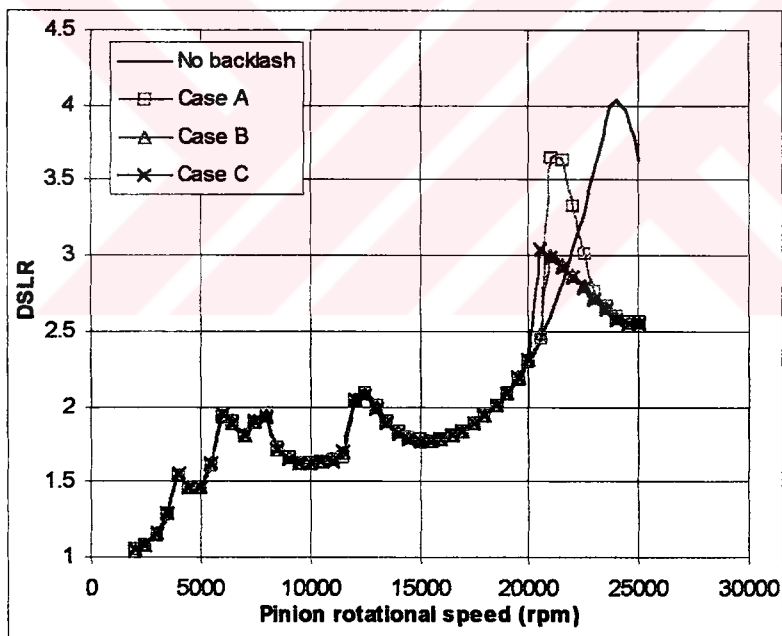
Figure 5.48 DSLR graph (ξ=0.08)
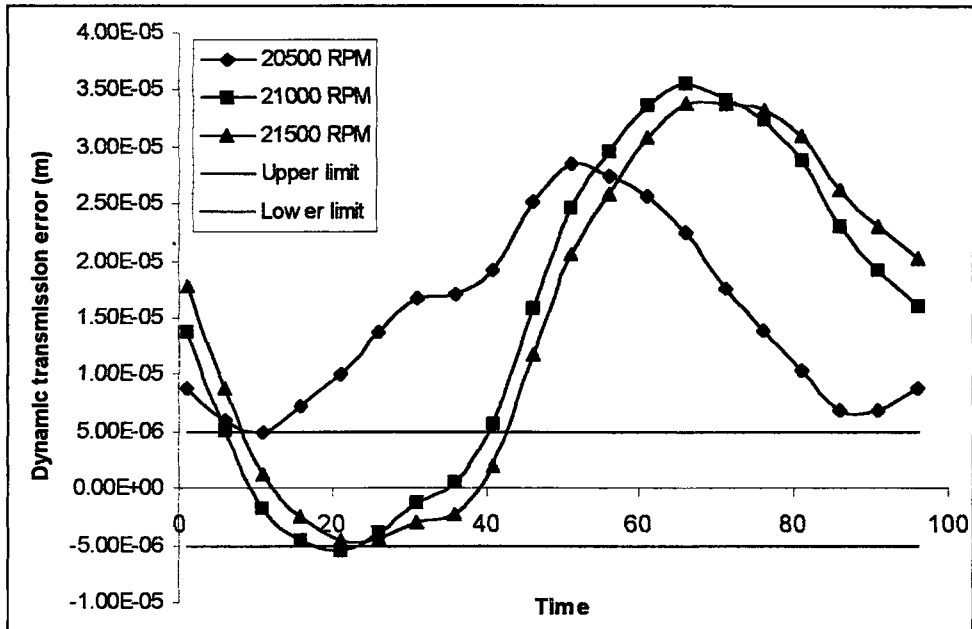
Figure 5.49 Dynamic transmission error graph Case A (ξ=0.1)
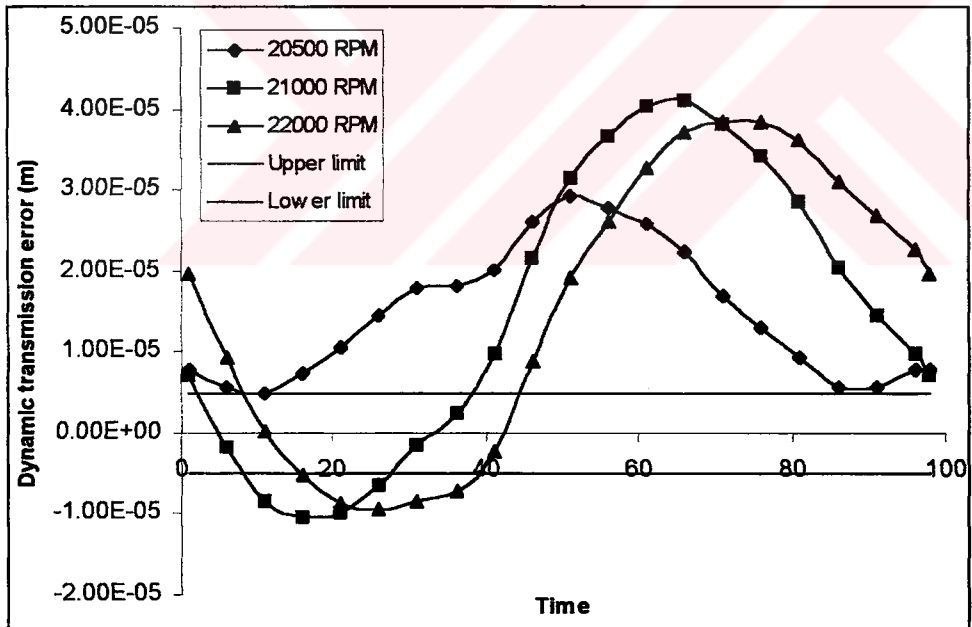
Figure 5.50 Dynamic transmission error graph Case A (ξ=0.08)
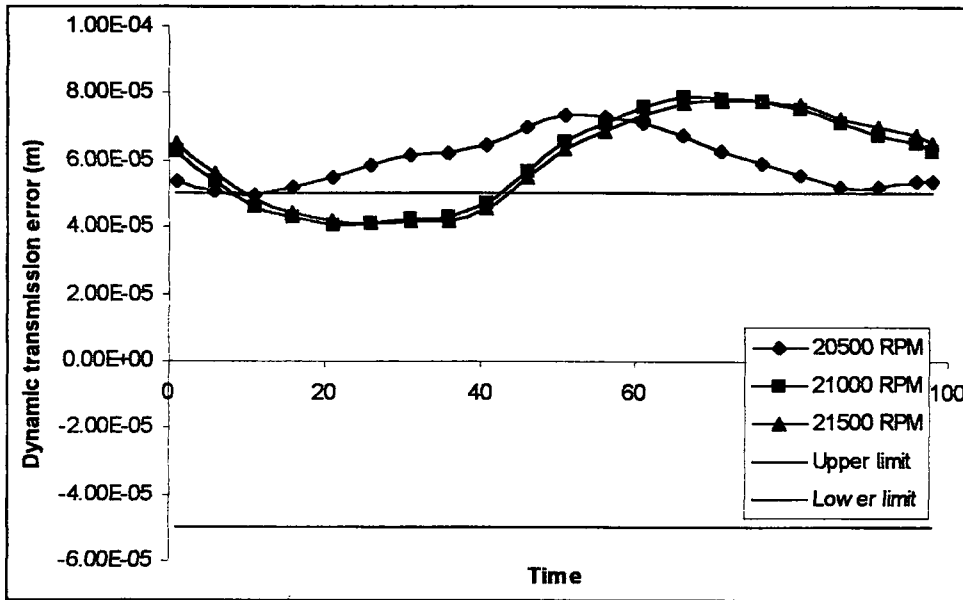
Figure 5.51 Dynamic transmission error graph Case B (ξ=0.1)
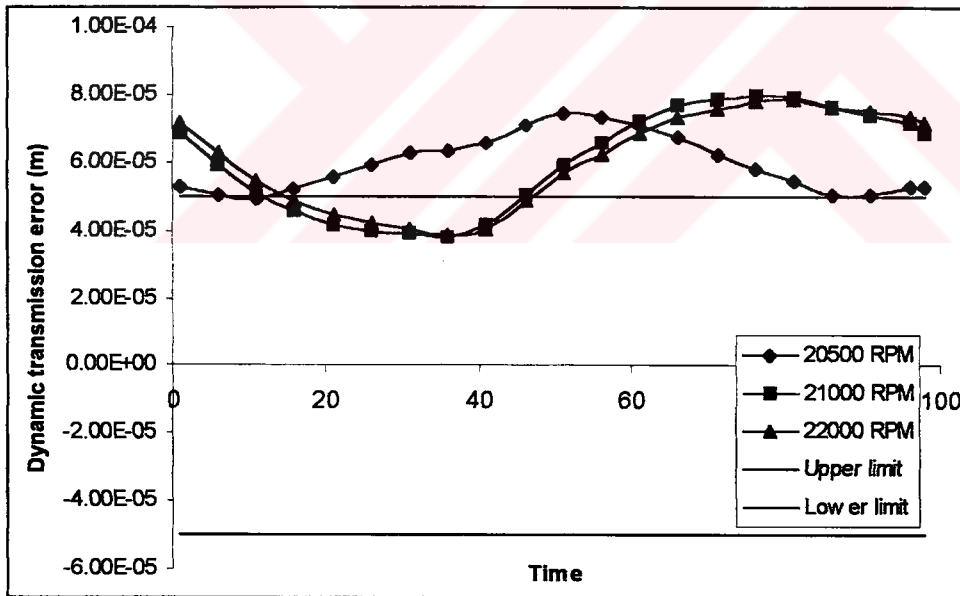
Figure 5.52 Dynamic transmission error graph Case B (ξ=0.08)

124

apparent as the damping ratio is decreased which results in an increase in the average mesh stiffness.

Figure 5.51 and Figure 5.52 show the dynamic transmission error between gears for mesh damping ratio of 0.1 and 0.008 for Case B. Figure 5.51 and Figure 5.52 show that Case A has single-sided impact in both cases.

Up to a certain frequency the system is certainly linear since tooth separation does not take place, however when it reaches to the speed at which backlash is effective (20500 rpm in this case) tooth separation occurs

and dynamic transmission error suddenly increases as there is no restoring force in the system. This causes a sudden increase in DSLR as well.

As the backlash is increased from zero up to a certain value, first double-sided impact then single-sided impact take place. Once tooth separation occcurs, a further increase in backlash does not affect the system response at this speed.

CHAPTER VI

CONCLUSIONS AND RECOMMENDATIONS

6.1 Conclusion

In this thesis, firstly, the computer code NLGRD developed for nonlinear dynamic analysis of gear-shaft-bearing systems, is modified further to compute dynamic bearing forces and make a modal analysis of the corresponding linear system. A user interface which is written in VB 5.0 is also added to the program which allows the user to model the system more easily by using graphical construction. Thus user errors in modeling are tried to be minimized by this new visual interface. Although there exist several dynamic models which consider spur gears, they are neither as accurate as NLGRD for complex configuration nor as professional as the interface of NLGRD. Therefore, the resulting model and the computer code is the most advanced one developed until now.

The dynamic model consists of finite element models of two shafts that are coupled by a typical nonlinear three degrees of freedom spur gear model, which had been used successfully by other authors. The finite element modeling allows one to construct any possible configuration for a single stage gear mesh such as a gear pair on simply supported shafts or overhung shafts, etc. It also allows the user to construct stepped shafts. Thus this new code, NLGRD, has a flexible preprocessor that makes it possible to study more than one configuration by the same computer program. Another important feature of

126

this code is the solution technique. Backlash type nonlinearity in the three degrees of freedom spur gear mesh is modeled by describing functions which allows one to express the dynamic equations of a nonlinear system in frequency domain. Hence nonlinear differential equations are simply converted into nonlinear algebraic equations. Since only a limited number of coordinates are affected from nonlinearity (the three coordinates of the spur gear mesh) system matrices are partitioned and a new method suggested in a previous study is used to reduce the size of the problem to the number nonlinear coordinates and solve them with an iterative process. This method reduces the computational time considerably. Time variation of stiffness is considered in the model by taking the average value of the mesh stiffness in the gear mesh interface, but including the excitation effect of the time varying mesh stiffness through a periodic displacement function representing loaded static transmission error.

In this thesis, secondly, results obtained by NLGRD are validated by comparing them with Munro's and Kubo's experimental results. The results are found to be in good agreement with the experimental results, although some deviations are observed. Reasons for these deviations are explained in the related sections.

The results obtained by NLGRD are also compared with the results obtained from the models of Özgüven (1988b) and Lin (1994). The change of dynamic to static load ratio with rotating speed is found to be similar.

In the last part of this thesis, several parametric studies are performed to understand the effects of several parameters on dynamic behavior of the geared rotor systems, such as mean load, module, center distance, parabolic profile modifications and linear profile modifications. The effect of tooth separation is also studied. In this study the following conclusions are drawn :

127

- Mean load increases the static transmission error as well as the difference between the maximum and minimum values of the static transmission error, which in turn, however does not change the dynamic to static load ratio. This suggests that dynamic to static load ratio is a system property which is independent of the transmitted load and therefore the same dynamic to static load ratio can be safely used at off design loads. Dynamic load itself and dynamic transmission error increases, though.

- As the module is increased static transmission error decreases since both gear and tooth dimensions take larger values and so the difference between maximum and minimum values of STE decreases too. This decreases the dynamic load and therefore the dynamic to static load ratio. Dynamics of the system is also affected from an increase in module since the equivalent gear mass increases which in turn shifts the torsional resonance to lower frequencies.

- There is almost a linear relation between maximum dynamic to static load ratio and module on logarithmic scale. An empirical equation is suggested for the calculation of the maximum dynamic to static load ratio as a function of gear module in a given geared rotor system. The following observations are made as a result of this part o the study :

1. By using a few experimental data for different modules, the dynamic response of a specific geared rotor configuration can be determined for all possible gear modules at a certain speed.

2. As the relationship between dynamic to static load ratio and module is linear on logarithmic scale, in an experimental study logarithmically increasing values of modules are to be used.

3. As the module takes larger values, maximum dynamic to static load ratio approaches to unity.

- A change in center distance changes contact ratio which affects the Fourier components of static transmission error. A small change in contact ratio, which in turn changes dynamic to static load ratio slightly do not affect the Fourier components of static transmission error considerably up to a critical value, after which higher harmonics overtake the main harmonic, and a subharmonic peak takes larger values than the main resonance peak amplitude. However, as the contact ratio is reduced further so that it approaches to unity, dynamic to static load ratio approaches to unity but of course, showing slight increases around resonance frequency.

- When the contact ratio is integer, the difference between maximum and minimum of static transmission error graph is minimum.

- Case studies have shown that high loaded static transmission error does not always imply high dynamic to static load ratio. The difference between maximum and minimum values of static transmission error as well as the shape of static transmission error curve are the basic factors determining the dynamic response.

- Rectangular wave approximation does not simulate static transmission error when profile modification is applied.

- Parabolic and linear profile modifications decrease dynamic to static load ratio. There is almost a linear relation between maximum dynamic to static load ratio and amplitude of modification. Linear profile modification is much more effective than the parabolic profile modification in reducing dynamic to static load ratio.

- The slope of the linear modification line is steeper than the parabolic one. From manufacturing point of view, this shows that linear profile modification is more sensitive to manufacturing errors and tolerances than parabolic profile modification.

- When there is tooth separation, the dynamics of the system becomes truly nonlinear and resonance frequency shifts to lower frequencies since due to backlash average mesh stiffness decreases. Damping value and the amount of backlash have significant effects on double-sided impact.

- As the backlash is increased from zero to a certain value, it is observed that first double-sided then single-sided impact take place. Increasing backlash beyond a critical value does not have an effect on dynamic to static load ratio.

- Although increasing backlash decreases the maximum dynamic to static load ratio, it does not have any effect on dynamic to static load ratio at off resonance and subresonances where tooth separation does not take place.

6.2 Recommendation

In this study a comprehensive finite element model is developed mainly for the dynamic analysis of spur gears. The flexibility of the finite element method is the main advantage of this code. Several different single stage spur gear mesh configuration can be analyzed by the same code. This model considers backlash in spur gear pair. The gear mesh interface is modeled as a three degree of freedom spur gear model, which includes the relative displacement along the pressure line between gear pair and rotational motion of gears about their pivot points. Although this model works perfectly for spur gears, a more advanced helical gear mesh interface can be inserted into the finite element model.

130

Blankenship and Singh (1995a) has developed a twelve degree of freedom linear helical gear mesh interface. Having extended the interface to include backlash, this dynamic gear mesh interface can be integrated in NLGRD. So an improved version of NLGRD, which considers both helical and spur gears can be developed.

In this case the number of nonlinear coordinates will increase. This will result in a more complicated interface between two shafts. However, attention must be paid to the iteration technique.

The user interface, Visual Geared Rotors (VGR), can be extended to show the mode shapes of geared rotor system graphically.

REFERENCES

Blankenship, G. W. and Kahraman, A., 1995a. "Steady State Forced Response of a Mechanical Oscillator with Combined Parametric Excitation and Clearance Type Non-Linearity", Journal of Sound and Vibration, Vol.185, No. 5, pp. 743-765.

Blankenship, G. W. and Singh R., 1995b. "Analytical Solution for Modulation Sidebands Associated with a Class of Mechanical Oscillators", Journal of Sound and Vibration, pp. 13-36.

Blankenship, G. W. and Singh, R., 1995c. "A New Gear Mesh Interface Dynamic Model to Predict Multi-Dimensional Force Coupling and Excitation", Mechanism and Machine Theory, Vol. 30, No. 1, pp. 43-57.

Blankenship, G. W. and Singh, R., 1995d. "Dynamic Force Transmissibility in Helical Gear Pairs", Mechanism and Machine Theory, Vol. 30, No. 3, pp. 323-339.

Budak, E. and Özgüven, H.N., " A Method for Harmonic Response of Structures with Symmetrical Nonlinearities", Proceedings of the 15th International Seminar on Modal Analysis and Structural Dynamics, Vol. 2, pp. 901-915, Leuven, Belgium, September 17-21,1990

Budak, E. and Özgüven, H.N., "Iterative Receptance Method for Determining Harmonic Response of Structures with Symmetrical Nonlinearities", Mechanical System and Signal Processing, Vol. 7, No.1, pp.75-87

Cai, Y., 1995. "Simulation on the Rotational Vibration of Helical Gears in

Consideration of the Tooth Separation Phenomenon (A New Stiffness Function of Helical Involute Tooth Pair)", Transactions of ASME, Vol. 117, pp.460-468.

Comparin, R. J. and Singh, R., 1990. "Frequency Response Characteristics of a Multi-Degree-of-Freedom System with Clearances", Journal of Sound and Vibration, Vol. 142, No. 1, pp. 101-124.

Fisher, A., 1968. "Factors in calculating the load carrying capacity of helical gears", Machinery, Vol. 98, pp. 545-552.

Genta, G. and De Bona F., 1990. "Unbalance Response of Rotors: A Modal Approach with Some Extensions to Damped Natural Systems", Journal of Sound and Vibration, Vol. 140, No. 1, pp. 129-153.

Gregory, R. W., Harris, S. L. and Munro, R. G., 1963-1964. "Dynamic behavior of spur gears", Proceedings of the Institution of Mechanical Engineers, Vol. 178, pp. 207-226.

Hagiwara, N., Ida, M. and Kikuch, K., 1981. "Forced vibration of a pinion-gear system supported on journal bearings", Proceedings, International Symposium on Gearing and Power Transmission ,Tokyo, pp.85-90.

Harris, S. L., 1958. "Dynamic loads on the teeth of spur gears", Proceedings of the Institution of Mechanical Engineers, Vol. 172, pp. 87-112.

Iwatsubo, T., Arii, S. and Kawai, R., 1984. "Coupled lateral-torsional vibration of rotor system trained by gears", Bulletin of the Japanese Society of Mechanical Engineers, Vol. 27, pp. 271-277.

Kahraman, A. and Singh, R., 1990. "Non-Linear Dynamics of aSpur Gear Pair", Journal of Sound and Vibration, Vol. 142, No. 1, pp. 49-75.

Kahraman, A. and Singh R., 1991a. "Non-Linear Dynamics of a Geared Rotor-Bearing System with Multiple Clearances", Journal of Sound and Vibration, Vol. 144, No. 2, pp. 469-506.

Kahraman, A and Singh, R., 1991b. "Interactions Between time-Varying Mesh Stiffness and Clearance non-Linearities in a Geared System", <u>Journal of Sound and Vibration</u>, Vol. 146, No. 1, pp. 135-156.

Kahraman, A. and Blankenship G. W., 1996. "Interactions Between Commensurate Parametric and Forcing Excitations in a System with Clearance", <u>Journal of Sound and Vibration</u>, Vol. 194, No. 3, pp. 317-336.

Kim, Y. B., 1995. "Quasi-Periodic Response and Stability Analysis for Non-Linear Systems: A General Approach", <u>Journal of Sound and Vibration</u>, Vol. 1992, No. 4, pp. 821-833.

Kohler, H. K., Pratt, A. and Thomson, A. M., 1970. "Dynamics and noise of parallel axis gearing", <u>Proceedings of the Institution of Mechanical Engineers</u>, Vol. 184, pp. 111-121.

Kujath, M. R. and Liu K. F., 1992. "On Vibration of a Class of Linear Time-Varying System", <u>Journal of Sound and Vibration</u>, Vol.156, No.3, pp. 481-504.

Lin, H. H. and Huston, R., 1986. "Dynamic loading on parallel shaft gears", <u>NASA CR 179473</u>

Lin, H. H. et. al, 1994. "Dynamic Loading of Spur Gears with Linear or Parabolic Tooth Profile Modifications", <u>Mechanism and Machine Theory</u>, Vol. 29, No. 8, pp. 1115-1129.

Litvin, F. L. , et. al, 1995. "Computerized Design and Generation of Low-Noise Helical Gears with Modified Surface Topology", <u>Transactions of ASME</u>, Vol. 117, pp. 254-261.

Kücükay, F., 1984. "Dynamic behavior of high speed gears", <u>Proceedings of the 3rd International Conference on Vibrations in Rotating Machinery, Institution of Mechanical Engineers</u>, pp. 81-90.

Maliha, R., 1994. "Non-Linear Dynamic Analysis of Geared Rotors to Internal

Excitation by Using Describing Functions and Finite Element Method", Phd Thesis, Middle East Technical University, Ankara,Turkey.

Mitchell, K. D. and Mellen, D. M., 1975. "Torsional-lateral coupling in a geared high-speed rotor system", American Society o Mechanical Engineers Paper 75-DET-75.

Mitchell, K. D. and Daws, J. W., 1983. "A basic approach to gearbox noise prediction", Society of Automotive Engineers Transactions, Vol. 9, pp. 3366-3379.

Nakada, T. and Utagawa, M., 1956. "The dynamic loads on gears caused by the varying elasticity of the mating teeth of spur gears", Proceedings of the Sixth Japanese National Congress on Applied Mechanics, pp. 493-497.

Nakamura, K., 1967. "Tooth separations and abnormal noise on power-transmission gears", Bulletin of the Japanese Society of Mechanical Engineers, Vol. 10, pp. 846-854.

Tanrikulu, Ömerand Kuran, Bayındır and Özgüven, H.N and İmregün, Mehmet, " Forced Harmonic Response Analysis of Nonlinear Structures Using Describing Functions", American Institute Aeronautics and Astronautics, Vol.31, No.7, pp.1313-1320.

Özgüven, H. N. and Houser, D. R., 1988a. "Mathematical Model Used in Gear Dynamics - A Review", Journal of Sound and Vibration, Vol. 121, No. 3, pp. 383-411.

Özgüven, H. N. and Houser, D. R., 1988b. "Dynamic Analysis of High Speed Gears by Using Loaded Static Transmission Error", Journal of Sound and Vibration, Vol. 125, No. 1, pp. 71-83.

Özgüven, H. N., 1991. " A Non-Linear Mathematical Model for Dynamic Analysis of Spur Gears Including Shaft and Bearing Dynamics", journal of

Sound Vibration, Vol. 145, No. 2, pp. 239-260.

Padmanabhan, C. and Singh, R., 1992. "Spectral Coupling Issues in a Two-Degree-of- Freedom System with Clearance Non-Linearity", Journal of Sound and Vibration, Vol. 155, No. 2, pp. 209-230.

Padmanabhan, C. and Singh, R., 1995a. "Analysis of Periodically Excited Non-Linear Systems by a Parametric Continuation Technique", Journal of Sound and Vibration, Vol. 184, No. 1, pp. 35-58.

Padmanabhan, C. and Singh R., 1995b. "Dynamics of a Piecewise Non-Linear System Subject to Dual Harmonic Excitation Using Parametric Continuation", Journal of Sound and Vibration, Vol. 184, No. 5, pp. 767-799.

Perret, J. and Liaudet, 1996. "An Original Method for Computing the Response of a Parametrically Excited Forced System", Journal of Sound and Vibration, Vol. 196, No. 2, pp. 165-177.

Pilipchuk, V. N., 1996. "Analytical Study of Vibrating Systems with Strong Non-Linearities by Employing Saw-Tooth time Transformations", Journal of Sound and Vibration, Vol. 192, No. 1, pp. 43-64.

Rettig, H., 1975. "Vibrations in gear drives; test results and calculation method for dynamic tooth forces", Proceedings of the International Federation of the Theory of Machines and Mechanisms 4th World Congress, Newcastle

Rook, T. E. and Singh R., 1995. "Dynamic Analysis of Reverse-Idler Gear Pair with Concurrent Clearances", Journal of Sound and Vibration, Vol. 182, No. 2, pp. 303-332.

Ross, A., A., 1927. "High speed gears", American Gear Manufacturers Association paper

Sinha, S.C. and Wu, D. H., 1991. "An Efficient Computational Scheme for the Analysis of Periodic System", Journal of Sound and Vibration, Vol. 151, No. 1, pp. 91-117.

Strauch, H., 1953. " Zahnradschwingunen (Gear vibrations)", Zeitschrift des Vereines Deutscher Ingiere, Vol. 95 pp. 159-163.

Toda, A. and Tordion, G. V., 1979. "Dynamic behavior of a mechanical system with gear trasnmission error", Proceedings of the International Federation of the Theory of Machines and Mechanisms 5th World Congress, Montreal, pp. 1130-1133.

Tomlinson, G. R. and Lam, J., 1984. "Frequency Response Characteristics of Structures with single and Multiple Clearance-Type Non-Linearity", Journal of Sound and Vibration, Vol. 96, No. 1, pp. 111-125.

Tordion, G. V., 1963. "The mechanical impedance approach to the gear dynamics of geared systems", American Gear Manufacturers Association Paper 209.04

Vinayak, H. et. al, 1995. "Linear Dynamic Analysis of Multi-Mesh Transmissions Containing External Rigid Gears", Journal of Sound and Vibration, Vol. 185, No. 1, pp. 1-32.

Yoon, K. Y. and Rao, S. S., 1996. "Dynamic Load Analysis of Spur Gears Using a New Tooth Profile", Journal of Mechanical Design, Vol.116, pp. 1-6

Zeman, J., 1957. "Dynamische zusatzkrafter in zahnbradgetrieben", Zeitschrift des Deutscher Ingiere, Vol. 99, pp. 244

APPENDIXE A

A.1 Nomenclature of Spur Gears

Spur gears are used to transmit rotary motion between parallel shafts; they are usually cylindrical in shape, and the teeth are straight and parallel to the axis of rotation.

The terminology of gear teeth is illustrated in Figure A.1. The **pitch circle** is a theoretical circle upon which all calculations are usually based. The pitch circles of a mating gears are tangent to each other. A **pinion** is the smaller of the mating gears. The larger is often called **gear**.

The **circular pitch** is the distance, measured on pitch circle, from a point on one tooth to a point on an adjacent tooth. Thus the circular pitch is equal to the sum of the **tooth thickness** and **width of space.**

The **module** is the ratio of the pitch diameter to the number of teeth. The customary unit of length used is the millimeter. The module is the index of gear tooth size in SI.

A pair of meshing gears, consisting of a pinion and a gear, must have exactly the same module, of course, to mesh properly.

The **addendum** is the radial distance between the **top land** and the pitch circle. The **dedendum** is the radial distance from the **bottom land** to the pitch circle. The **whole depth** is the sum of the addendum and dedendum.

The **clearance circle** is a circle that is tangent to the addendum circle of the mating gear. The **clearance** is the amount by which the dedendum

in given circle exceeds the addendum of its mating gear. The **backlash** is the amount by which the
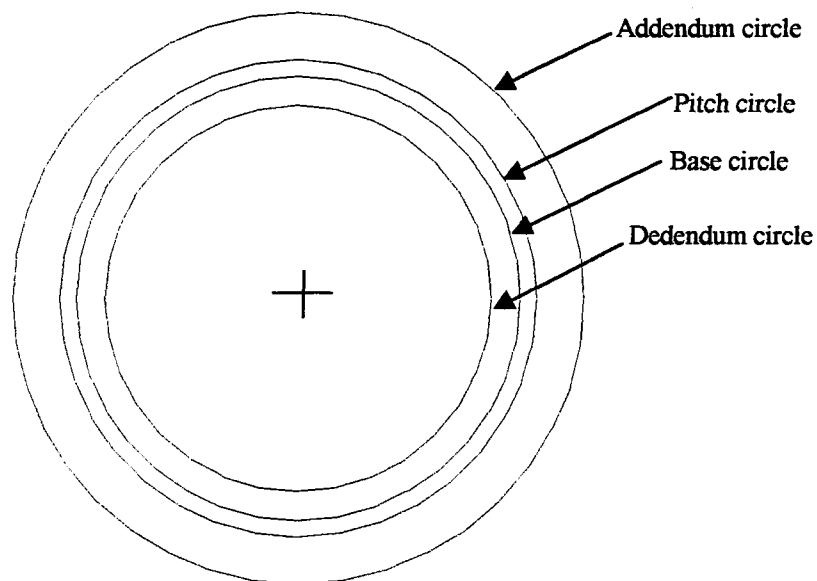
Figure A.1 Nomenclature of gear teeth

Table A.1 Basic tooth dimensions

FORMULAS FOR TOOTH DIMENSIONS FOR PRESSURE ANGLE OF 20 AND 25	
Addendum	m
Dedendum	1.25m
Working Depth	2m
Whole Depth (min)	2.25
Tooth Thickness	m/2
Fillet Radius of Basic Rack	0.300m
Clearance (min)	0.25m
Clearance Shaved or Ground Teeth	0.35m
Minimum Number of Teeth	
20 deg.	18
25 deg.	12
Width of Top Land	0.25m

m : module

139

width of a tooth space exceeds the thickness of the engaging tooth measured on the pitch circles.

A.2 Basic Tooth Dimensions

A tooth system is a standard which specifies the relationships involving addendum, dedendum, working depth, tooth thickness and pressure angle, for the purpose of standardizing cutting tool. The standard also achieves interchangeability of gears of all tooth numbers but of the same pressure angle and module.

Table A.1 lists the basic tooth dimensions for full-depth teeth having pressure angles 20° and 25°. The 20° pressure angle is most widely used. The 25° angle tooth is used mostly when a pinion with the least number of teeth is desired.

The addendum listed in Table A.1 are for gears having tooth numbers equal to or greater than the minimum numbers listed, and for these numbers there will be no undercutting. For a fewer numbers of teeth a modification called the **long and short addendum system** should be used.

A.3 Contact Ratio

The contact ratio, a number which indicates the average number of pairs of teeth in contact, can be calculated by Equation A.1

$$m_c = \frac{u_a + u_r}{p \cos(\phi)} \tag{A.1}$$

$$u_a = \left[(r_3 + a)^2 - r_{b3}^2 \right]^{1/2} - r_3 \sin(\theta) \tag{A.2}$$

$$u_r = \left[(r_2 + a)^2 - r_{b2}^2 \right]^{1/2} - r_2 \sin(\theta) \tag{A.3}$$

140

where

r_2 and r_3 : pitch circle's radius of the driven and driving gear

a : addendum

r_b : base circle radius

θ : Pressure angle

p : circular pitch

A.4 Varying the Center Distance

When a pair of meshing gears having involute teeth are separated by increasing center distance slightly. Clearance or backlash, now exists between the teeth. When the center distance is increased, new pitch circles having larger radii are created because the pitch circles are always tangent to each other. However the base circles are a constant and fundamental characteristic of the gears. This means that an increase in center distance changes the inclination of the line of action and results in a larger pressure angle. Notice, too, that a tracing point on the new pressure line will still generate the same involute, the normal to the tooth profiles still passes through the same pitch point, and hence the law of gearing is satisfied for any center distance.

A second effect of increasing the center distance is the shortening of the path of contact. The contact ratio can be defined as the length of the path of contact to the base pitch. The limiting value of this ratio is unity.; otherwise, periods would occur in which there would be no contact at all. Thus the center distance cannot be larger than that corresponding to a contact ratio of unity.

APPENDIXE B

PROFILE MODIFICATION

For convenience the same amount and length of profile modification are assumed to be applied to the tooth tip of both pinion and gear. Since modifying the root of one member has the same effect as modifying the tip of the mating member, all modification is assumed to be applied at the tooth tips. Extra care must be taken in modifying the roots of gear teeth, because of their complex geometry. This is particularly true for gears with small number of teeth. In some extreme cases with low-contact-ratio gears, root modification can destroy the effects of tip modification, making it preferable to employ only tip modification.

The minimum tip relief should be equal to twice the maximum spacing error plus the combined tooth deflection evaluated at the highest point of single tooth contact. A typical tooth profile showing both the unmodified(true involute) profile and a modified profile is illustrated in Figure B.1. Note that although, in Figure B.1, the length of modification is shown as vertical distance (parallel to axis of tooth), it is actually defined in terms of the gear roll angle

The optimum length of tip relief will allow loading pass smoothly from one tooth to the next. The length required depends on the contact ratio. Tip relief should not extend to the pitch radius unless the contact ratio is at least 2.

True involute
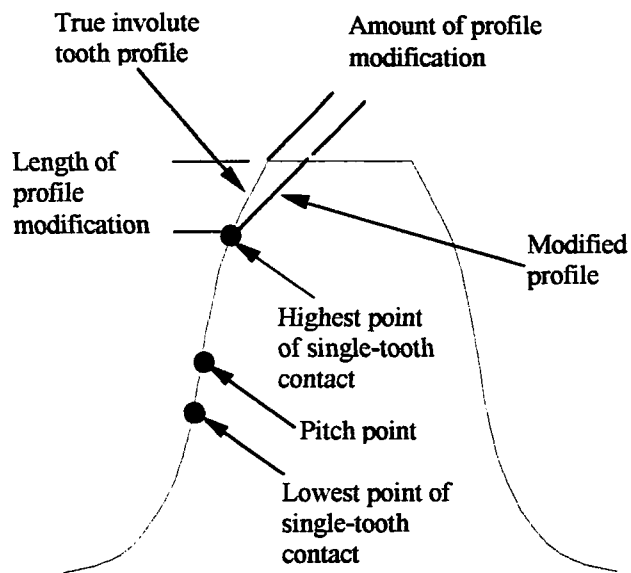tooth profile

Amount of profile
modification

Length of
profile
modification

Modified
profile

Highest point
of single-tooth
contact

Pitch point

Lowest point of
single-tooth
contact

Figure B.1 Gear tooth with linearly modified tooth profile

143

APPENDIXE C

USER MANUAL

C.1 Installation

The VGR version 2.0 is a user friendly interface which controls several sub codes. These codes are :

- NLGRD version 2.0 (Non-Linear Geared Rotor Dynamics)

- LDP version 10.1 (Load Distribution Program)

- Pine version 1.0

NLGRD version 2.0 is a finite element program which computes the dynamic to static load ratio, dynamic transmission error, bearing forces and natural frequencies of a geared rotor sytem.

LDP version 10.1 computes the several key issues of gears by static analysis, of which the loaded static transmission error has the most significance for this study.

Pine version 1.0 converts the output of VGR version 2.0 to the format of LDP version 10.1.

The four computer code, VGR, NLGRD, LDP and Pine must be installed properly to run the VGR version 2.0.

The VGR version 2.0 must be installed under the directory named :

C:\VGR\ Vgr20.exe

The NLGRD version 2.0 must be installed under the directory named :

C:\VGR\NLGRD\Nlgrd20.exe

The LDP version 10.1 must be installed under the directory named :

C:\VGR\LDP\Ldp101.exe

The Pine version 10 must be installed under the directory named :

C:\VGR\PINE\Pine10.exe

C.2 Visual Geared Rotors

The Visual Geared Rotors (VGR) consists of two sub programs. These are :

- NLGRD

- LDP

The VGR is able to prepare input data for both program. The LDP part of the program is placed in frames named LDP and the NLGRD part of the program is placed in frames named NLGRD. The parts which are common to LDP and NLGRD are placed in frames named NLGRD/LDP. All units are in SI standards. The units of the input data is indicated next to the input boxes.

Before going further, firstly user must construct the system geometrically, because the computer code, VGR, could automatically detect the order and type of the basic elements. If system is constructed in a wrong way. For instance clicking the stop button is forgotten, shaft one and two cannot be differentiated or gear and pinion have the same code number which may result in wrong matching of the input data.

When the user save the program files, VGR automatically creates the following files :

- *.vgr

- *.ldp

- *.shp

- File.vgr

*.vgr file holds the input data which is necessary for NLGRD version 2.0 to run, basically the material and geometric properties of the basic elements that are present is the system.

*.ldp file holds the input data which is necessary for LDP version 10.1 to run. However the format of this file is not appropriate for LDP version10.1. It must be converted by Pine version 1.0 through VGR version 2.0.

*.shp file holds the dimensions and place of basic object pictures in it. Thus when a preexist file is opened VGR is able to construct the system graphically.

File.vgr is a file which is automatically opened by NLGRD version 2.0. It holds the name of the input file name which is going to be read by

146

NLGRD version 2.0 and the name of the other output files that is going to be written by it. These are

- *.mod (holds the modal analysis output)

- *.dsl (holds the dynamic to static load ratio data)

- *.brf (holds the bearing forces)

- *.brd (holds the bearing displacements)

- *.msh (holds the dynamic transmission error data)

When the user run the Pine version 1.0, File.pin is automatically created under the directory in which Pine version 1.0 is placed. It contains the source and the target file names. Pine version 1.0 automatically opens this file.